POLITECNICO DI MILANO

Facoltà di Ingegneria dei Sistemi

Laurea di secondo livello in Ingegneria Biomedica

Scattering - Parameters measurement system for automatic matching network setup in MRI

Relatori: Prof. Andrea Aliverti;

Prof. Klaas Prüssmann.

Correlatore: PhD Matteo Pavan

Tesi di Laurea di:

Roberto Parrinello

Matr.735105

Anno Accademico 2009-2010

Scattering - Parameters measurement system for

automatic matching network setup in MRI

Supervisors: Prof. Andrea Aliverti;

Prof. Klaas Prüssmann.

Advisor: PhD Matteo Pavan

Master thesis by:

Roberto Parrinello

735105

Academic Year 2009-2010

Alla mia kikka

Acknowledgements

Ringraziamenti

Ringrazio il professore Andrea Aliverti, per la sua attenta e costante supervisione durante tutto il periodo Erasmus, per la sua disponibilita´ nel fornirmi aiuto nella stilazione e correzione della Tesi.

Voglio ringraziare i miei genitori che hanno avuto un ruolo determinante, sostenendomi durante i miei studi, ma soprattutto nella formazione come persona, con duro lavoro, fatica e tanta pazienza; Mia sorella, che mi ha insegnato a lottare per ottenere quello che voglio e che bisogna puntare sempre in alto, cercando con tutte le proprie forze di realizzare i propri sogni; La mia cara nonnina, una persona davvero speciale, che mi ha sempre appoggiato in tutte le mie scelte, che mi ha saputo consigliare con molta saggezza e che da sempre costituisce il tipo di persona che spero di diventare un giorno. Per tutte queste ragioni devo a loro quello che sono oggi.

Ringrazio tutti gli amici che ho incontrato a Milano durante questi anni universitari e che hanno contribuito, ognuno a suo modo, a rendere piu´ piacevole questo soggiorno e meno lungo questo viaggio che mi ha portato fino alla laurea.

Ringrazio tutti i miei amici con cui sono cresciuto in sicilia, che mi hanno supportato e che non si sono mai tirati indietro aiutandomi quando avevo bisogno di loro e che, nonostante la lontananza, continuano ad essere un punto di riferimento nella mia vita, come se non ci fossimo mai separati.

Infine ringrazio la persona che piu´ di tutti mi ha supportato nei momenti tristi ed elogiato in quelli felici, che mi ha regalato in tutti questi anni tanti momenti indimenticabili che portero´sempre con me e che mi ha fatto capire che la vita puo´essere veramente bella.

Contents

Sommario

Lavorando indipendentemente, Felix Bloch dell'università di Stanford e Edward Purcell della Università di Harvard realizzarono il primo esperimento sulla risonanza magnetica con successo per studiare i componenti chimici nel 1946. Dr Bloch e Dr Purcell furono premiati con il Premio Nobel per la Fisica nel 1952. All'inizio degli anni ottanta i primi scanner di risonanza magnetica (MRI) divennero disponibili, producendo immagini dell'interno del corpo umano. La risonanza magnetica (MRI) è una tecnica di imaging usata prima di tutto nel campo medico per produrre immagini dell'interno del corpo umano di alta risoluzione. L'MRI è basata sul principio di risonanza magnetica nucleare (NMR), una tecnica spettroscopica usata dagli scienziati per ottenere informazioni microscopiche in ambito chimico e fisico riguardo le molecole. Questa tecnica fu chiamata risonanza magnetica invece che risonanza magnetica nucleare (NMRI) a causa della connotazione negativa associata con la parola nucleare alla fine degli anni settanta. La risonanza magnetica viene usata come tecnica di imaging tomografica, in quanto produce una immagine del segnale della NMR in una fetta sottile attraverso il corpo umano. Col passare del tempo l'MRI si è trasformata dalla sola tecnica di imaging tomografica ad una tecnica di imaging di volume. Quindi una MRI può essere ritenuta simile ad uno scanner di tomografia computerizzata (CT) poiché produce una immagine di cross-sezione del corpo. Guardare un'immagine del corpo di una cross-sezione può essere comparata al guardare all'interno di una fetta di pane ottenuta tagliandolo. A differenza di uno scanner CT, l'MRI non usa raggi X. Al contrario usa un forte campo magnetico e onde radio per produrre una immagine computerizzata molto chiara e dettagliata dell'interno del corpo umano. Infatti gli scanner MRI di nuova generazione forniscono immagini 2-D e 3-D altamente dettagliate della anatomia umana. MRI è comunemente usata per esaminare il cervello, la colonna vertebrale, i legamenti, l'addome, e il bacino pelvico. Il fenomeno di NMR si basa sull'eccitazione all'interno di un oggetto (come ad esempio un paziente), posizionato in un campo magnetico polarizzato, irradiando l'oggetto con un'energia RF per ottenere la frequenza di Larmor. Nella applicazioni diagnostiche medicali che sono

4

tipicamente caratterizzati dal posizionamento del paziente, da esaminare, in una coil RF con un amplificatore RF di potenza. La stessa o un'altra coil e un preamplificatore RF sono usati, inoltre, per ricevere il segnale NMR emanato dal volume del paziente disteso all'interno del campo della RF coil. Per assicurare il massimo trasferimento di potenza tra l'amplificatore di potenza RF e la coil RF, e allo stesso modo tra la coil e l'amplificatore del ricevitore NMR, la impedenza di input della coil deve essere simile all'impedenza di output dell'amplificatore e all'impedenza di input e a quella del preamplificatore. Questo risultato può essere raggiunto usando una RF coil matching network. Dal passato ad oggi, diverse tecniche sono state usate per affrontare questo problema e provare a "matchare" l'impedenza, in modo da ottenere le migliori prestazioni di rapporto segnale rumore (SNR) e immagini con elevata risoluzione. Questo problema è anche legato con i due tipi diversi di RF coil: coil di volume e coil di superficie e quale di questi è migliore per l'MRI. Il più grande vantaggio delle coil di volume è la loro abilità di generare elevati campi omogenei polarizzati circolari B_1, che si traduce in un segnale omogeneo di uguale sensitività nelle operazioni di ricezione. I due maggiori svantaggi di questi coil sono: la loro geometria fissa e il fatto che sono dei risonatori singoli di volume e perciò non riescono ad esplorare i benefici di una misurazione multi-canale. Le coil di superficie offrono una grande libertà rispettando la loro forma e la loro geometria in un array. Sono usate comunemente disposte attorno alla regione di interesse. Comunque, con coil larghe è difficile ottenere elevate prestazioni, facilità di gestione, e comfort per il paziente allo stesso tempo. Per un ottimo SNR ed elevate velocità di calcolo, gli array di coil hanno bisogno di adattarsi bene alla parte anatomica di interesse, che può variare significativamente in forma e grandezza in soggetti diversi. Cambiamenti tra un paziente e l'altro nella geometria dell'array indurrà variazioni nel loading e nel mutual coupling. Una volta ottenuta la massimizzazione delle performance del SNR, queste variazioni richiedono robuste e specifiche strategie di tuning, matching e decoupling. Klaas Prüssmann, nel 2009, ha introdotto il concetto di array geometricamente adattabili, affrontandolo solo per il caso specifico di imaging per il polso. Per questa ragione fu costruito un array di otto canali manualmente adattabile per il polso per un'MRI di 3 Tesla. L'array si adatta alla grandezza di polsi diversi attraverso un semplice meccanismo di scorrimento ed è stato progettato per assicurare delle performance di SNR robuste in un intervallo ampio di valori differenti di

loading e coupling. Ma sarebbe impensabile in un setup clinico adattare e modificare ogni volta manualmente il matching e il tuning di un array di coil che dipende da pazienti diversi o da misurazioni diverse. Per tale motivo, Matteo Pavan, nel 2010, presenta un sistema di matching con un Metodo Automatico Modulare (AMM) che può facilmente essere esteso a matchare l'impedenze di output di molti canali diversi allo stesso tempo. Un punto da sottolineare di questo sistema è la capacità che ha di ottenere un matching di impedenze su qualsiasi punto desiderato del piano complesso. La parte principale di questo circuito di matching è un chip di guadagno nelle radiofrequenze e di fase (AD8302, *Analog Device*), dove un segnale di riferimento fisso, generato da un Oscillatore di Voltaggio Controllato (VCO) è introdotto in un doppio ibrido (con direttività migliore di 40 dB) e grazie all'isolamento tra le diverse porte dell'ibrido è possibile separare le onde principale e riflessa. Queste due onde sono introdotte nel chip di guadagno e di fase che restituisce come output due voltaggi costanti, uno proporzionale alla differenza di fase tra l'onda principale e quelle riflessa e l'altro proporzionale al rapporto del modulo dell'onda principale e il modulo dell'onda riflessa. Quindi i due diversi voltaggi sono dipendenti tra loro e il chip non è lineare. Infatti, quando la fase rilevata è vicina allo zero, il sistema non riesce a distinguere le fasi dove la differenza è di 180°. Questo lavoro di tesi è stato sviluppato nel laboratorio di MRI del dipartimento di Biomedica nell'università ETH di Zurigo, Lo scopo di questa tesi è il miglioramento del sistema precedentemente usato da Pavan attraverso la creazione e l'uso di un modo innovativo di misurare le rispettive impedenze per il sistema automatico di matching. In particolare gli obbiettivi di questo nuovo sistema sono:

- Nel nuovo sistema il segnale, in uscita dal doppio ibrido, è diviso in due diverse onde in modo totalmente indipendente una dall'altra.

- Questo nuovo sistema può garantire una buona linearità delle misurazioni dell'impedenza e può differenziare i valori di impedenza in tutta la Smith Chart senza nessun tipo di problema di differenziazione di fase.

- E' possibile non soltanto misurare i parametri di scattering di riflessione S_{11} e S_{22} che erano calcolate anche nel sistema precedente, ma anche i parametri di scattering di trasmissione S_{12} e S_{21} che sono molto importanti per una calibrazione più precisa della matching network e per un calcolo più preciso dell'impedenza.

Questa tesi offre una solida base per ulteriori sviluppi riguardo un sistema di matching hardware automatico per la risonanza magnetica di 7 Tesla. Il nuovo sistema sviluppato è facile da usare come schiacciare un tasto, con un Errore di Impedenza molto buono anche se ancora leggermente peggiore rispetto al sistema precedente. Comunque la più importante proprietà di questo nuovo sistema è la capacità di misurare i parametri S_{12} e S_{21} senza nessuna aggiunta o cambiamento nell hardware. Grazie a questo sistema sarà possibile effettuare una calibrazione a Due Porte durante un'acquisizione di MRI di un campione (es: paziente) con tutto l'hardware necessario all'interno della stanza di MRI. Ciò può offrire una misurazione di impedenza più specifica e accurata dei cambiamenti della coil in minor tempo (una misura di una impedenza impiega meno di 100 ms). Possibili sviluppi, focalizzati in un sistema migliore senza però aumentare il tempo globale di una misurazione di impedenza, potrebbero essere: un'ottimizzazione del sottocampionamento con un migliore filtro digitale, implementato nell'algoritmo del PIC nella parte di processore che può diminuire l'Errore di Impedenza; un miglioramento nella qualità del segnale proveniente dai due mixer con una differenza maggiore tra l'onda PRINCIPALE e quella RIFLESSA che può permettere un migliore calcolo della differenza di fase; l'implementazione dell'algoritmo interamente all'interno del PIC con un minor numero di comunicazioni tra il PIC e il PC che può garantire un calcolo più veloce dell'impedenza finale; l'aumento del numero di canali da due, già implementati nell'algoritmo e testati, fino a 16 canali, che l'hardware permette di usare ma senza nessun tipo di cambiamento, ma che per mancanza di tempo non si è riusciti a testare.

La tesi è divisa in 4 capitoli:

- Il primo capitolo comincia con una introduzione degli argomenti principali della MRI richiamando i principi fondamentali della MRI e i fenomeni che accadono durante un

acquisizione di MRI. Successivamente viene fatta una breve descrizione dell'hardware della MRI, con un'analisi più dettagliata dei differenti tipi di coil usati per l'imaging. Inoltre vengono esposti i diversi tipi di matching network manuali e automatici dal passato fino allo stato dell'arte. Il paragrafo correlato con l'obiettivo di questa tesi conclude il primo capitolo.

- Il secondo capitolo fornisce tutte le informazioni riguardo la radiofrequenza e alcuni concetti basilari necessari legati alla RF come ad esempio l'SNR, il fattore di Qualità, i componenti elettrici e la teoria della linea di trasmissione. Tutte queste informazioni servono a comprendere meglio il cuore della tesi basata sul calcolo del coefficiente di riflessione e del calcolo dell'impedenza corrispondente e mostrare questi valori nella Smith Chart. Il secondo capitolo termina con la spiegazione dei parametri S e dei differenti metodi usati per raggiungere la stabilità e la minore figura di rumore.

- Il terzo capitolo descrive, dopo una breve introduzione sul Network Analyzer, tutte le diverse parti che permettono a questo strumento di registrare il segnale e di fornire la misura dell'impedenza. Dopodiché ogni sezione del Network Analyzer viene confrontata con il nuovo sistema provvedendo a fornire tutte le informazioni riguardanti la fase di progettazione e costruzione. Le quattro sezioni elencate sono: La sorgente di stimolo; il device per la separazione del segnale; la parte dedicata alla ricezione del segnale; il Processore / Display per il calcolo e la revisione dei risultati.

- Il quarto ed ultimo capitolo presenta i risultati ottenuti riguardanti, prima il processo di calibrazione e successivamente le misure delle impedenze attraverso un'analisi quantitativa e statistica dei dati. Inoltre, usando schemi e grafici è stato possibile mostrare il confronto tra i dati misurati dal Network Analyzer e quelli del nuovo sistema. Questi risultati sono ottenuti da misurazioni di cambiamenti teorici di impedenza. Alla fine, Vengono presentate le conclusioni di questo lavoro mostrando i limiti incontrati e proponendo sviluppi futuri con l'intento di migliorare il sistema precedentemente sviluppato.

Abstract

Working independently, Felix Bloch of Stanford University and Edward Purcell of Harvard University made the first successful nuclear magnetic resonance experiment to study chemical compounds in 1946. Dr Bloch and Dr Purcell were awarded the Nobel Prize for Physics in 1952. In the early 1980s, the first "human" magnetic resonance imaging (MRI) scanners became available, producing images of the inside of the body. Magnetic resonance imaging (MRI) is an imaging technique used primarily in medical settings to produce high quality images of the inside of the human body. MRI is based on the principles of nuclear magnetic resonance (NMR), a spectroscopic technique used by scientists to obtain microscopic chemical and physical information about molecules. The technique was called magnetic resonance imaging rather than nuclear magnetic resonance imaging (NMRI) because of the negative connotations associated with the word nuclear in the late 1970s. MRI started out as a tomographic imaging technique, that produced an image of the NMR signal in a thin slice through the human body. MRI has advanced beyond a tomographic imaging technique to a volume imaging technique. So an MRI is similar to a computerized topography (CT) scanner in that it produces cross-sectional images of the body. Looking at images of the body in cross section can be compared to looking at the inside of a loaf of bread by slicing it. Unlike a CT scan, MRI does not use x-rays. Instead, it uses a strong magnetic field and radio waves to produce very clear and detailed computerised images of the inside of the body. Current MRI scanners produce highly detailed 2-dimensional and 3-dimensional images of the human anatomy. MRI is commonly used to examine the brain, spine, joints, abdomen, and pelvis. The NMR phenomenon can be excited within a sample object, such as a human patient, positioned in a polarizing magnetic field, by irradiating the object with radio frequency (RF) energy at the Larmor frequency. In medical diagnostic applications, this is typically accomplished by positioning the patient to be examined in an RF coil with an RF power amplifier and the same or a different RF coil and a RF preamplifier are used to receive the NMR signal emanating

from the patient volume lying within the field of the RF coil. To ensure maximum power transfer between the RF power amplifier and the RF coil, as well as between the coil and the NMR receiver preamplifier, the coil input impedance must match the amplifier output impedance and the preamplifier input impedance. This can be achieved by using an RF coil matching network. Several techniques have been used trough time to face this problem and try to match the impedance in such a way to obtain the best SNR performances and high image resolution. This problem is also related with the two types of RF coils: volume coils and surface coils and which one is better to use in MRI. The main advantage of volume coils is their ability to generate highly homogeneous circularly polarized B_1 fields, which translate into equally homogeneous signal sensitivity in "receive" operation. The two main disadvantages of these coils are their fixed geometry and the fact that they are single volume resonators, thus they do not exploit the benefits of multiple-channel detection. Surface coils offer great freedom with respect to their shape and geometric layout in an array. They are commonly arranged such as to tile the region of interest. However, with large coil counts it is a challenge to achieve high performance, ease of handling, and patient comfort at the same time. For optimal SNR and encoding performance, the coil array needs to closely fit the anatomy of interest, which may vary significantly in shape and size for different subjects. Patient-to-patient changes in array geometry will induce variations in the loading and mutual coupling of the coil elements. Given the goal of maximizing SNR performance, such variations require precise tuning, matching, and decoupling strategies. *Klaas Prüssmann*, in 2009, has introduced the concept of a geometrically adjustable array that he has explored for the specific task of wrist imaging. Therefore, a manually adjustable eight-channel wrist array has been constructed, targeting proton MRI at 3 Tesla. The array accommodates individual wrist sizes by a simple sliding mechanism and was designed to ensure robust SNR performance in a wide range of loading and coupling conditions. But it would be unthinkable in a clinical setup to manually adjust the matching and tuning of an array of coils depending on different patients or different measurements. This led *Matteo Pavan* in 2010 to develop a modular Automatic Matching Method (AMM) system that can be easily extended to match the output impedance of many different channels at the same time. An underlying point of this system is the capability of matching impedances to any desired point of the complex plane.

The core of the matching network is an RF gain and phase detector chip (AD8302, *Analog Device*), where a fixed reference signal, generated by a Voltage Controlled Oscillator (VCO), is fed into a double hybrid (directivity better than 40dB) and thanks to isolation between different ports of the hybrid is possible to separate the forward and the reflected waves. Those two waves are fed into the gain and phase chip detector that gives at the output two constant voltages, one proportional to the phase difference between the forward and the reflected wave and the other proportional to the ratio of the magnitude of the forward and reflected waves. So the two voltages are dependent of each other and the chip is non linear. In fact, when the detecting phase differences are close to zero, the system does not distinguish phases that differ of 180°. This thesis has been developed in the MRI lab of the Biomedical Department in the ETH University of Zürich. The scope of this thesis is to improve of the previous system used by *Matteo Pavan* through the creation and application of an innovative way to measure the respective impedance for the automatic matching network setup. In particular the goals of this new system are:

- The signal after the double hybrid is divided in two different waves totally independent of each other,

- To guarantee a good linearity of the measurements of the impedance and can differentiate the values of the impedance in all the Smith Charts without any problems in the phase differences.

- It is possible to measure not only the reflection scattering parameters S_{11} and S_{22} that were computed even in the previous system, but also the transmission scattering parameters S_{12} and S_{21} that are very important for a more precise calibration of the matching network and for the precise computation of the impedance to be matched.

This thesis offers a solid basis to start further development in automatic hardware matching network setup for a 7 Tesla Magnetic Resonance. Using the newly developed system ia as

simple as the touch of a button, with a very good Impedance Error but still less accurate than the previous one. However the most important property of this new system is the capability to measure the S_{12} and S_{21} parameters without any changes or additions to the hardware. Therefore it is possible to execute a Two Port calibration during an MR image acquisition of a sample (as a patient) with all the hardware inside the MRI room. This can offer a more specific and accurate impedance measure of the coil's changes in less time (a measure of one impedance takes less than 100 ms). Possible improvements, focused on the improvement of the system without increasing the global time used to measure an impedance, could be: an optimization of the undersampling with a better digital filter, implemented in the algorithm of the PIC in the processor part that can decrease the Impedance Error; an improvement of the quality of the signal from the two mixers with a bigger difference between the FORWARD and REFLECTED waves that can permit a better computation of the phase shift; the implementation of the algorithm entirely inside the PIC with less communication between the PIC and the PC that can guarantee a faster computation of the final impedance; The increasing of the number of the channels from 2, already implemented in the algorithm and already tested, up to 16 channels, that the hardware can permit without any kind of changes but It was not done for lack of time.

The thesis is dived into four chapters:

- The first chapter starts with an introduction of the basis topic of the MRI recalling the fundamental principles of the MRI and the phenomenon that happens during the MRI acquisition. Then there is brief description of the hardware of an MRI scanner and a more detailed analysis of the different types of coils used for imaging. It also exposes the different kinds of manually and automatic matching networks from the past to the state of the art of this device. The paragraph related to the purpose of this thesis concludes the first chapter.

- The second chapter provides all the information about the radio frequency background and some necessary basic concepts related with the RF such as SNR, Quality Factor, electric components and line theory. All this information is needed to better comprehends the core of the thesis based on the computation of the reflection coefficient and the respective impedance and showing these values in the Smith Chart. The second chapter ends with an explaination about the S-parameters and the different methods to reach the stability and the lowest noise figure.

- The third chapter describes, after a brief introduction of the Network Analyser, all the different parts required by this instrumentation to record the signal and provide the impedance measurement. Then every section of the Network Analyser is compared with the new system providing all the information about the design and manufacturing process. The four sections clarified are: Source for stimulus; Signal-separation devices; Receiver that provides detection; Processor/display for calculating and reviewing the results.

- The fourth and final chapter presents the results of, firsthly; first, the calibration process and then; the impedance measure through quantitative analysis and statistics. Trough charts and graphs the comparison between the data provided by Network Analyser and the new systematic. These results are obtained from the execution of the measurements of theoretic impedance changes. Finally, conclusions of this work are presented showing the limits encountered and proposing future developments with the aim of improving the system so far developed.

Chapter 1

Magnetic Resonance Imaging: RF Coil Matching Networks

1.1 Why MRI?

In medicine it is important to use images both for clinical diagnosis and also to understand causes of disease. Images are created through the interaction between some kind of energy and the tissue under observation; all measured parameters from this interaction can represent (eventually after data processing) biological tissue's features that can be viewed in two or three dimensions. Magnetic resonance imaging (MRI) can discriminate, for example, liver and spleen tissue that have the same X-ray transparency, and also permit you to take $2D$ pictures with any orientations or volume images, without using ionizing radiations. Furthermore, is possible to study the functionality of biological structures. This makes MRI extraordinarily versatile, and provides a fertile ground for innovative academic research into novel applications. Technological advancements in basic hardware led to expand the role of MRI as an experimental tool, this advancements involve people specialized in fields such as electrical engineering, physic, computer science and medicine.

1.1.2 The origin of the signal

MRI belongs to a larger group of techniques which are based on the principles of the nuclear magnetic resonance (NMR). The NMR experiment described by Purcell and Bloch in 1946, can acquire a signal with no means to integrate the spatial information so as to generate an image. Since the word "nuclear" has an unfortunate connotation for the public, this imaging technique was called MRI to avoid misconceptions. NMR was mainly used for spectroscopic analysis before the principles of MRI were introduced by Lautherbur and Mansfield independently in 1973. MRI can provide more information than other imaging modalities since MR signal is sensitive to several tissue parameters. MRI operates by observing the absorption or emission of power as transitions are induced between the nuclear energy levels. Normally, the energy levels are nearly degenerate, making this a very difficult task. However, application of an external magnetic field can split the energy nuclear energy levels. Transitions between the nuclear energy levels can then be induced by an oscillating magnetic field, usually in the radio frequency (RF) range. The frequency where absorption or emission of power occurs corresponds to a matching of the energy of the incident radiation to the energy level splitting. These transitions can then be observed experimentally through their absorption and emission of radiation. The local environment of the nuclei in solids and liquids is influenced by fluctuations, both static and dynamic, caused by neighboring nuclei and electrons that couple to the nuclear magnetic moment. These fluctuations will shift and broaden the absorption. Measurement of these shifts provides information on the static fluctuations in the systems. Measurement of the width of the line, and the associated relaxation times, provides information on the dynamic fluctuations in the system. The most important contribution arises from fluctuations at the resonance frequency. Thus, MRI provides a method to observe the magnitude of the local fluctuations at a particular frequency and measurements at several frequencies can be used to map the fluctuation spectrum. Water provides an ideal sample for introductory experiments in MRI. The signal from the hydrogen is quite strong and the properties of the system can be varied over a wide range. The MRI experiment utilizes pulsed techniques to measure the position, width, and relaxation time of the resonance. Pulsed techniques, which are now used in most applications, use linear

response theory to relate the response after a short perturbation to the more familiar continuous absorption method [1-5]. A strong magnetic field will tend to orient nuclear spins and induce a magnetization of the sample along the direction of the field. The direction of the magnetization can be changed very efficiently by applying RF pulses at the spin precession frequency, the Larmor frequency.
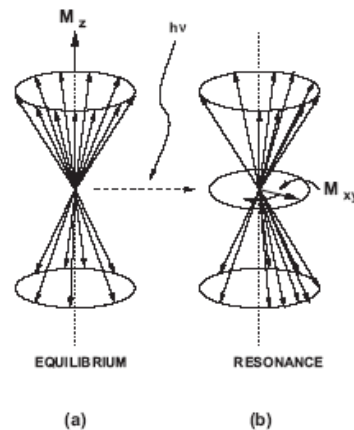
Figure 1.1: RF magnetic field disturb the equilibrium of *M (see RF Circuit Design [10])* .

With an appropriate choice of pulse height, duration and phase the sample can be brought into any magnetization state desired, but after the pulse it will relax back to thermal equilibrium, with the magnetization again directed along the field. One application of MRI is to study the relaxation processes. One distinguishes three types of relaxation. In the first place there is the interaction with the spins with "the rest of the system". The spin distribution is out of thermal equilibrium and will lose energy to the other degrees of freedom in the system. As a result the magnetization will relax towards its equilibrium value. The relaxation time associated with these processes is called the longitudinal relaxation time, τ_1. The second type of relaxation process involves interactions between the spins. These redistribute energy between the spins but leave the total energy of the spin system unchanged, so only the components perpendicular to the field relax. The relevant relaxation time is called transverse relaxation time, τ_2. A third effect is the so called free induction decay (FID).
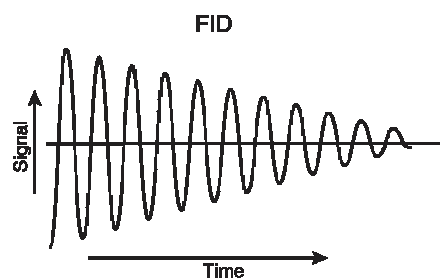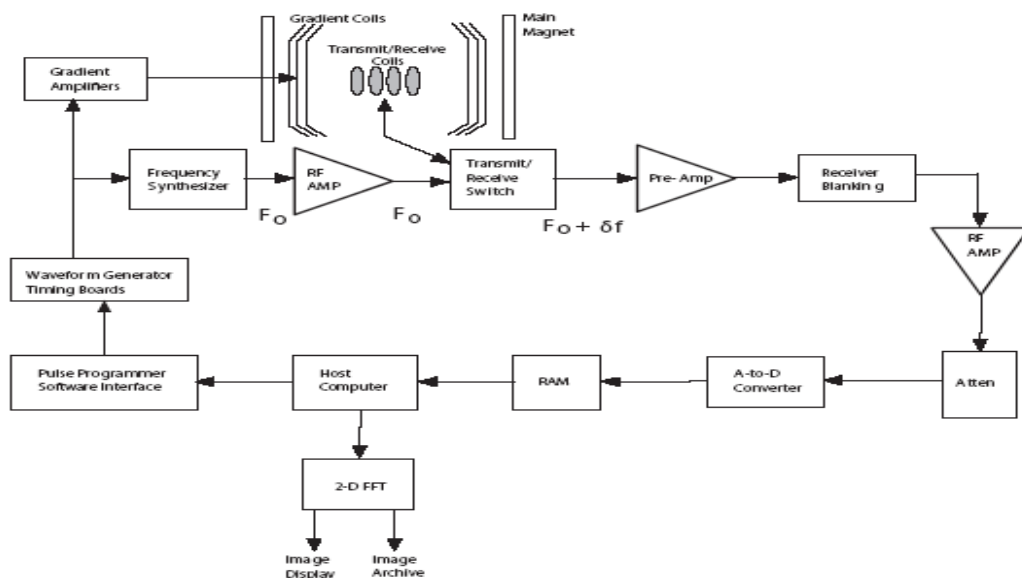
Figure 1.2: FID

When the total magnetization is put at some angle with respect to the magnetic field, it starts to precess. If all the spins would precess at exactly the same frequency, one would observe the transverse component of the magnetization decay with τ_2. In fact, it seems to decay much faster. Due to variations in its environment, every spin sees a slightly different field. This means that the local precession frequencies are slightly different, some spins precess faster than others. However, although it appears that the transverse magnetization decays, this is not a relaxation process. As long as there are no interactions, the spins know where they came from, and if all the spins or all the fields were inverted, the process is perfectly reversible; all the spins precess backward to where they came from. The idea of separating the reversible and the irreversible processes is one key feature of pulse MRI. Typical experiments go as follows. To measure τ_2, rotate, with what is called a τ_2 pulse, the magnetization into the x − y plane (z is along the magnetic field). Quickly the magnetization signal in the x−y plane will disappear. Wait a while, and then, using a pulse with appropriate amplitude and duration (a π pulse) rotate all the spins by 180°. Wait a while longer and the signal reappears; most the spins are back. However, some of the spins have interacted with other spins, etc. and got lost. Consequently, the echo is smaller than the original signal, and furthermore, it becomes increasingly smaller when the delay between the $\pi/2$ and the π pulse is increased. From the echo height versus delay time one can obtain the transverse relaxation time τ_2. A similar experiment is used to measure τ_1. Rotate the spins by 180° so that the magnetization points along the −z axis, wait and rotate them by 90°. Now the signal in the x−y plane corresponds to the remaining total magnetization that you had in the −z direction. Again, with increasing

delay this becomes smaller, indicating $\overrightarrow{B_0}$ how quickly the total magnetization decays. The peak of the FID signal (immediately after the $\pi/2$ pulse) as a function of π is proportional to $|2\exp(-\tau/\tau_1)-1|$ and this may be used to determine τ_1. Another application of MRI is to form an image. For this scope is necessary to perform the spatial localization of the MR signals which is normally a two steps process. First a slice of the body is selected for imaging (*selective excitation*). Second a magnetic field gradient can be applied along to any or a combinations of following directions *x*, *y*, and *z*, and according to a pre-established imaging sequence to generate an image with a specific orientation (*spatial encoding*). In order to generate an image, it is necessary to measure the spatial variation of MR parameters such as spin density, or the spin-lattice relaxation time, τ_1. These variables are not independent of the spatial coordinates of the spin system. These measurements are made by adding other space dependent magnetic fields to the static magnetic field so that the magnetization precesses at different frequencies depending on its space position. We may add to the uniform field $\overrightarrow{B_0}$ a linear spatially varying magnetic field gradient. The gradient gives a linear variation of Larmor frequency with position. For a given *z* all the spins that lie in that plane *xy* have the same Larmor frequency, so it is possible to select and excite only an assigned slice. Once the slice has been selected, the frequency and phase of the precessing macroscopic magnetic moment can be made a function of position within the slice. By briefly turning on the G_y gradient field, immediately after the selective excitation (slice selection), the precessional phases of the rotating macroscopic magnetization can be manipulated. Turning on the *Gy* gradient means the precessional frequency (the Larmor frequency) now varies along the *y*-direction. Then a magnetic field gradient in the *x*-direction, *Gx*, is switched on immediately the Larmor frequency becomes a function of *x* position. To obtain the proton density $\rho(x; y)$ is possible by taking the inverse 2*D* Fourier transform of the demodulated FID signal. The sequence of *Gz*, *Gy*, *Gz* gradient and RF pulses is known as a pulse sequence. Depending on the sequence of gradient and RF pulses the *k*space (the abstract platform onto which data are acquired, positioned, and then transformed into the desired image) can be scanned in a number of ways. These pulse sequences can be extremely complicated and can include other manipulations

such as spin echo, fat suppression, spin inversion and gradient echo. The manner, and in particular the speed, in which the *k*space is scanned is crucial to determine temporal variations in localized spin properties that occur ad example due to the variations in blood flow [6-10].

1.2   Hardware

The basic components of MRI hardware are shown in Figure 1.5. The patient is positioned within the main magnet by a computer controlled table with a positioning accuracy of $1\,mm$. The scan room is surrounded by an RF shield. The shield prevents the high power RF pulses from radiating out through the hospital and it also prevents the various RF signals from television and radio stations to be detected by the scanner. The shield is a copper or stainless steel known as a Faraday shield.   Maintaining the integrity of this Faraday shield is very important to minimize noise contamination of the final images. MRI rooms have one or two holes in the shield that let cables to enter and exit from the MRI room for experimental setup.   These holes in the shield acts like waveguides with a cutoff-frequency that permit to stop all the noise. It is important to do not insert conductors through this holes because the conductor eliminates the waveguide effect letting noise to enter [9].

Figure 1.3: Basic components of MRI hardware

1.2.1   PC

Every MRI system has a minimum of two computers.   The main or host computer controls the user interface software. This software enables the operator to control all functions of the scanner either directly or indirectly. Scan parameters may be selected or modified, patient images may be dis- played or recorded on film or other media, and postprocessing operations such as region-of-interest measurements or quantification can be performed. The second computer system is a dedicated image processor used to process the detected data.   This processor is controlled by software provided by the manufacturer and it controls all components on the system.   The RF components under control of the computer are the radio frequency source and pulse programmer. The source produces a sine wave of the desired frequency. The Pulse programmer shapes the RF pulses. The computer also controls the gradient pulse programmer which sets the shape and amplitude of each of the three gradient fields.   The gradient amplifier increases the power of the gradient pulses to a level sufficient to drive the gradient coils. The two-dimensional Fourier transform is performed by an array processor in fractions of a second so the computer off loads the Fourier transform to this faster device. The scan room must be shielded also to prevents distortion of the image on the monitor.

1.2.2   Main Magnet

The main magnet is the most expensive component of the magnetic resonance imaging system.   The main magnet is a superconducting magnet, that means it is an electromagnet magnet made of superconducting wire. Superconducting wire has a resistance approximately equal to zero when it is cooled to a temperature close to absolute zero ($\simeq 4\,K$) by immersing it in liquid helium. Once current is caused to flow in the coil it will continue to flow as long as the coil is kept at liquid helium temperatures.

Some losses do occur over time due to infinitely small resistance of the coil but these losses are on the order of a *ppm* of the main magnetic field per year. Coil and liquid helium tank are surrounded by a refrigerator which acts as a thermal buffer between the room temperature ($293\ K$) and the liquid helium. The primary consideration in magnet quality is the homogeneity or uniformity of the magnetic field. One factor affecting magnet homogeneity is the magnet design. Large-bore solenoidal magnets generally have the best homogeneity over the largest volume. Short-bore magnets tend to have smaller regions of good homogeneity due to the reduced number of magnet windings used. Open-design magnets will also have reduced regions of good homogeneity. Magnetic field homogeneity is usually expressed in units of ppm relative to the main field over a certain distance. High homogeneity means the magnetic field changes very little over the specified region or volume. The protons in this region resonate at the same frequency in a coherent manner and thus induce the maximum possible signal. Great effort is taken during magnet manufacturing and installation to ensure the best homogeneity possible. However, manufacturing imperfections or site problems (e.g., nearby steel posts, asymmetrical metal arrangements) may produce significant field distortions. It is possible to analyze the distortions and characterize them by a mathematical shape of the field then a coil known as a shim coil is used to correct them. Main magnets are manufactured with magnetic shielding that can surround the magnet (passive shielding) or that can be generated by a second set of superconducting magnet windings surrounding the main field (active shielding). A strong magnetic field provides a better SNR and better resolution in both frequency spatial domains.

1.2.3   Shim coils

The primary requirements of the main magnet is that its field must be uniform. In most cases, the magnetic field is not uniform and for this reason "shim" coils are frequently employed. Shim coils are a set of coils built to produce a field that is polarized in the same direction as the main field of known spatial dependence. Therefore, if the main

magnet's non-uniformity is known, the shim coils can be set to carry gradients that cancel (using superposition) the inhomogeneous components of the main field. $\vec{B_0}$ inhomogeneities correction is better if it is done over a small volume, so when more than one slice is acquired it is possible to modify, for each slice acquisition, the field of the shimming coils to correct $\vec{B_0}$ inhomogeneities in that particular slice volume. The design of the shim coil may be passive in that the magnet structure holds pieces of metal (shim plates) or small magnets that correct the field distortions, or active in that there are loops of wire through a current passes and generate a field for correction. Both types of inhomogeneous correction may be used together. Passive shimming is generally performed at the time of magnet installation as a one-time event. Active shimming (also called electrical shimming) is usually performed on a regular basis during system maintenance.

1.2.4 Gradient coils

Three gradients are used, one each in the x, y, and z directions, to produce the orthogonal field variations required for imaging. They are all generated by the flow of electrical current through separate loops of wire mounted into a single form known as the gradient coil. Variations in gradient amplitude are produced by changes in the amount or direction of the current flow through the coil. There are four aspects that are important in assessing gradient system performance: maximum gradient strength, rise time or slew rate, duty cycle, and techniques for eddy current compensation. Gradient strength is measured in units of $mTm^{-1}ms^{-1}$, with typical maximum gradient strengths may be $30 - 40\ mTm^{-1}ms^{-1}$. These maximum gradient strengths allow thinner slices or smaller FOV to be obtained without changing other measurement parameters. Another quantity often used to describe maximum gradient amplitudes is the effective gradient amplitude G_{eff}. This is the vector sum of all three gradients.

The response of a gradient coil to the flow of current is not instantaneous. Gradient pulses

require a finite time known as the rise time to achieve their final value. This rise time can be $0.2\text{--}0.5ms$, which defines a rate of change or slew rate for a gradient pulse. High-performance amplifiers allow shorter rise times (faster slew rates), enabling shorter gradient pulse durations and/or interpulse delays within a pulse sequence. The duty cycle of the gradient amplifier is another important measure of gradient performance. The duty cycle determines how fast the amplifier can respond to the demands of a pulse sequence. Large duty cycles allow high-amplitude gradient pulses to be used with very short interpulse delays.

Another complication of gradient pulses are the eddy currents. Eddy cur- rents are electric fields produced in a conductive medium by a time-varying magnetic field. In MRI systems, eddy currents are typically induced by the ramping gradient pulse in the body coil located inside the gradient coil and the cryoshield (the innermost portion of the magnet cryostat) outside the coil. These currents generate a magnetic field that opposes and distorts the original gradient pulse. Two approaches are commonly used for compensation. One method pre-distorts the gradient pulse so that the field variation inside the magnet is the desired one. This pre-distortion may be done via hardware or software. A second approach uses a second set of coil windings surrounding the main gradient coil. This approach is called an actively shielded gradient coil, analogous to the actively shielded magnet described previously. The current flow through the shield coil reduces the induced eddy currents. Typical scanners use both methods of eddy current compensation.

1.2.5   Exciting Signal Generation

The radio frequency transmitter system is responsible for generating and broadcasting the RF pulses used to excite the protons. The RF transmitter contains four main components: a frequency synthesizer, the digital envelope of RF frequencies, a high-power amplifier, and a coil or antenna. Each RF pulse must have both a frequency and a phase defined. The frequency synthesizer produces the center or carrier frequency for

the RF pulse, the master clock for the measurement hardware during the scan and also controls the relative phase of the RF pulse.

The RF envelope is stored as a discrete envelope or function containing a range or bandwidth of frequencies. It is mixed with the carrier frequency prior to amplification to produce an amplitude- or phase-modulated pulse centered at the desired frequency.

The RF power amplifier is responsible for producing sufficient power from the frequency synthesizer signal to excite the protons. The amplifier may be solid state or a tube type. Typical RF amplifiers for MR scanners are rated at $2 - 30\ kW$ of output power. The actual amount of power required from the amplifier to rotate the protons from equilibrium depends on the field strength, coil transmission efficiency, transmitter pulse duration, and desired excitation angle.

The final component of the RF system is the transmitter coil. Although transmitter coils can be made of any size and shape they must designed to generate an effective $\vec{B_1}$ field perpendicular to $\vec{B_0}$.

Another feature that transmitter coils must have, is to produce uniform RF excitation over a desired volume. This volume can be defined within the coil like the space where all protons experience the same amount of RF energy.

1.2.6 RF Coils

Radio frequency coils, also known as RF resonators and RF probes, are key components in a magnetic resonance imager. They are called RF coils because they resonate at a specific radio frequency. In particular RF coils create the $\vec{B_1}$ field which rotates the net magnetization in a pulse sequence. They also detect the transverse magnetization when it precesses in the xy plane. RF coils can be divided into three general categories: transmit and receive coils, receive only coils, and transmit only coils. An imaging coil must resonate, or efficiently store energy, at the Larmor frequency. All imaging coils are composed of an inductor, or inductive elements, and a set of capacitive elements. The resonant

frequency, of an RF coil is determined by the inductance (L) and capacitance (C) of the circuit. Some coils are adjusted or tuned to the patient to achieve the maximum efficiency in RF transmission.

Transmitting Coils

Two types of coil polarity are used: linear polarized and circularly polarized (also called quadrature coils). In an linear polarized system, a single coil system is present and the RF pulse is broadcast as a plane wave. A plane wave has two circularly rotating components, rotating in opposite directions at the same frequency f_0. For the MR purpose, only the component rotating in the same direction as the protons induces resonance. The other component is absorbed by the patient as heat. For this reason two circularly polarized coils can be used. In a circularly polarized transmitting system, two coils are present, one rotated $90°$ from the other. Phase shifted RF pulses are broadcast through each coil. A 40% improvement in efficiency from the transmitter system is achieved for a circularly polarized system compared to an equivalent linear polarized system for the same proton rotation. Transmitting coils must generate a very uniform magnetic field. Any inhomogeneity will introduce a distortion in the images.

Receiving Coils

For large-volume studies such as body or head imaging, the transmitter coil often serves as the receiver coil. For smaller-volume studies, receive-only surface coils are usually used. These coils are small, usually ring-shaped, have high sensitivity but limited penetration, and are used to examine anatomy near the surface of the patient's body. Phased-array coils use two or more smaller surface coils to cover a larger area. The small coils are configured so that there is minimal interference between them. There are some problem to consider. Usually a receiving coil is connect directly to an high gain, low noise amplifier, so if we want to transmit the maximum power from the coil to the

amplifier we need to match the impedance of the coil with the input impedance of the amplifier, but, as we will see in the next sub-chapter the amplifier has an minimum in its noise figure if it sees at the input an impedance that usually is different from the impedance needed to satisfy the matching condition. So, the designer must choose if to transmit the maximum power of if to have a low noise amplifier. To complicate this tradeoff, in an array coil system, there is the problem due to the signal coupling between close coil. To have a low coupling between the coils, the impedance that each coil sees at its output end should be enough high to avoid the current to flow. For this reasons often the receiving coils are connected directly to a high gain, low noise amplifier with an high input impedance. As the same like in the transmitting system, in the receiving system a quadrature detector can be used. The quadrature detector is a device which separates the M_x and M_y signals from the signal detected at the output of the RF coil. The heart of a quadrature detector is a device called a doubly balanced mixer (DBM). The doubly balanced mixer has two inputs and one output. The quadrature detector typically contains two doubly balanced mixers, two filters, two amplifiers, and a $\pi/2$ phase shifter. When a RF coil is used as both a receiver and transmitter is then usually called a transceiver coil. Since a RF coil can be used for both reception and transmission of a MR signal, and to gain insight of the parameters involved in the design on a RF coil, the Principle of Reciprocity might be invoked. This principle allows us to calculate the induced voltage and to deduce the field produced by resonant circuit at any point. MRI coils can also be divided in two major groups: volume coils and surface coils.

Volume Coils

Some of them are: Helmholtz coil, saddle coil, high-pass and low-pass birdcage coils and TEM resonator coils. The birdcage coil has become the most widely used since is able to produce a very uniform $\vec{B_1}$ field over large volume in the coil. A different type of coil has been recently introduced to meet the needs of the so called parallel imaging. This Kind of imaging sequence is able to parallel acquire signals coming from different coil elements to speed up the acquisition process [32]. This imaging scheme is based on the

coil sensitivity and it is denominated the SENSitivity Encoding technique (SENSE).

Figure 1.5: Example of volume coil provides high signal-to-noise ratio and a high RF homogeneity over the volume of interest (Bruker BioSpin, http://www.bruker-biospin.com/rf_coils.html)

Surface Coils

Surface coils have become an important tool to produce high quality images and spectra in Magnetic Resonance Imaging and Spectroscopy. The idea of using a surface coil is intuitively attractive because, as is well known, the closest the coil is to the object being imaged, the more signal is expected. It is well known that surface antennae can produce a high SNR but poor uniformity. Therefore, an optimal design of a MRI coil should be able to generate a good homogeneity of the field and high penetration capacity (good SNR). Unfortunately, spatial uniformity and high-efficiency cannot be optimized simultaneously. Increasing the homogeneity will increase the required power and decrease the SNR[32].

Figure 1.6: Example of a surface coils that offers a wider selection of positioning options and It enables the examination of joints in stretched or bent positions (Noras MRI products, http://www.noras.de)

1.2.7   T/R Switch

If a transmit and receive coil is used, a device called T/R switch must be used too. When we transmit a RF pulse to excite the protons, we want this power to be coupled into the coil and we do not want to lose power through the receiving system that, in addition, it could be damaged because the power we send is very high.

A T/R switch has two working state, the transmitting mode and receiving mode. When it is working in the transmitting mode it avoids that the exciting RF pulse flows through the receiving system, when it is working in the receiving mode it lets the signal from the protons flows to the scanner but not to the RF generator.

A simple T/R switch can be made of a few electronic components such as PIN diode and a $\lambda/4$ line (that can be implemented with an inductor and some capacitors). To switch from the transmitting state to the receiving state there is an high voltage signal coming from the scanner that change the bias of the PIN diodes. The main feature that a T/R switch must have it is a great isolation. A PIN diode is a diode that acts with a reverse bias as a low capacitance that stops the RF signal. With a forward bias a typical PIN diode will

have an RF resistance of about 1Ω, making it a good RF conductor. The PIN diode makes a good and fast RF switch.

1.2.8   Signal Acquisition

The data acquisition system is responsible for measuring the signals from the protons and digitizing them for later postprocessing.

The signals produced by the protons are usually $nV - \mu V$ in amplitude and MHz frequency. In order to process them, amplification is required, which is usually performed in several stages. The initial amplification is performed using a low-noise, high-gain preamplifier located inside the magnet room or built into the coil itself. This signal is further amplified, and then attenuated. The attenuator used is a variable attenuator that permit to the level of the signal to digitalize to fit the input amplitude range of the ADC converter. ADCs digitalize each analog signal at a rate determined by the sampling time t_C. It is important that the input signal amplitude fits exactly the input voltage range of the ADC. If the input signal is higher than the maximum signal that the ADC can convert the signal is clipped and if the maximum input signal is too low compared with the maximum signal that the ADC can convert, resolution is decreased.

When the desired signal amplitude is reached the signal is demodulated to a lower frequency, filtered and afterward digitalized with ADCs (Analog to Digital Converters). Due to the fact that the input signal has a limited bandwidth centered at the Larmour frequency f_0, it is possible to undersample this signal whit a sampling frequency $f_c < f_0$ where $f_c = 1/t_c$. The result of this operation represents the input signal sampled and demodulated to an intermediate frequency f_c. Care must be taken when the sampling frequency f_c is chosen because it must be below the Nyquist frequency to avoid signal aliasing. The spectrum of a sampled signal is the infinite sum of the shifted spectrum of the original signal (see Figure 1.4). The shift is equal to f_c, so for a limited bandwidth signal if f_c is lower than the central signal frequency, f_0, demodulation is done.
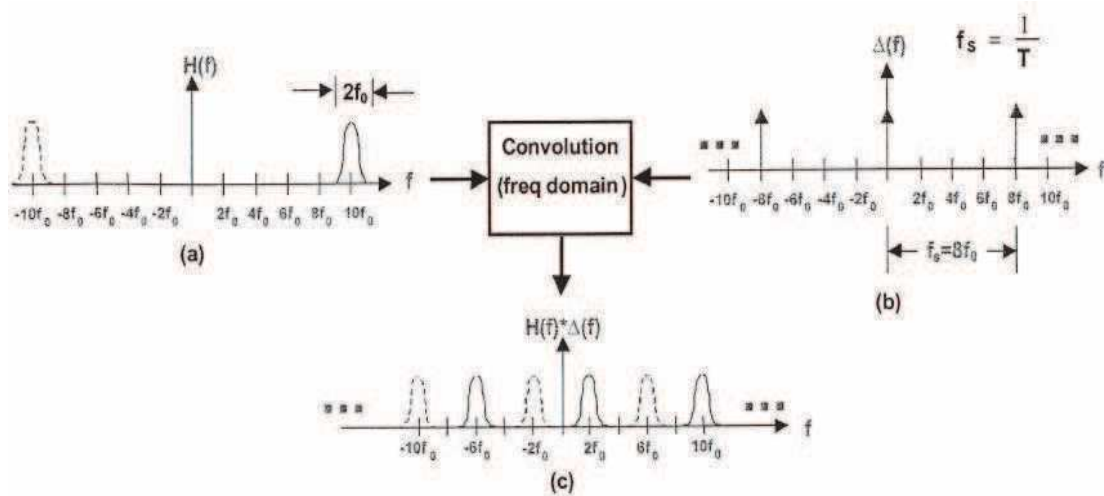
Figure 1.4: ADC undersampling: sampling the input signal means to compute the convolution of the fourier transform of the signal to sample (a) with the signal in (b). The result in (c) is the fourier transform of the ADC output signal. Notice that because $f_c < f_0 - \Delta f$ there is no aliasing.

The digital signal can be now filtered, demodulated to audio range in a digital way. Also quadrature and Fourier transform can be performed digitally. We saw that demodulation and digitalization can be performed in a single step and that is what is normally done in an MRI system. However, for high field system (for example for 7T system), where the signal is too fast to be directly digitalized, the signal is analog demodulated, than filtered with bandpass filters and finally digitized using analog-to-digital converters (ADCs). Digitalization allows better signal transmission and manipulation com- pared to the analog ones and allows data to be easily stored. Typically array coils have a separate preamplifier and ADC for each coil in the array. Usually 14 bit ADC are used and the dynamic range of the receiver chain is limited almost entirely by the effects of the digitization.

1.3   RF Coil Matching Network

As is now well known, the NMR resonance phenomenon can be excited within a sample object, such as a human patient, positioned in a polarizing magnetic field, by irradiating the object with RF energy at the Larmor frequency. In medical diagnostic applications, this is typically accomplished by positioning the patient to be examined in an RF coil with an RF power amplifier. Upon cessation of the RF excitation, the same or a different RF coil and a RF preamplifier are used to receive the NMR signal emanating from the patient volume lying within the field of the RF coil. The NMR signal is usually observed in the presence of linear magnetic field gradients used to encode spatial information into the signal. In the course of a complete NMR scan, a plurality of NMR signals are typically observed. The signals are then used to derive NMR imaging or spectroscopic information about the object studied. To ensure maximum power transfer between the RF power amplifier and the RF coil, as well as between the coil and the NMR receiver preamplifier, the coil input impedance must match the amplifier output impedance and the preamplifier input impedance. Additionally, the RF coil impedance must match the characteristic impedance of the transmission line coupling the RF coil to either the RF power amplifier or the preamplifier. This can be achieved by using different kind of RF coil matching networks.

From the past to nowadays several techniques were used to faces this problem. The first technique used was an adjustable impedance matching networks. A problem which arises with conventional NMR RF coil matching networks is that such circuits are dependent for proper operation of the quality factor, Q, of the coil which is subject to change with the size of the object in it. Thus, a large person (e.g. one weighing over 220 pounds) will lower the Q of the coil much more than a smaller person. A lower value of Q generally results in an impedance mismatch because a drop in the value of Q results in a concomitant reduction in the input impedance of the coil. To regain optimum input impedance, conventional matching networks require either electrical connections to be moved, capacitor values substituted, or variable capacitors or inductors to be adjusted. However, the substitution of components having discrete value or the movement of electrical connection may permit only a finite number of NMR RF coil loads to be impedance matched. Equally undesirable is the use of adjustable

capacitive and inductive elements near the bore of NMR magnet due to their affect on the homogeneity of magnetic fields. It is therefore that *Patrick L. Jaskolski in 1987,* invented an NMR RF coil impedance matching device which overcomes the shortcomings of the conventional device as discussed hereinabove [14]. The invention is based in an NMR scanner apparatus includes an RF coil for transmitting and receiving radio frequency signals. When the coil is operated in the transmitting mode, it is coupled to a source of RF energy. In the receiving mode, the RF coupled to a radio frequency receiver. A matching coil is provided for coupling the NMR RF coil to the source of RF energy and to the receiver using mutual inductance. To this end, in operation, the matching coil is disposed in the magnetic flux field of the RF coil. On this way, as it possible to see in Fig. 1.5, the change in the quality factor Q therefore results in a change in the input impedance, Z_{in}, seen by the RF power source resulting in an impedance mismatch and Z_{in}, can be adjusted by varying the coupling between the matching coil inductance and the NMR RF coil inductance.
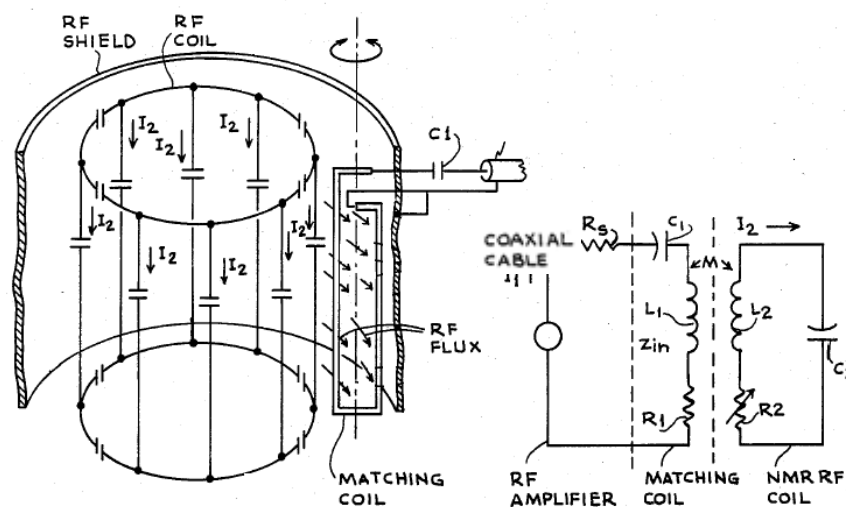
Figure 1.5: NMR RF coil impedance matching device utilizing variable mutual inductance

Two years later *William H. Harrison* invented a new MRI system having a remote tunable impedance matching network used to remotely adjust the input impedance of an RF coil to the 50 ohms (or other) impedance of a transmission line and other remotely located RF

equipment. The RF coil requiring tuning typically is housed within a static magnet and gradient coil structure where its load impedance may vary considerably (it depends upon the size and composition of the object being imaged which is inherently coupled to the RF coil). the technique necessarily must transmit RF signals of predetermined frequency. Typically exciting pulses of RF energy of a specified frequency are transmitted via an RF coil structure into an object to be imaged and, a short time later, radio frequency NMR responses are received by the same or similar RF structure. As is already understood in the art, one significant limiting factor on the quality of such images is the attainable SNR of the RF responses which must be detected and processed [15]. The signal level is enhanced and raised above the noise floor by the use of resonant circuits in the RF coil assembly that is used to transmit and/or receive the RF energy. This invention (Fig.1.6) includes a transmission line between the MRI processing circuits and the RF coil assembly or "applicator" which must necessarily be remotely housed within the cryogenic magnet and magnetic gradient coils. the SNR is optimized when the RF coil/applicator is resonated so that the impedance looking into the coil/applicator is "matched" or made equal (50 ohms) to the transmission line impedance that connects it to the processing equipment. The load impedance seen by the coil/applicator will vary considerably depending upon the mass and composition of the material being imaged. In the past, optimum performance (best SNR) was obtained by making an inconvenient internal impedance adjustment to the RF coil each time a new object was to be imaged. This new tuning device requires only two controls, and which remotely corrects the undesired impedance variation (any phase angle of predetermined magnitude) [21].
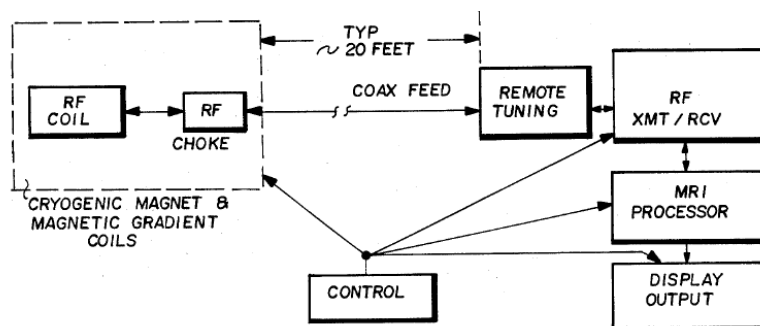

Figure 1.6: It is a schematic block diagram of an MRI system utilizing the remote tuning network

1.3.1   Automatic RF Matching Network with probes of fixed shape

In many NMR experiments, time is of the essence, and this is particularly true in certain biological and medical applications. Now, it is clear that one of the essential prerequisites of a successful experiment is correct tuning and matching of the probe so that it presents an impedance of typically 50 ohms resistive. Depending on the probe design being used, this can take a considerable time-as long as a minute. Further, if the tuning and matching change during the course of an experiment, for example by the sample's conductivity and/or size changing, an extra complication is introduced that may need to be resolved as quickly as possible. In helping to design an imaging system for use during neurological operations, *F. Hwang, D. I. Hoult in 1998* have been confronted with the need for reliable probe tuning and matching in the shortest time possible. During a short break in the operating procedure, a split probe is placed about the patient's head, a 1.5-T magnet moves quickly down the operating theater into position about the patient, imaging and angiography are performed, and then the magnet retreats, after which half the probe is removed and the surgery proceeds on the basis of the fresh images. In this situation, where the probe is dismantled, reassembled, and generally maltreated, a reliable and rapid automatic tuning and matching system is required, but this system has several difficulties in the design and implementation [16]. However it is not restricted to one particular application, but is pertinent to the whole NMR discipline. Very little has been published previously on this topic. If a change in, or of, the sample alters the probe Q factor by no more than a factor of, say, ± 3 during the course of an experiment, or indeed from experiment to experiment, use of a preamplifier of *excellent* noise figure can allow a *good* noise figure to be obtained over a prescribed loading range without change of matching. This strategy, and related techniques for quadrature coils, is described by *Sorgenfrei and Edelstein (1996)* and is helpful if the small loss of sensitivity can be tolerated; for example, in imaging experiments. With a transmit/receive probe, if the variation of transmitter flip angle inherent in this method is acceptable (up to roughly 20% above and beyond the variation one would expect by re-matching), only the tuning then needs to be adjusted. In this regard, a patent by *Sugiura (1986)* describes the use of the NMR signal's amplitude as an indication of probe detuning. A suitable correction voltage is then applied to a "varicap"

diode. Of course, such a probe cannot be used for transmission, and various manufacturers of commercial equipment have devised means for varying tuning capacitors remotely so as to overcome this difficulty. A patent by *Haragashira (1989)* attempts to deal with automatic correction of both tuning and matching. The impedance of the probe is assessed by detecting repeatedly the amplitude and phase of the standing wave on the probe's cable during low power transmission. The directions of change in the tuning and matching necessary to bring the impedance to 50 ohms are then calculated, and the tuning and matching capacitors repeatedly adjusted, with the aid of computer controlled motors, until the desired impedance is obtained. This method is computationally intensive and suffers from several drawbacks. Using the particular probe design specified in the patent, the stability of correction is questionable, and the inventor admits that, in some circumstances, the algorithm used may not converge to the right answer. Making accurate standing wave measurements at frequencies above about **100** MHz is difficult as the perturbation to the cable continuity caused by the presence of detection diodes and their capacitance then becomes important. Further, the method limits the length of the cable from the probe to the standing wave detector to multiples of a half wavelength. *Hwang and Hoult* were intrigued as to why automatic tuning and matching was not available in the NMR community in general (although their application was medical, their interests also cover traditional high resolution spectroscopy), and therefore they embarked on a program to understand the difficulties and to try to produce an autonomous device that was not dependent on "real time" computations. They first examined in more detail the traditional manual method of tuning and matching with a bridge and showed that the main problem lies with the choice of probe circuitry. Assuming that the tuning and matching can be adjusted electrically (for example, with motors), they then extended the bridge method to create, with the aid of the NMR receiver, two analogue negative feedback servo-loops that control tuning and matching and adjust them swiftly and correctly. Finally, they took into account those readers who had digital receivers and described how the method can easily be extended to cover their needs.
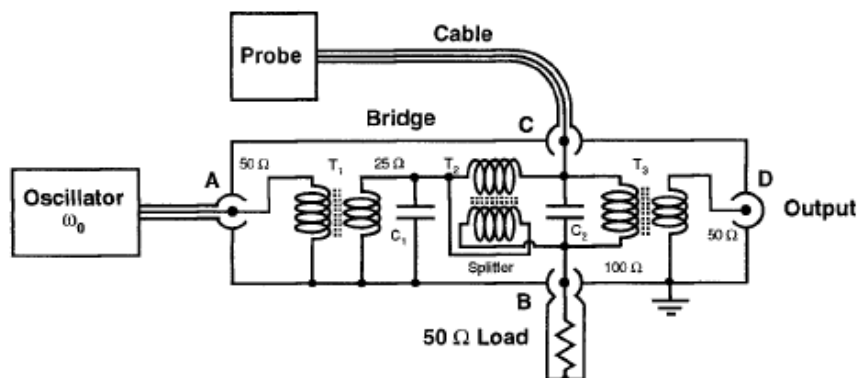
Figure 1.7: A simple four port, 50 ohms bridge. When the loads on ports **B** and C are equal, there is no output at port *D*. Each transformer is tuned with an appropriate capacitance to remove residual reactance. The capacitances for transformers T_2, and T_3 are combined as capacitor C_2.

So the main problem in the design of any automatic tuning and matching device is the lack of orthogonality of the two probe adjustments, and that the use of an inductively coupled probe with a tuned matching coil resolves the difficulty. The complex amplitude of the output from a simple four-port bridge then accurately reflects small errors in matching and tuning, whereas quadrature phase-sensitive detection delivers that amplitude as two error signals. An additional difficulty is that the phase of the complex error signal depends on cable length. Thus *variable* phase-sensitive detection is required if an arbitrary cable length from the probe to the detection bridge is needed. In this regard, the use of the NMR spectrometer is the obvious way of getting round the problem. However, recognizing that some users may not be able to vary the phase of the NMR receiver, provision has been included in the final design for manual adjustment of phase. In some instruments, it is impossible to turn on the receiver while also having available a signal at the Larmor frequency for the bridge. There is then no option but to employ the instrument with a separate detector that mimics a spectrometer output. This is the bridge of Fig. 1.7 plus a simple base band *I-Q* demodulator, or less optimally, a standing wave detector. However, such a detector's dynamic range is limited, its orthogonality is highly frequency-dependent and it is difficult to make at ultra-high frequencies.

1.3.2   Automatic RF Matching Network with probes of flexible shape

There are many examples of pioneering work in interventional MRI over the last 15 years. These include great strides in prostate imaging using endorectal coils, high-resolution imaging of arterial plaque using receiver coils within arteries or nearby veins, and catheter visualization for MR-guided surgery. Other researchers have developed endourethral, transesophageal, and even stent-based imaging techniques. However, in these interventional techniques the probe tuning is usually accomplished with fixed elements or is performed manually at the end of a length of coaxial cable (or both). Early work in MR emphasized the fundamental importance of probe integrity (tuning and matching) in achieving a high signal-to-noise ratio (SNR). Several investigators have examined and identified the key tradeoffs for the remote tuning and matching of probes with respect to image quality. Tuning is necessary, but it is time-consuming and difficult. Indeed, coil designers often advocate the use of probes of fixed shape to avoid the problem of tuning and matching. However, interventional environments are seldom static, and relaxing the constraints of fixed or repeatable probe shapes can address various clinical difficulties with interventional probes. Hence, investigators have worked on schemes that either require no tuning or automatically tune the probe once it is in place. Ocali and Atalar developed a "loopless" catheter coil that acts as a whip antenna within the body. It has a distributed nature, so its tuning and matching are insensitive to changes in shape, and it is capable of imaging with high SNR over the long extent of a vessel. However, its radial reception profile is somewhat limited, which makes it most appropriate for imaging long thin structures or for tracking. Automatic probe tuning has been addressed in many contexts outside of MR, including devices for tuning and matching radio antennas. These methods usually involve switched tuning elements, which are not suitable for MRI because they use motors to adjust component values. The constraints of using an inductive probe at the end of a lossy transmission line, and within the magnetic interference- sensitive environment of an MRI scanner, make this task more difficult. Hwang and Hoult argued strongly for the use of an inductively coupled MR probe, and described a robust closed-loop feedback system for tuning and matching such a probe. While their method successfully orthogonalizes "tuning" and "matching," it is mechanically impractical to use mutual inductance as a remotely-tunable

variable for many interventional applications. Early work with receive-only surface coils introduced varactor-diodes as voltage-controlled tuning elements. Hirata used varactor-diodes to design a closed-loop automatic tuning and matching circuit for a flexible EPR surface resonator. Rousseau developed a microcontroller-based automatic tuning scheme for MRI with varactor-diodes. However, their device measures the power received in a flexible coil using an external transmitter and tunes the coil according to a precomputed heuristic algorithm. The procedure takes about 1 min to complete, and it involves physically disconnecting the coil from the scanner. While this scheme could work interventionally, Venook and Hargreaves's study proposes an entirely new circuitry (Fig. 1.8) that can tune a device in line with the scanner in under 1 s at the touch of a button.
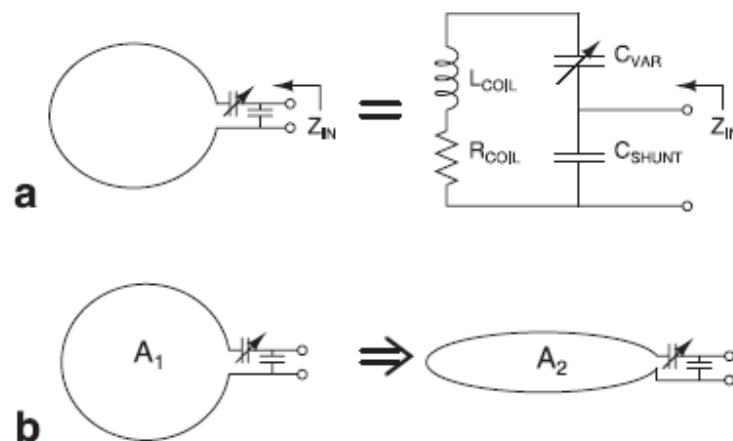
Figure 1.8: a: Probe topology, lumped-element equivalent circuit. **b:** Change in the probe area and inductance with change in the probe shape.

Interventional MRI presents the new challenges of a dynamic sample environment, coil topology constraints, and the need for miniaturization. Previous approaches to coil tuning address some, but not all, of these challenges. In this work, well explained by Fig. 1.9 they presented an efficient method for automatic varactor tuning of a flexible interventional RF receiver coil and they demonstrate the SNR benefit of imaging with a small interarticular coil in a cadaveric porcine knee as compared to a surface coil. They believed the probes must be

flexible to be safe and effective. Because this flexibility makes probes susceptible to centerfrequency shifts, automatic tuning devices such as the one presented here could maximize the clinical benefits of interventional MR procedures.
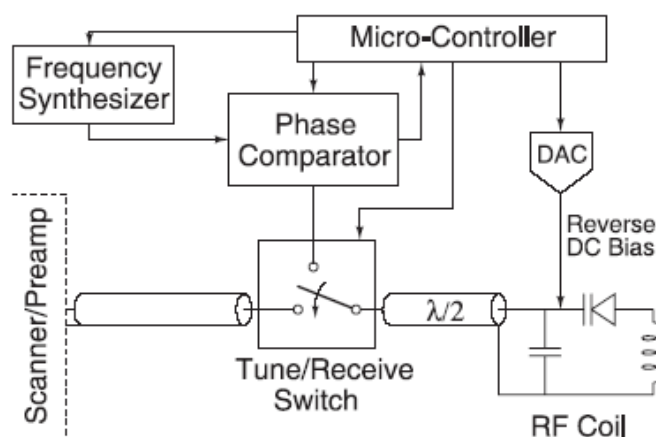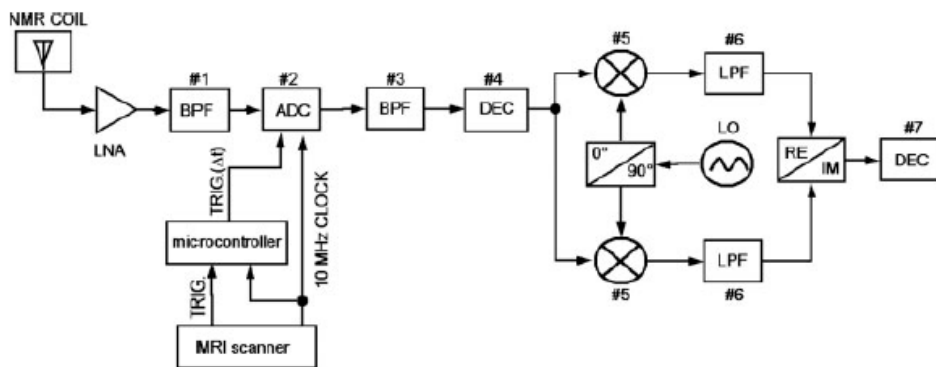

Figure 1.9 Block diagram of autotuning circuitry. The microcontroller enables the frequency synthesizer and sets it to oscillate at the Larmor frequency, measures the voltage output from the phase comparator, sets the RF coil's center frequency via a DAC, and operates the tune/receive switch.

1.3.3 Digital Multiband Receiver

In recent years, parallel-phased array signal detection methods in combination with high duty cycle and high signal bandwidth applications have set new requirement for MR receiver systems in terms of number of independent RF receiver channels and digital postprocessing speed. Modern, clinical MRI systems are typically based on scalable receiver architectures with up to 128 independent receivers, each capable of 16-bit digitization at an acquisition bandwidth of 1 MHz. Such receiver systems are highly optimized for high-speed data acquisition and postprocessing at a single Larmor frequency band only. As a result, they show limited flexibility for applications with extended acquisition lengths and detection bandwidths in comparison to standard MRI. Relevant examples, where more flexible receiver systems would be advantageous, include magnetic field monitoring (MFM), for example, to accurately

measure k-space encoding simultaneous to 1H data acquisition by using non proton NMR probe magnetic field sensors, and interleaved multinuclear spectroscopy applications. *In 2009 Sipilä and Schulte* has described a scalable, multichannel, multi-frequency NMR receiver system based on off-theshelf components. The receiver has been designed to act as a flexible add-on toolkit, and can be synchronized with a clinical MRI scanner for parallel operations. In traditional heterodyne type MR receivers, the RF signal gets digitized after down-conversion. In addition to relaxing analog-to-digital conversion (ADC) requirements, the analog demodulation step provides phase-coherent acquisition (aka. phaselocking). In contrast to this, this approach is based on high-speed direct sampling and subsequent digital signal processing (DSP). Accordingly, changing between the different Larmor frequency bands is not any more dependent on appropriate analog demodulation, and thereby increases the system flexibility for multinuclear acquisition purposes. Because of the high-bandwidth direct-sampling scheme, multiple signals can be detected simultaneously as long as the corresponding frequency bands do not overlap. Thus, high sampling rate receivers can be conveniently applied for simultaneous multi-nuclei MR detection. In addition, the MR data acquisition can be accompanied with simultaneous acquisitions of other signals, such as ECG (electrocardiography) or EEG (electroencephalography). On the negative sides, the resulting larger raw data volumes lead to an increased workload for the subsequent DSP. This can become time wise limiting in certain high duty cycle data acquisitions [17]-[18].


Figure 1.10: Block diagram of the implemented IQ-detection based on direct-sampling and digital direct-conversion topologies. The timing circuitry required for the operation is accordingly shown. TRIG and TRIG (Δt) corresponds system, ''start sequence'' trigger, and the delayed one, respectively. BPF, LPF, and DEC stand for band-pass filter, low-pass filter, and decimation, respectively.

Time is not the only limiting factor that can affect this invention, but also the Noise from the preamplifiers (LNAs: low noise amplifiers) together with the thermal noise due to losses in patient and coil elements, that can determine the final signal-to-noise ratio (SNR) of the receive chain. A single LNA performs best, when the matched coil presents the so-called optimum noise impedance to the preamplifier. However, an array coil presents an impedance matrix to the LNAs which typically has non-diagonal elements due to element coupling. This leads to noise coupling and reduces the final SNR, if the noise matching is not corrected for the coupling. *Findeklee1 in 2009* found the way how the noise matching can be generalized for the case of array coils. This allows the coil designer to achieve true optimum SNR for a selected imaging region.

Figure 1.5.3.1 shows an equivalent circuit of a noisy single channel receiver chain. The coil is represented by the impedance Z_c, the noise voltage U_c and the signal voltage U_s. The noise figure F of an LNA can be defined as the ratio of SNR of the input signal in absence of LNA-noise to the SNR of the output signal including LNA-noise – with the thermal coil noise Whereby Z^H denotes the com $\overline{U_c U_c^H} = \sim(Z_c + Z_c^H).1$ the line over-expressions denotes the covariances of the noisy sources.
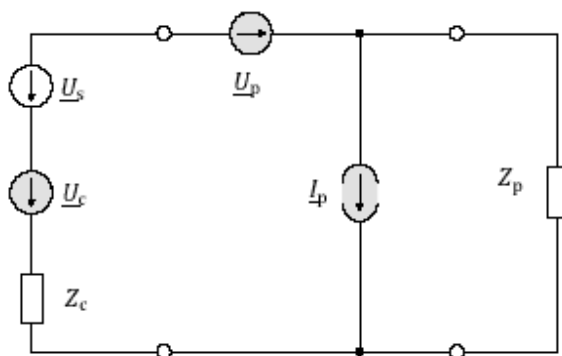
Figure 1.11: Noisy single channel chain

The noise figure is a function of the coil impedance Z_c but is not a function of the preamplifier input impedance Z_p. The optimum coil impedance $Z_{c,opt}$ for the lowest possible noise figure F_{opt} can be derived as:

$$Z_{c,opt} =: R_{c,opt} + jX_{c,opt} \quad , \quad \left| Z_{c,opt} \right| = \sqrt{\frac{\overline{U_p U_p^H}}{\overline{I_p I_p^H}}} \quad , \quad X_{c,opt} = \frac{\mathrm{imag}\,\overline{I_p U_p^H}}{\overline{I_p I_p^H}} \tag{1.1}$$

If the coil impedance $Z_c =: R_c + jX_c$ deviates from this optimum, the noise figure increases

$$F = F_{opt} + \frac{G_{I_p}}{R_c}\left| Z_c - Z_{c,opt} \right|^2 \tag{1.2}$$

(G_{Ip} denotes the thermal noisy conductance that generates the same noise as I_p) and the SNR at the LNA output can be expressed by:

$$SNR_{out} \sim \underline{U}_s^H \left(Z_c F_{opt} + F_{opt} Z_c^H + 2\left(Z_c - Z_{c,opt} \right) G_{I_p} \left(Z_c - Z_{c,opt} \right)^H \right)^{-1} \underline{U}_s. \tag{1.3}$$

Figure 1.12 shows a two-element array coil attached to two preamplifiers with $Z_p = \infty$.
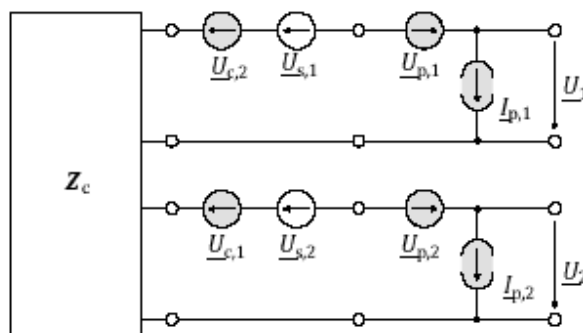
Figure 1.12: Noisy chain for two elements

The noise current source $I_{p,1}$ contributes with - $Z_{c;2,1} \cdot I_{p,1}$ in port 2 and vice versa (noise coupling). It can be shown that for the case of array coils the just derived SNR expression can be interpreted as a matrix equation, if the optimized combination, presented by Appelbaum (1986), Roemer (1990) and Pruessmann (1999) is used:

$$SNR_{out} \sim \overline{\boldsymbol{U}}_s^H \left(\boldsymbol{Z}_c [F_{opt}] + [F_{opt}] \boldsymbol{Z}_c^H + \left(\boldsymbol{Z}_c - [Z_{c,opt}] \right) \left[2G_{I_p} \right] \left(\boldsymbol{Z}_c - [Z_{c,opt}] \right)^H \right)^{-1} \overline{\boldsymbol{U}}_s \tag{1.4}$$

In this equation, the squared brackets have to be evaluated channel-wise forming diagonal matrices, and the parameters $Z_{c,opt}$ and G_{Ip} have to be interpreted as parameters of the single LNAs, including the matching circuits attached to the same. Z^H now denotes the transpose complex conjugate of Z. Using network theory, a similar expression can derived for a weighted combination of power $\tilde{P}$. In this function, the signal power received in each individual LNA impedance $Z_p = R_p + jX_p$ is divided by a corresponding real scalar Φ:

$$\tilde{P} \sim \underline{\mathbf{U}}_s{}^H \left(\mathbf{Z}_c[\Phi] + [\Phi]\mathbf{Z}_c{}^H + (\mathbf{Z}_c - [Z_p{}^H]) \left[\frac{\Phi}{2R_p}\right] (\mathbf{Z}_c - [Z_p{}^H])^H \right)^{-1} \underline{\mathbf{U}}_s \qquad (1.5)$$

It can be shown that for $[\Phi] := [F_{opt}]$, both of the above functions have the same optimum impedance $[Z_{c,opt}] = [Z_p{}^H]$, if $\mathbf{Z}_c[F_{opt}] + [F_{opt}]\mathbf{Z}_c{}^H$ is positive-semidefinite. This means, that the optimum matching condition in many realistic cases can be found by modifying the LNA inputs such that they present the complex conjugate of their own single channel optimum impedance, and provide a matching such that the weighted power sum – each channel power divided by the individual (adapted) gain and noise figure – at the LNA outputs is maximized. Afterwards, the LNA input modification is removed. If all LNAs have the same noise figure and the coil is reciprocal, this method of matching is equivalent to the method of using the active antenna impedance as proposed by *Maaskant in 2007*. In this proposed noise matching method the SNR was improved by more than 6% (without preamplifier decoupling). Simulations show that for multi element coils with decoupled nearest neighbors, but residual mutual couplings from more distant coil elements, an even greater improvement can be expected.

1.3.4   Mechanically Adjustable Coil Array

As we already know, MRI relies mainly on two types of radiofrequency (RF) coils: volume coils and surface coils. Most clinical systems are equipped with volume coils based on the birdcage principle that can serve for both RF transmission and reception. The main advantage of birdcage coils is their ability to generate highly homogeneous circularly polarized B1 fields,

which translate into equally homogeneous signal sensitivity in receive operation. One disadvantage of these coils is their fixed geometry. However, the most important drawback of single volume resonators is that they do not exploit the benefits of multiple-channel detection. The simultaneous use of multiple receiver coils was pioneered in the late 1980s. In these works, receiver arrays were used to enhance the signal-to-noise ratio (SNR) of MR data. In the late 1990s, parallel MRI introduced another use of receiver arrays by exploiting the diversity of individual receive sensitivities for spatial signal encoding. Both benefits of multiple-channel MR detection, that is, SNR gains and spatial encoding capability, are rooted in the fact that multiple receiver coils partly capture the inherent spatial diversity of the electromagnetic RF fields that emanate from the imaging target. Recent theoretical and experimental work suggests that to make optimal use of array detection a large number of small surface coils should closely surround the imaging volume. Surface coils offer great freedom with respect to their shape and geometric layout in an array. Most commonly, simple loop structures such as circles and rectangles are arranged such as to tile the region of interest. However, with large coil counts it is a challenge to achieve high performance, ease of handling, and patient comfort at the same time. For optimal SNR and encoding performance, the coil array needs to closely fit the anatomy of interest, which may vary significantly in shape and size for different subjects. One way of achieving this is to use freely configurable coil elements and form individually tailored arrangements. However, for large coil counts this is tedious to do in practice and requires cumbersome means of geometric fixation, which will often prove uncomfortable for the patient. Consequently, there is a need for integrated coil arrays that can be adjusted to individual anatomies in a simple and ergonomic manner. The mechanics of the geometric adjustment form one challenge in constructing such an array. However, geometric flexibility is demanding also with respect to electronic design. Patient-to-patient changes in array geometry will induce variations in the loading and mutual coupling of the coil elements. Given the goal of maximizing SNR performance, such variations require especially robust tuning, matching, and decoupling strategies. *Klaas Prüssmann*, in 2009, has introduced the concept of a geometrically adjustable array is explored for the specific task of wrist imaging. Exhibiting a large number of small, clinically relevant anatomical structures the wrist poses particularly high SNR requirements. These have been addressed with advanced rigid array

designs. However, even adult wrists vary up to 30% in circumference and thus promise significant benefits from size adjustment. Therefore, an adjustable eight-channel wrist array has been constructed, targeting proton MRI at 3 Tesla. The array accommodates individual wrist sizes by a simple sliding mechanism and was designed to ensure robust SNR performance in a wide range of loading and coupling conditions. The performance of the coil array was first studied in phantoms of various sizes and then demonstrated by wrist imaging in volunteers. The basic array geometry approximates the wrist as a truncated cone of variable diameter, entailing several advantages. Compared with rigid conventional wrist arrays, it covers a wider range of wrist sizes and offers more freedom for patient positioning because the hand can be placed in the coil at any rotation angle [19]. The additional flexibility necessary to accommodate individual deviations from the cone geometry is provided by flexible coil elements that passively adjust to the wrist surface. The geometrical adjustment is performed by a simple mechanism that closes the coil cone within seconds in a single operator move.
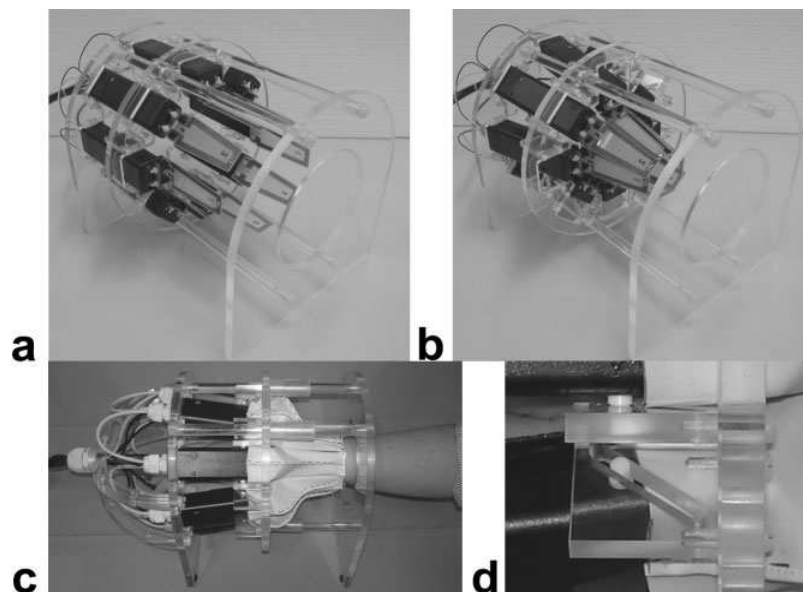
Figure 1.13: a,b: The assembled wrist array in open (a) and closed (b) state. To fit the array around an individual wrist the acrylic plate in the middle is shifted toward the subject. The flexible coil elements are pressed against the wrist by separate (transparent) sheets of polycarbonate. **c:** After padding with a thin layer of foam they were covered with easily cleanable biocompatible polymer material. The black boxes contain the matching and preamplifier electronics. **d:** The design details of the sliding cam mechanism. The white pin attached to the black box slides within the diagonal slot thus moving the coil element toward or away from the wrist.

A quantitative SNR study confirmed the sensitivity benefit of bringing the coil elements as close as possible to the individual sample. Geometrical flexibility inherently precludes inductive coil decoupling by precise mutual overlaps. Therefore, preamplifier decoupling has been used to limit coil-to-coil interaction. The remaining variable coupling among the coil elements and the variable loading lead to splitting and shifting of the primary coil resonances. These problems were successfully addressed by using a resonant π matching network that creates a robust frequency response plateau at the MR frequency.
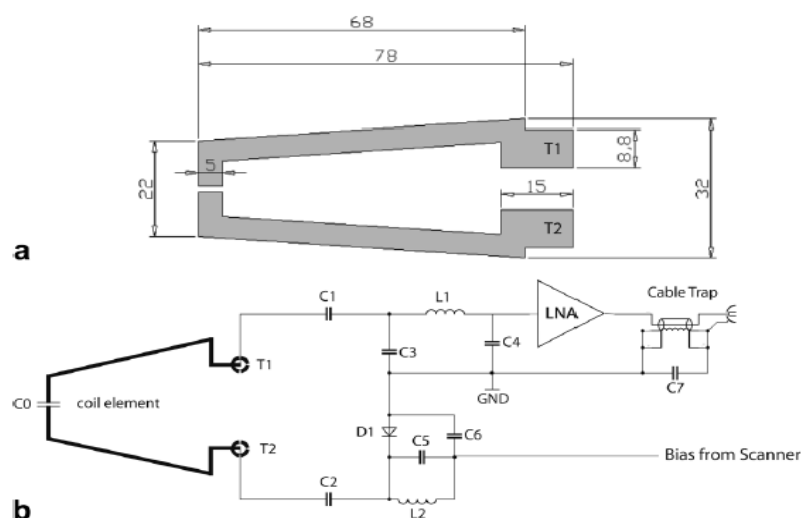
Figure 1.14: a: Dimensions of a single coil element in millimeters. The gap on the left is bridged by a capacitor and serves to limit the electrical length of the coil. The two terminals T1 and T2 on the right are connected to matching and preamplifier circuits. **b:** Schematic of the preamplifier board. The main components are the low-noise amplifier (LNA), the π matching network (C3, L1, and C4), the detuning trap (C5 and L2) and the coil element.

SNR measurements in phantoms and imaging of different sized wrists have confirmed these design considerations by revealing robust SNR performance over a wide range of loading and coupling conditions. Most importantly, the SNR was preserved in the critical center of the imaging volume, while strong coupling did take an SNR toll of up to 25% in the periphery. The robustness of the array performance is again confirmed by invariably high image quality

for all wrist sizes. High SNR yield is emphasized by the high resolution of these data as illustrated by the enlarged details (Figure 1.15). A range of small anatomical features that are not usually visible in MR images are readily discerned, including single fascicles of the median nerve, fine details of trabecular bone, and the inner structure of tendons.
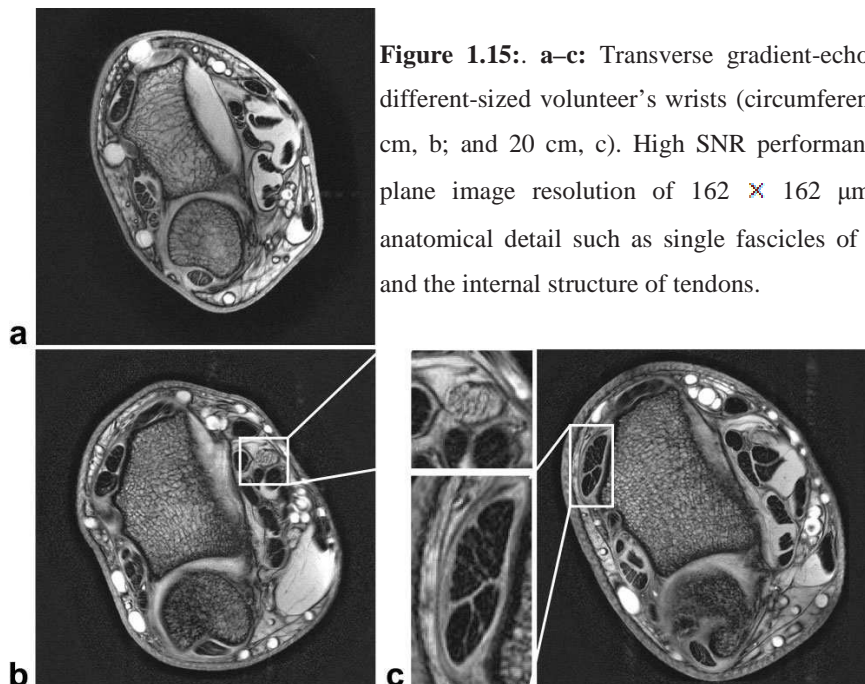
Figure 1.15:. **a–c:** Transverse gradient-echo images of three different-sized volunteer's wrists (circumference 15.5 cm, a; 18 cm, b; and 20 cm, c). High SNR performance enabled an in-plane image resolution of 162 $\times$ 162 μm^2, revealing fine anatomical detail such as single fascicles of the median nerve and the internal structure of tendons.

1.3.5   A Modular Automatic Matching Network System

So it is clear that a matching network is a very important device for MR signal detection. Since they are the first element in the chain between coils and the ADC (Analog to Digital Converter), their insertion loss cannot be compensate with preamplification and SNR is directly affected. A matching network that presents the wrong impedance at the input of the first low noise preamplifier can deteriorate substantially its noise figure (NF). To keep the coil matched to the impedance that gives the best noise figure of the preamplifier it is a challenge

when coil loading conditions are changing, when coils can be stretched to adapt to the anatomic region to be imaged; even more difficulties come whenever we have to consider coupling between different elements in a coil array. It would be unthinkable in a clinical setup to adjust manually matching and tuning of a coils array depending on different patients or different measurement. Pavan and Pruesmann in 2010 present a modular Automatic Matching Method (AMM) system that can be easily extended to match the output impedance of many different channels at the same time. An underlying point of this system is the capability of matching impedances to any desired point of the complex plane [20]-[21]. Remote impedance matching can be achieved through the use of a matching network made of varicaps (BB153 Philips), a varicap is a diode that changes its capacitance depending on its reverse bias voltage (in our case the range is 65.1-6.9 pF when the bias voltage is between 0 and 10 volts). The matching network we use is a PI matching network where the input and the output shunt capacitances are substitute with respectively two varicaps; another varicap is placed in series with the series inductance (37 nH) to have fully control of all the reactive elements of the matching network. The AMM system, (showed in Fig.1.16) consists of two main parts that are interfaced to an external PC through a microcontroller (PIC16F777, Microchip, with 14 analog to digital channels and internal oscillator clock). One main part of the system is the DAC (Digital to Analog Converter) module that is connected to the varciaps of the matching network and the second part is the RF circuitry capable of measuring the reflection coefficient seen by the preamplifier. A switch (controlled by the microcontroller) is determining whether the coil has to be connected to the reflection coefficient measurement circuit (since the characteristic impedance is set to 50 ohms, reflection coefficient measurement directly reflects the impedance we want to measure) or to the preamplifier of the MR reception chain. The switch is a SW-395 (*tyco electronics*) SPDT GaAs switch, insertion loss less than 0.5 dB, typical isolation 28dB, maximum switching time 5 µsec. Microcontroller and external PC are communicating to each other using a serial fiber optic connection (thought the use of a UM232 USB-Serial UART module, *ftdi chip*). The principle of operation is very simple, when the AMM system is in the idle mode the switch connects the output of the matching network to the preamplifier, the reflection coefficient circuit is isolated and the scanner can be used to image. Whenever we want to match any special impedance we have just to type it in the

external pc running MATLAB, this PC tells the microcontroller to isolate the scanner and connect to the matching network output the reflection coefficient measurement circuit, at this point a MATLAB script iteratively changes remotely the output voltage of the DAC (changing in this way the reactive elements of the matching network) and reads the corresponding new output impedance value until the desired impedance is reached. The DAC module is an AD5361 chip (*Analog Devices*), it has 16 channels and a resolution of 16 bit over the maximum range output voltage range +/- 10 V. Varicaps have to be only reverse biased, so half of the DAC voltage range cannot be used, this allows anyway to have 2^{15} different capacitance value over the range 6.9-65.1 pF and allows the matching network to reach 98304 different impedances almost all over the entire impedance complex plane. The DAC has already the capability of driving 5 different and independent matching networks but the chip itself modular and more AD5361 is can be connected together to extent the number of output channels. The major source of noise in the matching network is not actually *1/f* noise from the varicaps but very low frequency noise coming from the power modules of the DAC, the noise can be reduced with the use of big capacitance (50μF). The core of the reflection coefficient is an RF gain and phase detector chip (AD8302, *Analog Device*). A fixed reference signal (same frequency as proton frequency) is generated (only when the impedance measurement is performed, to avoid RF artifacts in the image) with a Voltage Controlled Oscillator (VCO), this reference is fed into a double hybrid (directivity better than 40dB) and thanks to isolation between different ports of the hybrid is possible to separate the forward and the reflected, those two waves are fed into the gain and phase detector that gives at the output two constant voltages, one proportional to the phase difference between the forward and the reflected wave and the other proportional to the ratio of the magnitude of the forward and reflected wave, no high speed digitizers are needed at all for reflection measurement. To have a very good directivity (this defines the sensitivity of the measurement to the reflection wave) they have chosen a tuned hybrid with the minimum number of reactive elements. The AD8302 chip is non linear when detecting phase differences close to zero and does not distinguish phases and differ to each other of 180°, these problems can be solved with a simple look up table for the linearization of its response function and with a variable delay line to detect whether two phases differ each other of 180° or not. Since the microcontroller has 14 ADC, 7 magnitude

and 7 phase information can be read at the same time. A typical impedance matching operation takes less than 3-4 minutes. This Automatic   Matching system has been implemented and tested in the 7 Tesla system. The advantage of this system is to be easily scalable to many independent channels suiting applications like receive array, notoriously hard to match due to elements coupling, mechanically adjustable coils and in general any coil that sees different load conditions. A good impedance measurement can be performed without high speed digitizers and impedances that minimize the noise figure of the preamplifier can be matched at any value of the complex plane. The matching network can work only for receive coils since high power could direct bias the varicaps, attention has to be paid to have a good linearization of the gain phase detection chip.
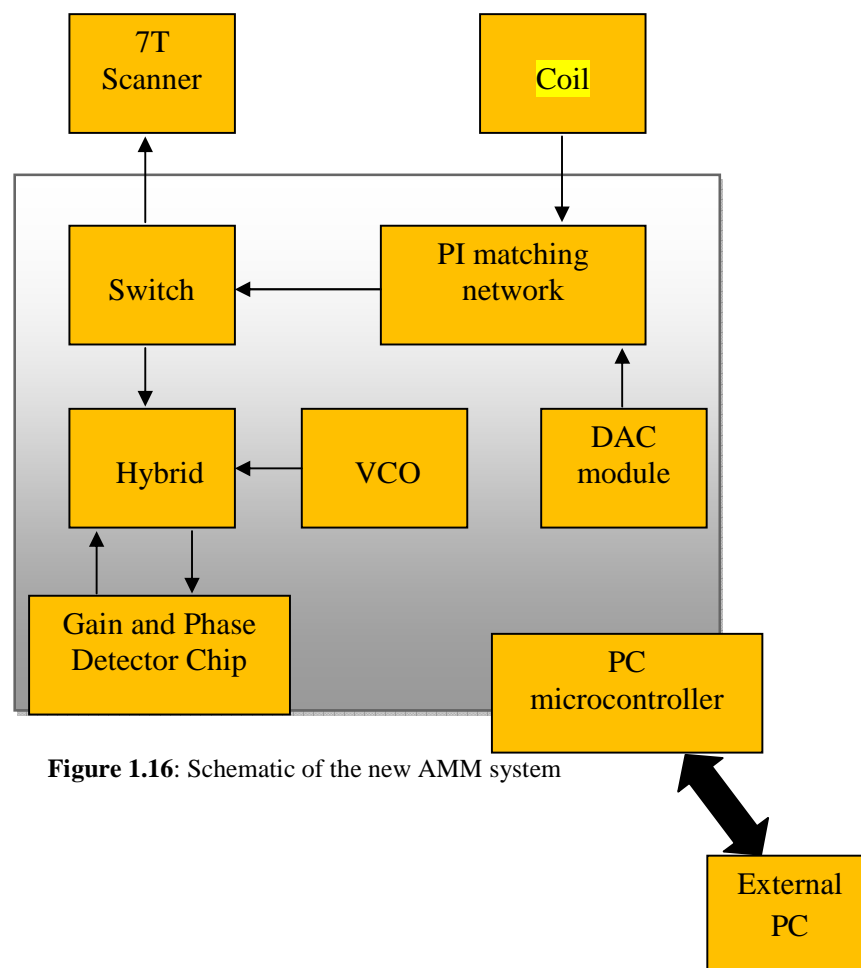
Figure 1.16: Schematic of the new AMM system

1.3.6   Scope of the Thesis

The Goal of this work is the improvement of the previous system used by Pavan through the creation and application of an innovative way to measure the respective impedance for the automatic matching network setup. In particular this new system permits to measure the forward wave and the reflected wave in an independent way, instead the chip used by the older system has to measure both waves at the same time as input and it gives two voltages as output. So in the AD8302 chip the computation of the impedance is dependent from an algorithm with both waves, instead in this new system the signal after the double hybrid (Directional Coupler) is divided in two different waves totally independent and they are used to compute directly from the signal the coefficients used to compute one specific impedance.

Another problem of the previous system implemented by Pavan is the non-linearity of the chip and for this reason it doesn't distinguish if the impedance can be summarized as inductance or capacitance (if it differs each other of a phase of 180°) in the Smith Chart (a specific graph used to show the different values of impedances). This new system instead can guarantee a good linearity of the measurements of the impedance and can differentiate the values of the impedance in all the Smith Chart without any kinds of problem in the phase differences.

Therefore with this innovative method to measure the impedance that belongs from the RF coil, it is possible to measure not only the reflection scattering parameters S11 and S22 that were computed even in the previous system, but also the transmission scattering parameters S12 and S21 (all these will be discussed and explained later) that are very important for a more precise calibration of the matching network and for the precise computation of the impedance to be matched.

So this new "Scattering-parameter measurement system for automatic matching network setup" includes the Directional Coupler connected with two Mixers and every Mixer receives one of the two waves (forward or reflection). Two external frequency generators provide the input signal, one for the Double Hybrid and the other one as the Local Oscillator (LO)for both Mixers. The two outputs of the Mixers are bandpass filtered and then through the PIC microcontroller are sampled and analyzed to obtain the values to compute with the external PC

the value of the impedance. Finally the new Modular Automatic Matching Network System can be summarized as it is possible to see in Fig.1.17.
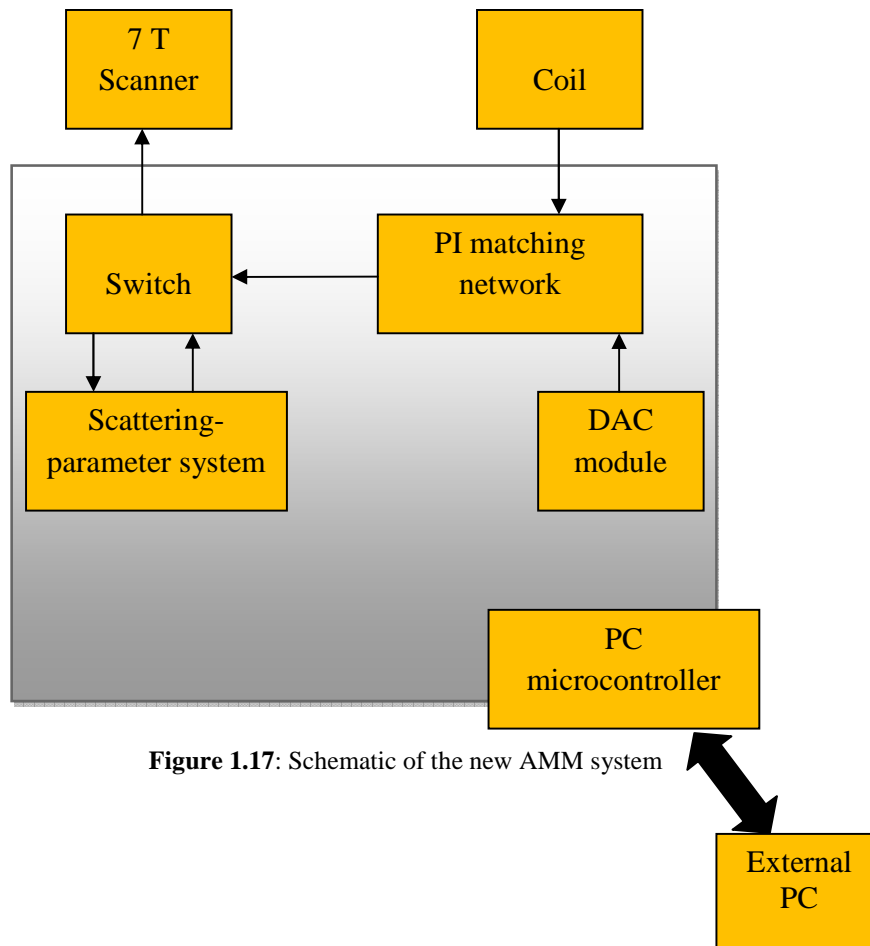

Figure 1.17: Schematic of the new AMM system

Chapter 2

Material and Methods:
Some Basic Concepts

Before to start to explain all the different steps used to develop the new Measurement Impedance System, it is necessary to explain and make it clears some basic concepts about the RF circuit, the differences between the electronic components at low frequency and at RF frequency and all the coefficients used to compute and show an impedance.

2.1   Radiofrequency Background

Radiofrequency (RF) is any frequency within the electromagnetic spectrum associated with radio wave propagation. Why are radiofrequencies different from lower frequencies?
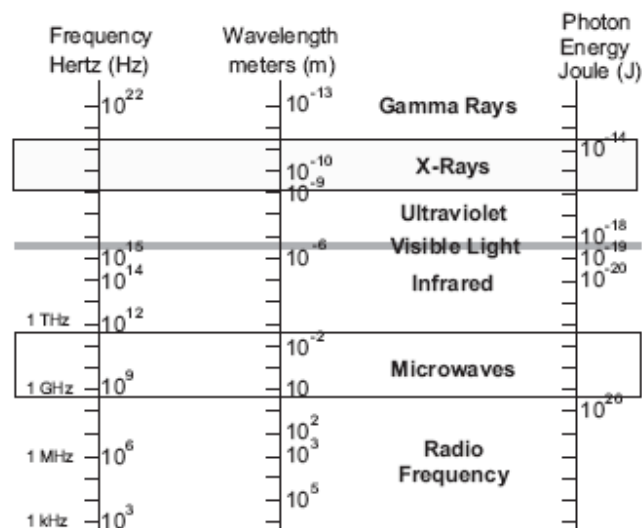
Figure 2.1: Electromagnetic spectrum

As the frequency increases and the associate wavelength of the electromagnetic wave becomes comparable with the dimension of the discrete circuit components, such as resistors, capacitors, inductances these components start to deviate to their ideal frequency response. At lower frequency the wavelength is large enough that there is insignificant phase variation across the dimension of a component but if the wavelength is on the same order of the dimensions of the component, the phase of a voltage or a current changes significantly over the physic extension of the device. In a transmission line, reflection could occur and this must be taken in account. Another difference is that in a conductor the radiofrequency does not propagate in the inner side because it spread inside with a certain penetration depth due to the skin effect. So all of these and other parameters such as SNR, Quality factor, and also the different behaviors and characteristics of the RF coils have to be taken in account when MRI and in particular RFs are used.

2.1.1 SNR in MRI

When performing any MR Imaging experiment always appears an undesirable component that is uncorrelated to the signal. The Brownian motion of electrons in the receiver coil might be responsible and is the result of the coil resistance and temperature. A MRI experiment then involves the combination of two important parameters, signal and noise. This can be referred as the Signal-to-Noise Ratio: Signal/Noise or S/N or SNR. It has been previously stated that a good coil design should include a high SNR. This parameter is an accepted standard for measurement of quality in MRI studies. The quality of the reconstructed images depends strongly on the SNR of the acquired signal. Modern Imaging techniques often demand very high speed and spatial resolution, so that the highest possible SNR is still required to avoid poor image quality. The optimization of the SNR is a major factor in the design of a RF receiver coil. So as we already said, the MR signal is determined by the magnetic field generated by the coil. However, noise always accompanies a signal that is not solely due to the coil itself, but the human body as well. Unlike the SNR of the NMR experiment, in MRI the

biological sample (patient) produces a resistance comparatively large since is a poor conductor, and contributes significantly in the noise figure induced in the coil. To include the biological sample resistance, Hoult and Richard proposed a new SNR expression:

$$SNR = \frac{Peak}{Signal} \propto \frac{\omega_0^{\overline{2}} i^{-1} B_\perp V_{sample}}{R_{eff}}$$

(2.1)

where ω_0 is the resonant frequency, V_{sample} is the voxel volume, $\vec{B_1}$ is the transverse linearly polarized magnetic field for unit current in the coil, R_{eff} is the effective resistance. The effective resistance includes contribution from the coil, electronics and the sample being imaged (patient).

$$R_{eff} = R_{coil} + R_{sample} + R_{electronics}$$

(2.2)

Since the electronics of a MR imager between 0.5 Tesla and 4 Tesla has improved significantly, imaging experiments carried out today on these systems it is possible to affirm that R_{eff} is approximately equal to R_{sample} (resistance caused by the patient). The noise in any MRI coil and the sample and is scribed by the Nyquist formula:

$$R_{eff} = \sqrt{4 \kappa T \Delta f R_{coil}}$$

(2.3)

where κ represent the Boltzmann's constant, T is the sample temperature, the resistance, R coil is used to represent the conductive losses of the coil itself as well as magnetic (eddy currents) and dielectric losses in the sample and surroundings structures. The noise is measured over a

defined spectral bandwidth Δf in Hertz. The SNR expression also dictates the size and geometry of the RF coil to be developed. In particular, analytical expression of the R_{eff} and $\vec{B_1}$ for simple geometries have been developed by Wang and co-workers who used the quasi-static approach to obtain a SNR formula. This produces accurate results for low field strengths (≤ 1 Tesla) in which the wavelength is much larger than the body size. Schell collaborators calculated the electromagnetic field of surface and volume coils by approximating the human body by a homogeneous half-space or cylinder depending on the type of coil to be used, to derive a general expression for the SNR in MRI. Ocali and Atalar introduced another approach to calculate the intrinsic SNR, based on the assumption of a superposition of a large number of plane waves to obtain an expression for the magnetic field. The idea is to minimize the total power deposition while maintaining a constant right-hand circular polarized component of the magnetic field at the point of interest. It is difficult to develop a simple relation between the imaging volume and the SNR of the associated RF coil, but it is still possible to see the increase of this parameter with the decrease of the coil's effective imaging as formulated in Eq. 2.1.

2.1.2   The RF coil as a coaxial transmission line

A medium to transmit the signal form the RF coil to the scanner is required, a coaxial (coax) or triaxial cable is usually used to connect the RF coil to the RF subsystem of the MR unit. The operation of the RF coil is not completely dependent upon the frequency response of the antenna itself but rather on the frequency characteristics of the transmission line-coil element combination. It also important to use a transmission line with a proper characteristics impedance to match the MR system, generally 50 omhs: the coaxial cable should then have a 50 ohms impedance as well. Another simple and practical technique that can be used to match the antenna to the transmission line is to use the λ/4 transformer. This implies that the coil should be matched to the coax by using a λ/4 piece of cable. Because the signal travels through a coaxial cable: a RF attenuation by the cable is present, and although small is not

negligible at some frequencies. A RF coil attached to a coaxial cable forms a transmission line which is inherently unbalanced. Because the inner and outer conductors are not coupled to the surface coil in the same way, they provide unbalance. Devices used to balance this unbalanced system are denominated *Baluns* (BALance to Unbalance)

2.1.3 The Equivalent Circuit of a Surface RF coil

Viewing a RF coil as a magnetic energy storage device is a key to a good coil design. Surface coils are generally operated as resonant circuits. Then, an equivalent circuit can be formulated to study the parameters affecting the design of a RF coil. This is done in most applications to provide maximum power transfer between the MR system and the coil. In a resonant circuit, equal amounts of energy are stored in the electric and magnetic fields, with the energy exchanging repeatrdly between the electric and magnetic fields. Electric fields with lossy dielectrics (patients) lead to increased resistance in the coil, the electric fields should be associated with the capacitors used for tuning and matching the coil rather than the stray electric filed of the coil. An easy way to represent a RF coil is using a resonant circuit composed of an inductor (L) a resistance ® and a capacitance (C). Consequently, using the Kirchhoffs law for circuit in Fig. 1.4, it can be obtained that the resonant frequency is:

$$\omega = 1/\sqrt{LC} \qquad (2.4)$$

In practice, the resistance cannot disappear totally so the current magnitude is never infinity. The current however would reach its maximum value at the resonant frequency.

2.1.4 The Quality factor of a RLC circuit

To provide a quantitative way to measure the quality of the circuit, a quality factor, Q can be defined as the energy stored divided by the energy dissipated per period. However, to calculate the inductance and resistance of a coil is not an easy task. The Q of a resonator can be expressed as:

$$Q = \frac{maximum\ energy\ stored}{average\ energy\ dissipated\ per\ cycle} = \frac{0.5\ I^2 L}{\pi/\omega I^2\ R_{coil}} = \frac{\omega L}{R_{coil}} \quad (2.5)$$

From Eq. (5) it can be said that a high Q should have a small resistance. The higher the Q, the higher the ratio of flux density produced to power dissipated in the coil. Typical values for loaded coils ranges from order of magnitude of 10 to 100. The relative values of R_{coil} and R_{sample} in Eq.2 can be determined by measuring the Q when the coil is empty and when it is loaded by a patient or a phantom. The best indicator of the coil sensitivity is the ratio:

$$\frac{Q_{empty}}{Q_{loaded}} = \frac{R_{coil} + R_{sample}}{R_{coil}} \quad (2.6)$$

provided the dielectric losses do not contribute to R_{sample} (patient). This ratio can be 5 times or more for a magnetic field strength of 1.5 Tesla, for this reason coil losses contribute less than 11% of the observed noise value. Therefore, a good coil design should have a $R_{sample} \gg R_{coil}$. A much simpler approach is to calculate Q according to the following expression:

$$Q = \frac{\omega}{\Delta\omega} \quad (2.7)$$

where $\Delta\omega$ denotes the bandwidth, which can be measured easily with the aid of a network analyzer. The measured Q factor includes the contribution of the capacitor's resistance, and one must be aware that many capacitor manufacturers specify the Q of their products. High quality chip capacitors are then recommended to be used in the design of a MRI coil, to avoid

unwanted resistance contributions coming from these electronic components which can drastically affect the quality factor.

2.1.5 Coil homogeneity

MR images present intensity variations caused by the magnet magnetic field ($\vec{B_0}$), the RF coil's field ($\vec{B_1}$) and eddy current compensation. In particular, the non-uniformity of the received field leads to unwanted variation in MR images. This effect pronounced with surface coils. A number of quality tests have been reported to measure image uniformity. This is normally carried out acquiring images under specific considerations. A crude manner quantify this parameter can be obtained by plotting the pixel variation across an axial phantom image.

2.2   RF Electronic Components

From conventional AC circuit analysis we know that a resistance *R* is frequency independent and that a capacitor *C* and an inductor *L* can simply be specified by their reactances *Xc* and *XL* as follows:

$$X_L = \omega L \tag{2.8}$$
$$X_c = \frac{1}{\omega C} \tag{2.9}$$

It is important to point out that resistances, inductances, and capacitances are not only created by wires, coils, and plates as typically encountered in conventional low-frequency electronics. Even a single straight wire or a copper segment of a printed circuit board (PCB) layout possesses frequency dependent resistance and reactance.

2.2.1   Resistors

Perhaps the most common circuit element in low-frequency electronics is a resistor whose purpose is to produce a voltage drop by converting some of the electric energy into heat. Thin-film chip resistors find application in RF circuits as surface mounted devices (SMDs). This is due to the fact that they can be produced in extremely small sizes. Because even a straight wire possesses an associated inductance, the electric equivalent circuit representation of a high frequency resistor of nominal value R is more complicated than a lower frequency one, and it has to be modified such that the finite lead dimensions as well as parasitic capacitances are taken into account. The two inductances L_l model the leads, while the
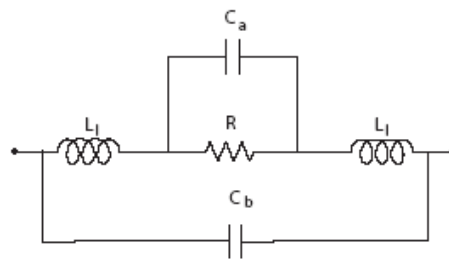
Figure 2.2: High frequency resistor model

capacitances are needed to account for the actual wire arrangement, which always represents a certain charge separation effect modeled by capacitance C_a, and inter-lead capacitance C_b. The lead resistance is generally neglected when compared with the nominal resistance R. Knowing the inductance of the leads, we can compute the impedance of the entire circuit as:

$$Z = j\omega L + \frac{1}{j\omega C + 1/R}$$

(2.10)

At low frequencies the impedance of the resistor is equal to R. However, as the frequency increases, the effect of the stray capacitance becomes dominant. Beyond the resonance, the

total impedance increases due to the lead inductance, which represents an open circuit or infinite impedance at very high frequencies. This example underscores the care that is required when dealing with resistors. Not all resistors exhibit exactly the same response, often resistors have multiple resonance point.

2.2.2   Capacitors

In most RF circuits, capacitors find widespread application for the tuning of filters and matching networks as well as for biasing active components such as transistors. Elementary circuit analysis defines capacitance for a parallel plate capacitor whose plate dimensions are large compared to its separation, as follows:

$$C = \frac{\epsilon A}{d} \tag{2.11}$$

where A is the plate surface area and d denotes the plate separation. Ideally there is no current flow between the plates. However, at high frequencies the dielectric materials become lossy (i.e. there is a conduction current flow). The impedance of a capacitor must thus be written as a parallel combination of resistance R_e and capacitance $1/(\omega C)$:

$$Z = \frac{1}{1/R_e + j\omega C} \tag{2.12}$$

To define the high frequency impedance model we must add now the inductance and the resistance associated with the leads.
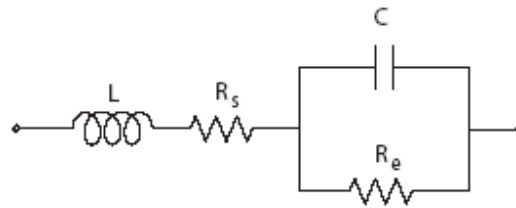
Figure 2.3: High frequency capacitor model

2.2.3   Inductors

Inductors generally are used in transistor biasing networks, as RF coils (RFCs) to short circuit the device to DC voltage conditions or for matching networks. Since a coil is generally formed by winding a straight wire on a cylindrical former, we know from our previous discussion that the wire represents an inductance and a resistance in addition. Moreover, adjacently positioned wires constitute separated moving charges, thus giving rise to a parasitic capacitance effect. The parasitic shunt capacitance *Cs* and series
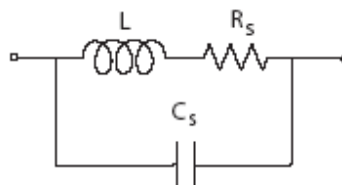
Figure 2.4: High frequency inductor model

resistance R_s represent composite effects of distributed capacitance and resistance, respectively. It is possible to build a inductor simply wrapping a wire, then we can estimate the inductance value via the formula:

$$L \simeq 0.394 \frac{a^2 n^2}{9a + 10b} \tag{2.13}$$

where *a* is internal radius of the coil in [*cm*], *b* is the length of the coil in [*cm*], *n* the number of turns and *L* the inductance in μH.
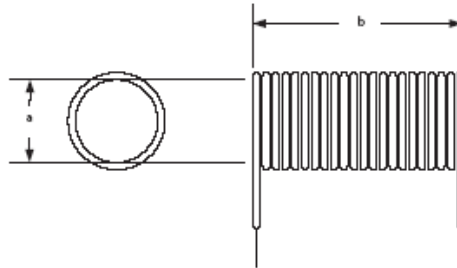
Figure 2.5: Inductor

2.3   Line Theory

When the electromagnetic wavelength is comparable with the dimension of the circuit, Kirchhoff´s circuit laws cannot be directly applied. The situation can be remedied, however, if the line is subdivided into elements of small, (mathematically speaking) infinitesimal length, over which voltage and current can be assumed to remain constant. For each section of length Δz, we can devise an equivalent electric circuit representation. To build the complete model of the entire line we would have to replicate Δz a large number of times. Therefore, the transmission line in general cannot be represented in terms of lumped parameters, but must be viewed as distributed parameters *R*, *L*, *C*, and *G*, where all circuit parameters are given in terms of unit length. As a rule of thumb, when the average size *l* of the discrete circuit component is more than a tenth of the wavelength, transmission line theory should be applied $(l \geq \lambda/10)$.

2.3.1 Two Wire Lines

The two-wire transmission line is one example of a system capable of transporting high-frequency electric energy from one location to another. Unfortunately, it is perhaps the most unsuitable way of transmitting high frequency voltage and current waves due to the fact that the wire pair acts as a large antenna, radiation loss tends to be very high.

2.3.2 Coaxial Cables

A more common example of a transmission line is the coaxial cable. It is used for almost all cases of externally connected RF systems or measurement equipment at frequencies of up to $10GHz$. A typical coaxial line consists of an inner cylindrical conductor of radius a, an outer conductor of radius b, and a dielectric medium layered in between. Usually the outer conductor is grounded, thus minimizing radiation loss and field interference.

2.3.3 Microstrip lines

It is a common practice to use planar printed circuit boards (PCBs) as the basic medium to implement most electronic systems. When dealing with actual RF circuits, we need to consider the high frequency behavior of the conducting strips etched on the PCBs. The ground plane below the current carrying conductor traces helps prevent excessive field leakage and thus reduces radiation loss. One of the disadvantages of single layered PCBs is that they have rather high radiation loss and are prone to "crosstalk" (interference) between neighboring conductor traces. To achieve high board density of the component layout, we should use substrates with high dielectric constants since they minimize field leakage and cross coupling.

2.3.4   Match

We can write the general Transmission Line Equation using the phasor notation and Kirchhoff's voltage law. The input and output voltage and current
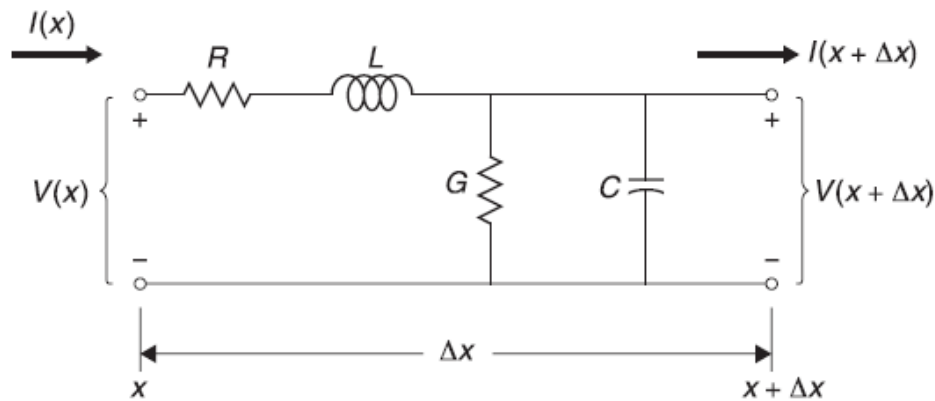
Figure 2.6: Line section of length Δz

of line section of length Δz represent in Figure 2.5 are related by:

$$(R + j\omega L)I(z)\Delta z + V(z + \Delta z) = V(z) \tag{2.14}$$

$$I(z) - V(z + \Delta z)(G + j\omega C) = I(z + \Delta z) \tag{2.15}$$

that we can express as a differential equation:

$$\lim_{\Delta x \to 0} -\frac{V(z + \Delta z) - V(z)}{\Delta z} = -\frac{dV(z)}{dz} = (R + j\omega L)I(z) \tag{2.16}$$

$$\lim_{\Delta x \to 0} \frac{I(z + \Delta z) - I(z)}{\Delta z} = \frac{dV(z)}{dz} = (G + j\omega C)V(z) \tag{2.17}$$

and their solutions are:

$$V(z) = V^+ e^{-kz} + V^- e^{+kz} \tag{2.18}$$

$$I(z) = I^+ e^{-kz} + I^- e^{+kz} \tag{2.19}$$

where k is called propagation constant and depends on the parameter R, G, L and C of the line. It is important to observe that 2.17 and 2.18 are general solutions for transmission aligned along the z-axis. The convention is such that the first term represents the wavefront propagating in the $(+z)$- direction, whereas the wavefront propagating in the $(-z)$-direction. This makes physical sense since the negative sign in the function with $k \geq 0$ ensures diminishing amplitudes. We can define now the line impedance as:

$$Z_0 = \frac{V^+}{I^+} = -\frac{V^-}{I^-}$$

(2.20)

Let us to apply a Z_l at the end of the transmission line like in Figure 2.6 If the load is matched to the line, that means $Z_l = Z_0$ no reflection occurs
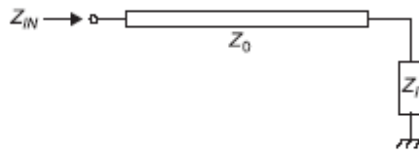
Figure 2.7: Transmission line terminated to a load Z_l

and the coefficient, V of the wavefront propagating in the $(-z)$-direction is zero. If the load is not matched, so $Z_l \neq Z = 0$ the coefficient, V of the wavefront propagating in the $(-z)$-direction is not zero and reflection occurs. It is possible to define the *reflection coefficient*, Γ_0 as the ratio of the reflected to incident voltage wave:

$$\Gamma_0 = \frac{V^-}{V^+}$$

(2.21)

$$\Gamma_0 = \frac{Z_l - Z_0}{Z_l + Z_0}$$

(2.22)

The larger mismatch, the larger reflection coefficient, the larger reflected voltage wave.
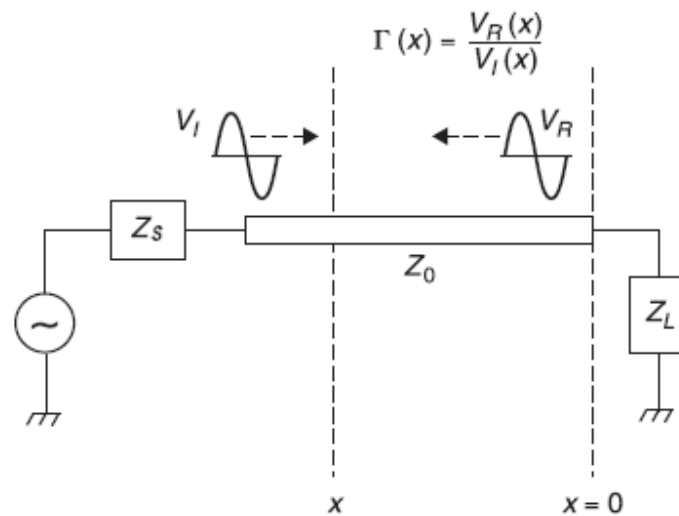
Figure 2.8: Meaning of Γ

If a generator with an equivalent output impedance Z_s is connected to a transmission line, reflection can occur at the source. The reflection coefficient at the source is define as:

$$\Gamma_s = \frac{Z_s - Z_0}{Z_s + Z_0} \tag{2.23}$$

There are two kind of matching, conjugate matching and load matching. Conjugate matching condition is $Z_0 = Z_l^*$ and in this case the maximum power is delivered but reflection occurs (unless Z_0 is real). Load matching condition is $Z_0 = Z_l$, so the power delivered is not maximized (unless Z_0 is real) but no reflection occurs.

2.3.5   The Smith Chart

Both length and operating frequency of the transmission line significantly influence the input impedance. To facilitate the evaluation of the reflection coefficient, P. H. Smith developed a graphical procedure based on conformal mapping principles. This approach permits an easy

and intuitive display of the reflection coefficient as well as the fine impedance in one single graph. Almost all computer-aided design programs utilize the Smith Chart for the analysis of circuit impedances, design of matching networks, and computations of noise figures, gain, and stability circles. Even instruments such as the network analyzer have the option to represent certain measurements in a Smith Chart format.
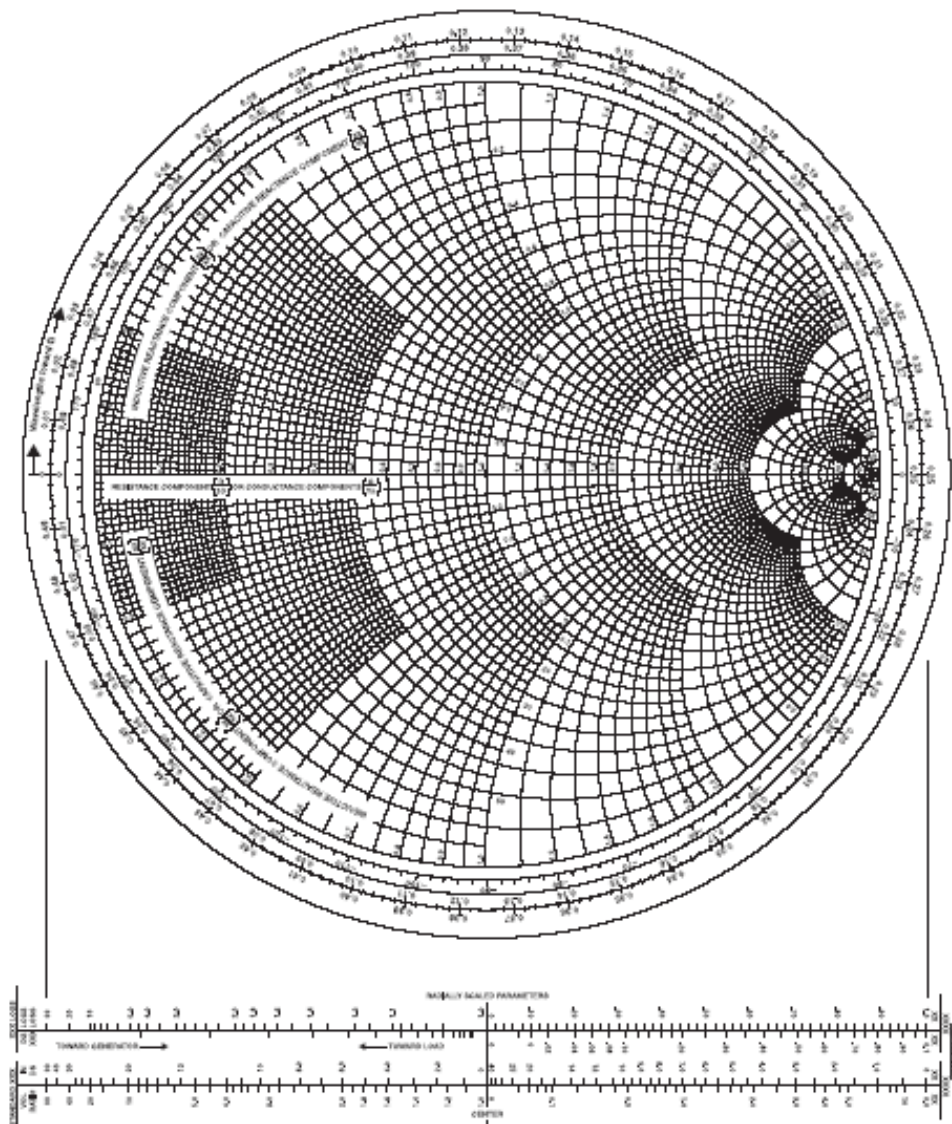
Figure 2.9: The Smith Char

2.4   HF Amplifier

Mainly thanks to preamplification it is possible to reach the high performance need in a MRI system. One of the main issue is to have the minimum noise figure (NF) to avoid to deteriorate the acquired signal. This NF is usually extremely high, so the only solution is to shift the input signal amplitude with an matching network system connected before the preamplification. The goal standard would be to have a noise figure below 1 *dB*. The design of a amplifier is the creation of a circuit environment in which a selected transistor performs as closely as possible to a set of design objectives. The circuit designer may have no influence over the transistor´s parameters. These are established by its geometry, quality of manufacture, and semiconductor physics. A generic single-stage amplifier configuration is embedded between input and output matching networks. Input and output matching networks are needed to reduce undesired reflections and thus improve the power flow capabilities. In terms of performance specifications, the following list constitutes a set of key amplifier parameters:

- Gain and gain flatness (in *dB*)

- Operating frequency and bandwidth (in *Hz*).

- Maximum output power (in *dBm*)

- Power supply requirements (in *V* and *A*)

- Input and output reflection coefficients

- Noise figure (in *dB*)

In addition, one often must consider such parameters as intermodulation distortion products, amplifier feedback, and heating effects. All of them can seriously affect amplifier

performance. Usually the circuit designer selects a transistor from a catalog and then the transistor is seen just as a two-port network described by a table of *S*-parameters taken over the entire frequency domain over which, it has gain. After the bias and heat sinking needs of the transistor have been satisfied, the RF design proceeds using the *S*-parameters and it is not important whether the device is a bipolar or field-effect transistor (FET) or any other device whose *S*-parameters suggest the prospect of gain.

2.4.1   S-Parameters

Scattering, or *S*-parameters are an extremely useful design aid that most manufacturers supply for their higher frequency transistors. *S*-parameters are widely used because they are easy to measure, easy to understand, convenient, and provide a wealth of information at a glance. *S*-parameters utilize normalized incident and reflected traveling waves to characterize the operation of the two-port network. Furthermore, with *S*-parameters, there is no need to present a short circuit to the two-port device, like in the measurement of other kind of parameters needs. A short-circuit measure it is not easy to do because an active device often does not want to see a short circuit applied to one of its ports. Often such a termination would cause an active device, such as a transistor, to become unstable, thus making measurements impossible. Let us now insert a two-port network between the source and the load. The following may be said for any traveling wave that originates at the source:

- A portion of the wave originating from the source and incident upon the two-port device (a_1) will be reflected (b_1) and another portion will be transmitted through the two-port device.

- A fraction of the transmitted signal is then reflected from the load and becomes incident upon the output of the two-port device (a_2).
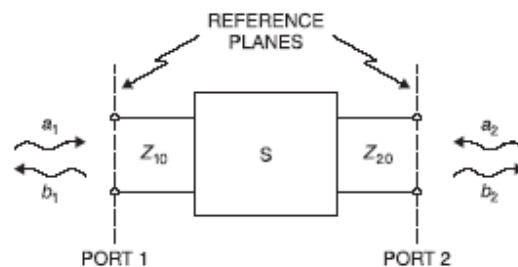
- A portion of the signal (a_2) is then reflected from the output port back toward the load (b_2), while a fraction is transmitted through the two-port device back to the source.

where:

$$a_i = \frac{V_{iIncident}}{\sqrt{Z_{i0}}} \qquad (2.24)$$

$$b_i = \frac{V_{iReflected}}{\sqrt{Z_{i0}}} \qquad (2.25)$$

and Z_{i0} is the characteristic impedance of the transmission line connected to the ith port network.

Figure 2.10: Incident and reflected waves of a two port device

It is obvious from the above discussion that any traveling wave present in the circuit is made up of two components. For instance, the total traveling wave component flowing from the output of the two port device to the load is made up of that portion of a_2 which is reflected from the output of the two-port device, plus that portion of $a1$ that is transmitted through the two-port device. Similarly, the total traveling wave flowing from the input of the two-port device back toward the source is made up of that portion of a_1 that is reflected from the input port plus that fraction of a_2 that is transmitted through the two-port device. If we set these observations in an equation form, we have:

$$b_1 = S_{11}a_1 + S_{12}a_2 \qquad (2.26)$$

$$b_2 = S_{21}a_1 + S_{22}a_2 \qquad (2.27)$$

that can be written as:

$$\begin{pmatrix} b_1 \\ b_2 \end{pmatrix} = \begin{pmatrix} S_{11} & S_{12} \\ S_{21} & S_{22} \end{pmatrix} \begin{pmatrix} a_1 \\ a_2 \end{pmatrix}$$

(2.28)

Suppose now that the transistor is embedded in a matched 50 Ohm system so S_{11} is the input reflection coefficient when the output is match terminated, S_{12} is the reverse transmission coefficient, S_{21} is the forward transmission coefficient and S_{22} is the output reflection coefficient when the input is match terminated. The individual S-parameters are evaluated using these relationships:

$$S_{11} = \left. \frac{b_1}{a_1} \right|_{a_2=0} \qquad S_{22} = \left. \frac{b_2}{a_2} \right|_{a_1=0} \qquad S_{21} = \left. \frac{b_2}{a_1} \right|_{a_2=0} \qquad S_{12} = \left. \frac{b_1}{a_2} \right|_{a_1=0}$$

(2.29)

2.4.2 Gain

There are various power gain definitions that are critical to the understanding of how an RF amplifier works. Let us assume that the two matching networks are included in the source and load impedances to simplifier our system configuration. The starting point of our power analysis is the RF source connected to the amplifier network.
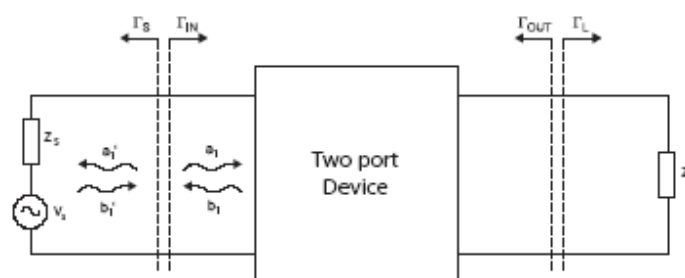
Figure 2.11: Insertion gain

From the *S*-parameters definition we can write:

$$b_s = b'_1 - a'_1 \Gamma_s = b'_1 (1 - \Gamma_{in} \Gamma_s)$$ (2.30)

The incident power wave associated with *b′*1 is:

$$P_{inc} = \frac{|b'_1|^2}{2} = \frac{1}{2} \frac{|b_s|^2}{|1 - \Gamma_{in} \Gamma_s|^2}$$ (2.31)

which is the power launched toward the amplifier. The actual input power P_{in} observed at the input terminal of the amplifier is composed of the incident and reflected power waves. With the aid of the input reflection coefficient Γ_{in} we can therefore write:

$$P_{in} = P_{inc}(1 - |\Gamma_{in}|^2)$$ (2.32)

Available power

The maximum power transfer from the source to the amplifier is achieved if the input impedance is complex conjugate matched ($Z_{in} = Z_{in}^*$) or, in terms of the reflection coefficients if $\Gamma_{in} = \Gamma_s^*$. Under maximum power transfer condition, we define the available power *Pa* as:

$$P_a = P_{in}|_{\Gamma_{in}=\Gamma_s^*} = \frac{1}{2} \frac{|b_s|^2}{1 - |\Gamma_s|^2}$$ (2.33)

Transducer power gain

We can next investigate the transducer power gain G_T, which quantifies the gain of the amplifier placed between source and load.

$$G_T = \frac{\text{power delivered to the load}}{\text{available power from the source}} = \frac{P_L}{P_a}$$ (2.34)

where
$$P_L = \frac{1}{2}|b_2|^2(1 - |\Gamma_L|^2)$$
(2.35)

and we obtain:
$$G_T = \frac{|b_2|^2}{|b_s|^2}(1 - |\Gamma_L|^2)(1 - |\Gamma_s|^2)$$
(2.36)

it is easy to show that:
$$G_T = \frac{(1 - |\Gamma_L|^2)|S_{21}|^2(1 - |\Gamma_s|^2)}{|(1 - S_{11}\Gamma_s)(1 - S_{22}\Gamma_L) - S_{21}S_{12}\Gamma_L\Gamma_s|}$$
(2.37)

Unilateral power gain

An often employed approximation for the transducer power gain is the so called unilateral power gain, G_{TU}, which neglects the feedback effect of the amplifier ($S12 = 0$). This simplifies the form of 2.29 to:

$$G_{TU} = \frac{(1 - |\Gamma_L|^2)|S_{21}|^2(1 - |\Gamma_s|^2)}{|1 - S_{22}\Gamma_L|^2|1 - S_{11}\Gamma_s|^2}$$
(2.38)

Insertion gain

We can rewrite the unilateral power gain such that the individual contributions of the matching networks become identifiable:

$$G_{TU} = G_s G_0 G_L$$
(2.39)

where
$$G_s = \frac{(1 - |\Gamma_s|^2)}{|1 - S_{11}\Gamma_s|^2} \quad G_0 = |S_{21}|^2 \quad G_L = \frac{(1 - |\Gamma_L|^2)}{|1 - S_{22}\Gamma_L|^2}$$
(2.40)

where G_s and G_L are the associate gain with the input and output matching networks and G_0 is the insertion gain of the amplifier.
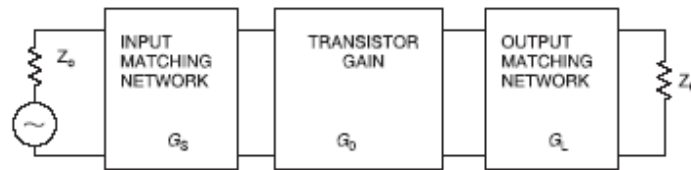
Figure 2.12: Insertion gain

Available power gain

The transducer power gain is a fundamental expression from which additional important power relations can be derived. For instance, the available power gain for load side matching $\Gamma_L = \Gamma_{out}^*$) is defined as:

$$G_A = G_T\big|_{\Gamma_L=\Gamma_{out}^*} = \frac{\text{power available from the amplifier}}{\text{power available from the source}} \tag{2.41}$$

or:

$$G_A = \frac{|S_{21}|^2(1 - |\Gamma_S|^2)}{(1 - |\Gamma_{out}|^2)|1 - S_{11}\Gamma_S|^2} \tag{2.42}$$

Power gain

Further, the power gain (operating power gain) is defined as the ratio of the power delivered to the load to the power supplied to the amplifier.

$$G = \frac{\text{power delivered to the load}}{\text{supplied to the amplifier}} = \frac{P_L}{P_{in}} = \frac{P_L}{P_A}\frac{P_A}{P_{in}} = G_T\frac{P_A}{P_{in}} \tag{2.43}$$

or

$$G = \frac{|S_{21}|^2(1 - |\Gamma_S|^2)}{(1 - |\Gamma_{in}|^2)|1 - S_{22}\Gamma_L|^2} \tag{2.44}$$

2.4.3   Stability

One of the first requirement that an amplifier circuit must meet is a stable performance in the frequency range of interest. This is a particular concern when dealing with RF circuits, which tend to oscillate depending on operating frequency and termination. The phenomenon of oscillations can be understood in the context of a voltage wave along a transmission line. If $/\Gamma_0/ > 1$, then the return voltage increases in magnitude (positive feedback) causing instability. Conversely, $/\Gamma_0/ < 1$ causes a diminished return voltage wave (negative feedback). Let us regard the amplifier as a two-port network characterized through its *S*-parameters and external terminations described by Γ_L and Γ_s. Stability then implies that the magnitudes of the reflection coefficients are less than unity:

$$|\Gamma_L| < 1 \qquad |\Gamma_s| < 1 \tag{2.45}$$

and

$$|\Gamma_{in}| < 1 \qquad |\Gamma_{out}| < 1 \tag{2.46}$$

It is possible to show that 2.38 are satisfied in a region of the smith chart delimited by a circle called *output stability circle*. Drawing the output stability circle in the smith chart, it is easy to see all the values of the load and source impedance that permit the amplifier to be stable. As the name implies, unconditional stability refers to the situation where the amplifier remains stable throughout the entire domain of the Smith Chart at the selected frequency and bias conditions. This applies to both the input and output ports. To have unconditional stability it must be:

$$k = \frac{1 - |S_{11}|^2 - |S_{22}|^2 + |\Delta|^2}{2|S_{12}||S_{21}|} > 1 \qquad |\Delta| < 1 \tag{2.47}$$

where *k* is called the Rollett factor and $\Delta = S_{11}S_{22} - S_{12}S_{21}$.

2.4.4   Stabilization Methods

If the operation of a amplifier is found to be unstable in the desired frequency range, an attempt can be made to stabilize the transistor. We recall that:

$$|\Gamma_{in}| = \left|\frac{Z_{in} - Z_0}{Z_{in} + Z_0}\right| > 1 \quad \text{and} \quad |\Gamma_{out}| = \left|\frac{Z_{out} - Z_0}{Z_{out} + Z_0}\right| > 1 \tag{2.48}$$

which implies $Re\{Z_{in}\} < 0$ and $Re\{Z_{out}\} < 0$. One way to stabilize the active device is to add a series resistance or a shunt conductance to the port. Stabilization through the addition of resistors comes at a prize: the impedance matching can suffer, there may be a loss in power flow, and the noise figure typically worsens due to the additional thermal noise sources that the resistors present.

2.4.5   Noise figure circles

In many RF amplifiers, the need for signal amplification at low noise level becomes an essential system requirement. Unfortunately, designing a low noise amplifier competes with such factors as stability and gain. For instance, a minimum noise performance at maximum gain cannot be obtained. It is therefore important to develop a method that allows us to display the influence of noise as part of the Smith Chart to conduct comparisons and observe tradeoffs between gain and stability. From a practical perspective, the key ingredient of a noise analysis is the noise figure of a two-port amplifier in the impedance form:

$$NF = NF_{min} + \frac{G_n}{R_s}|Z_s - Z_{opt}|^2 \tag{2.49}$$

where NF_{min} is the minimum noise figure, G_n is given by $G_n = 1/R_n$ where R_n is the equivalent noise resistance of the device and Z_{opt} is the value of the input impedance that gives the

minimum noise figure. From 2.41 it is possible to draw in the smith chart the noise figure circles that represent the value of Z_s where the noise figure is constant.

2.4.6 Multistage Network

When in a link there are two or more stage, it does not matter if they are amplifiers, optical links or other devices, because every stage is seen like a two port device that exhibits some features such as s-parameters, noise figure, intermodulation distortion and 1 dB compression point. Besides the typical input and output matching networks, a two stages link must have an additional so-called interstage matching network for matching the output of stage 1 with the input of stage 2. Under the assumption of optimally matched and lossless networks, let us summarize the most important dual-stage performance parameters.

Gain

The total power gain G_{tot}, of a dual-stage amplifier under linear operating conditions results in a multiplication of the individual gains G_1 and G_2, or in dB:

$$G_{tot} = G_1 + G_2 \tag{2.50}$$

Noise Figure

If F_1 and F_2 denote the noise figures associated with stages 1 and 2, the total noise figure F_{tot} is:

$$F_{tot}(dB) = G_1 + \frac{F_2 - 1}{G_1} \tag{2.51}$$

and the minimal detectable signal $P_{in;mds}$ at 3 dB above thermal noise at the input is given by $P_{in;mds} = kT\Delta f + 3dB + F_1$, the minimal detectable output power $P_{out;mds}$ becomes:

$$P_{out,mds} = kT\Delta f + 3 + F_{tot} + G_{tot} \qquad (2.52)$$

Dynamic Properties

The dynamic properties are also affected:

$$IP_{tot}(dBm) = \frac{1}{1/IP_1 + 1/(G_2 IP_2)} \qquad (2.53)$$

where IP_1 and IP_2 are the third order intercept points associated with stages 1 and 2. Finally the dynamic range is now reduced by the second stage by:

$$DR = IP_{tot} - P_{out,mds} \qquad (2.54)$$

Chapter 3

Material and Methods: Design of the S-Parameters Measurement System

3.1   General Description of a Network Analyser

To understand better The Design of the S-Parameters Measurement System is necessary to make first a general description of a Network Analyser (shown in the Figure 3. 1).

Figure 3.1: Network Analyser

Network Analysers have become one of the most important measurement tools for characterizing the performance of high-frequency components and devices. A modern vector Network Analyser can measure a component's magnitude, phase, and group delay, show port impedances on a Smith Chart, and, with time-domain capability, show the distance from a test port to an impedance mismatch or circuit fault. Understanding a Network analyser's capabilities and operation can help an operator derive optimum performance from the instrument. These analysers are available with a variety of test sets and calibration kits and

can be equipped with such options as time-domain capability for making distance-to-fault evaluations in transmission lines.

3.2   Network Analyser Architecture

Network Analysers differ in form and function from another tool commonly used to characterize communications systems and components, the spectrum analyser (Figure 3.2). Spectrum analysers measure unknown external signals. In contrast, Network Analysers utilize synthesized frequency sources to provide a known test stimulus that can sweep across a range of frequencies or power levels.
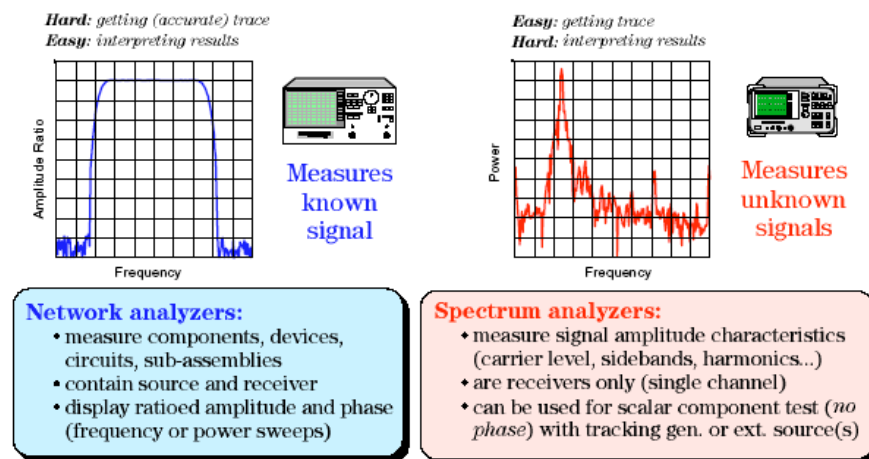
Figure 3.1: Network Analyzer VS Spectrum Analyzer

Network Analysers are used to measure components, devices, circuits, and sub-assemblies. They contain both a source and multiple receivers, and generally display ratioed amplitude and phase information (frequency or power sweeps). A Network Analyser is always looking at a known signal (in terms of frequency), since it is a stimulus-response system. With Network Analysers, it is harder to get an (accurate) trace on the display, but very easy to interpret the results. With vector-error correction, Network Analysers provide much higher measurement accuracy than spectrum analysers. Spectrum analysers are most often used to measure signal

characteristics such as carrier level, sidebands, harmonics, phase noise, etc., on unknown signals. They are most commonly configured as a single-channel receiver, without a source. Because of the flexibility needed to analyse signals, spectrum analysers generally have a much wider range of IF bandwidths available than most Network analysers. Spectrum analysers are often used with external sources for nonlinear stimulus/response testing. When combined with a tracking generator, spectrum analysers can be used for scalar component testing (magnitude versus frequency, but no phase measurements). With spectrum analysers, it is easy to get a trace on the display, but interpreting the results can be much more difficult than with a Network Analyser.

3.3   Network Analyser Hardware

In the Figure 3.3 is a generalized block diagram of a Network Analyser, showing the major signal processing sections.
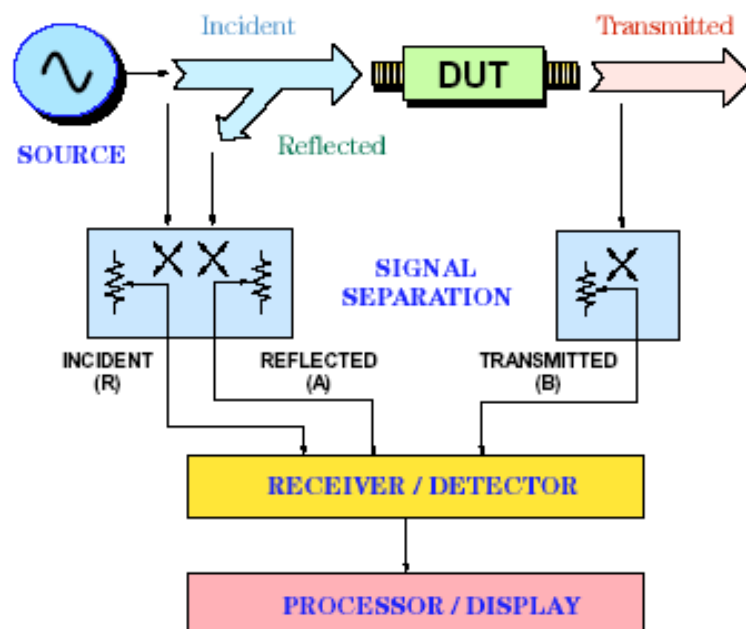
Figure 3.3: Network Analyzer Hardware

In order to measure the incident, reflected and transmitted signal, four sections are required:

1. Source for stimulus

2. Signal-separation devices

3. Receiver that provides detection

4. Processor/display for calculating and reviewing the results

They will each be examined in further detail in separate sections for a better comprehension of the general characteristics of the acquisition, computation and display of the impedance; which choice was made for the S-parameters Measuring System and why.

3.3.1   Source for stimulus

General characteristics

The signal source supplies the stimulus for the network analyzer stimulus-response test system. It is possible either sweep the frequency of the source or sweep its power level. Traditionally, network analyzers used a separate source. These sources were either based on open-loop voltage-controlled oscillators (VCOs) which were cheaper, or more expensive synthesized sweepers which provided higher performance, especially for measuring narrowband devices.
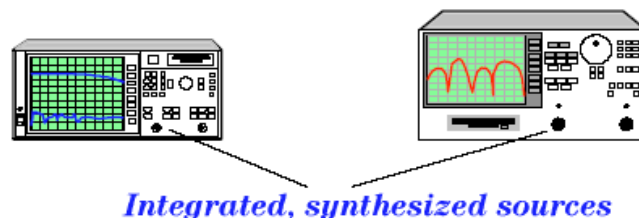
Figure 3.4: Source for stimulus

Implemented solution

The S-parameters Measuring System uses 2 synthesized sweepers (frequency generators) :

- The first one is used to generate the signal for the Directional Couplers with a sinusoidal signal with 298 MHz as the frequency (suited for 7 Tesla MRI);

- The second one is used to generate the Local oscillator (LO) for both Mixers (298,3 MHz)

Open-loop voltage-controlled oscillators (VCOs) are no longer used in this system because they provide lower performance than the frequency generators, especially for measuring narrowband devices. Excessive phase noise on open-loop VCOs degrades measurement accuracy considerably when measuring narrowband components over small frequency spans. This System is focused in only one frequency (very narrowband) and experimentally was proved that a change of the impedance at the output in the directional coupler correspond also a change in the input frequency of the source. This is the reason why two frequency generators were used and experimentally proved to be more stable in frequency even when the impedance of the Directional Coupler changes.

3.3.2   Signal Separation

General characteristics

The next major area covered is the signal separation block. The hardware used for this function is generally called the "test set". The test set can be a separate box or integrated within the Network Analyser. There are two functions that the signal-separation hardware must provide. The first is to measure a portion of the incident signal to provide a reference for rationing. This can be done with splitters or directional couplers. Splitters are usually resistive.

They are non-directional devices and can be very broadband. The trade-off is that they usually have 6 dB or more of loss in each arm (Figure 3.5).
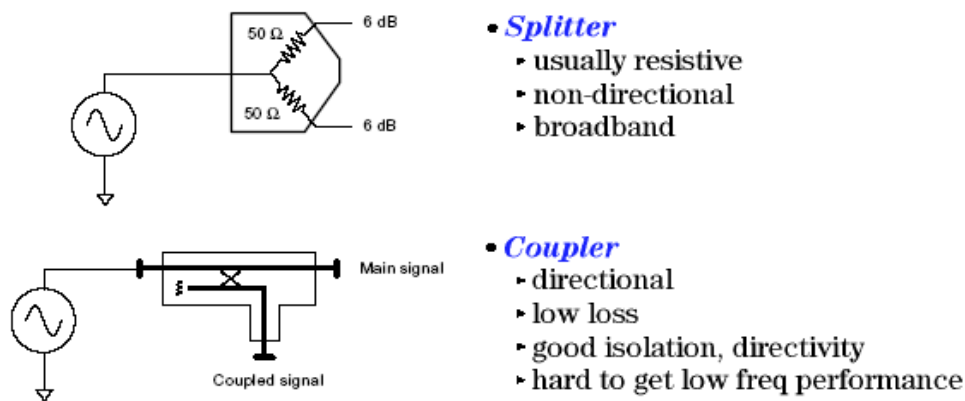
Figure 3.5: Splitter VS Coupler

Directional couplers can be built with very low loss (through the main arm) and good isolation and directivity. However, it is hard to make them operate at low frequencies. This can be a problem in RF Network Analysers, where low frequency coverage is important. The second function of the signal-splitting hardware is to separate the incident (forward) and reflected (reverse) traveling waves at the input of our Device under Test (DUT). Again, couplers are ideal in that they are directional, have low loss, and high reverse isolation. However, due to the difficulty of making truly broadband couplers, bridges are often used. Bridges are very useful for measuring reflection because they can be made to work over a very wide range of frequencies. The main trade-off is that they exhibit more loss to the transmitted signal, resulting in less power delivered to the DUT for a given source power. The Directional couplers are useful for measuring both the incident and reflected signals present at the input of the DUT. Directional couplers consist of a "through" path, and a "coupled" path that diverts a small amount of the power traveling along the through path (Figure 3.6).
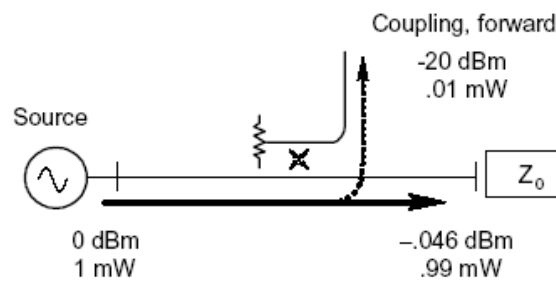
Figure 3.6: Coupling factor

The amount of coupled power is determined by the coupling factor:

Coupling factor (in dB) = –10 log (forward coupled power / incident power) (3.1)

For example, in a 20-dB coupler, the coupled power level is 20 dB less than the power level at the input port. In addition to the coupling factor, a directional coupler has other parameters, such as frequency response and directivity, that contribute to the overall power level seen at both the main output port and the coupled port. Ideally, a signal traveling in reverse through a coupler should not appear at the coupled port. In reality, some energy always appears at the coupled port because of the coupler's finite port-to-port isolation (Figure 3.7).
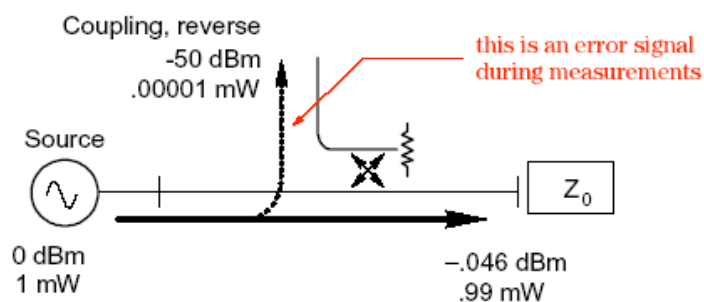
Figure 3.7: Coupling reverse factor

Isolation can be measured by sending power through the coupler in the reverse direction, and is defined as the leakage power at the coupled port relative to the incident power:

$$Isolation \ (in \ dB) = -10 \log (reverse \ coupled \ power \ / \ incident \ power) \tag{3.2}$$

One of the most important measured parameters for couplers is their directivity (Fig. 3.8). Directivity is a measure of a coupler's ability to separate signals flowing in opposite directions along the through path of the coupler. It can be thought of as the dynamic range available for reflection measurements. By definition, directivity is the coupling factor times any loss in the through path, divided by the reverse isolation (all terms are linear). In logarithmic terms, directivity is equal to the reverse coupling factor (isolation) minus the forward coupling factor minus the loss of the through arm (all terms in dB). When measuring forward and reverse coupling factors, the coupler must be terminated in a load impedance that is precisely equal to the characteristic impedance of the test system. Notice in the middle example of Figure 3.8 that adding loss (an attenuator for example) at the output of the coupler degrades raw (uncorrected) directivity by twice the value of the attenuator.
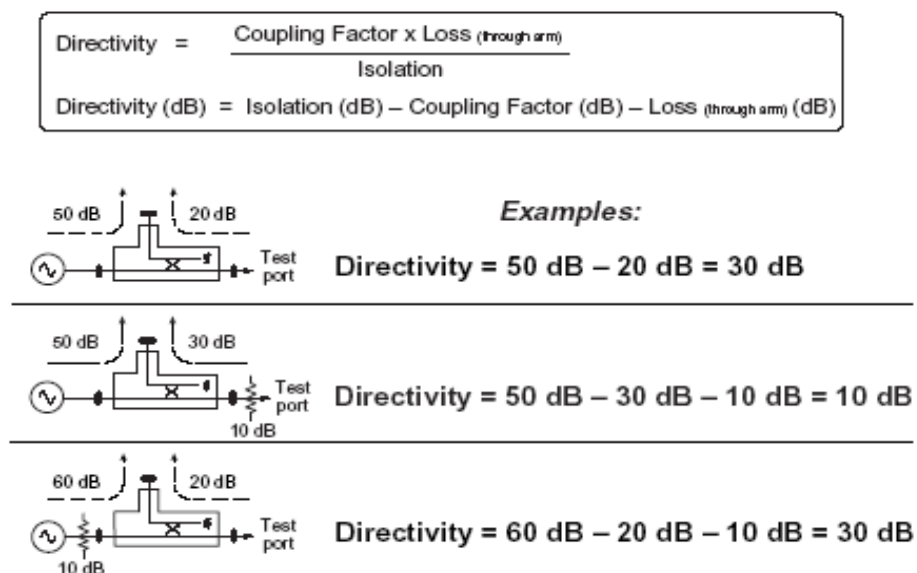
Figure 3.8: Directivity

This is why it is usually not a good idea to place attenuators or use lossy cables on any Network analyser test port that will be used for reflection measurements. Even when calibration is used to correct for the effect of the loss, the stability of the calibration will be worse (i.e., more drift will occur) due to the degraded raw directivity. Attenuation added between the source and the coupler has no effect on directivity, as shown in the lower example. While not shown, it is obvious that adding an attenuator on the coupled port would also not affect directivity since both the isolation and coupling term would be increased by the value of the attenuator. Errors due to finite directivity are often responsible for ripple patterns in many measurements of return loss. At the peaks of the ripple, directivity adds in-phase with reflections from the DUT. In some cases, directivity will cancel the DUT's reflection, resulting in a sharp dip in the return-loss response. One simple way to measure coupler directivity doesn't require forward and reverse measurements (Figure 3.9). This technique is useful for measuring a Network Analyser's effective directivity from the front-panel test ports. The first step is to place a short on the test port (the output of the coupler's through arm). Next, measure reflection and normalize the results (by saving data to memory and then displaying data divided by memory). The result is a 0 dB reference that includes the forward coupling factor and the through arm loss. The next step is to place a high-quality termination on the test port (a load from a calibration kit, for example). The signal now measured is only due to the leakage (directivity) error, based on the assumption of a perfect termination. Since the measurement has already been normalized, the measured value is the effective directivity of the coupler or analyser.
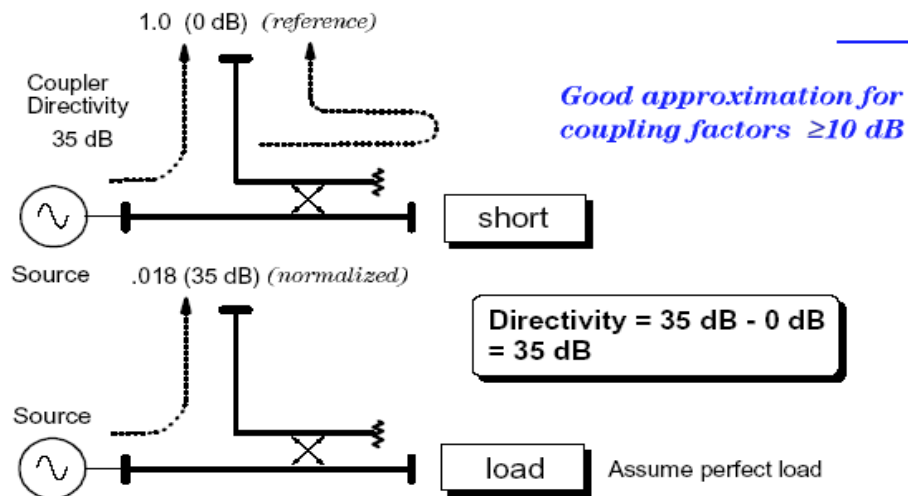
Figure 3.9: Measurement of coupler directivity

Directional bridges can also be used to measure reflected signals. In a directional bridge, if all four arms are equal in resistance, there will be a voltage null (this is the balanced condition). This happens if the test port is terminated with the characteristic impedance of the test system (typically 50 ohms). If the impedance at the test port is not 50 ohms, the voltage across the bridge is proportional to the mismatch presented by the DUT. By measuring both magnitude and phase across such a bridge, it is possible to measure the complex impedance at the test port. A bridge's equivalent directivity is the ratio (or difference in dB) between maximum balance (measuring a perfect Z_0 load) and minimum balance (measuring a short or open). The effect of bridge directivity on measurement uncertainty is exactly the same as for couplers.

Another kind of Directional Coupler is the Quadrature 3-dB hybrid, it is an important component widely applied in microwave but less in RF circuit design. It is a reciprocal four port networks that typically uses resonant quarter-wave length transmission line elements as its circuit building blocks. In the quadrature coupler, the input is split into two signals (usually with a goal of equal magnitudes) that are 90° degrees apart in phase.
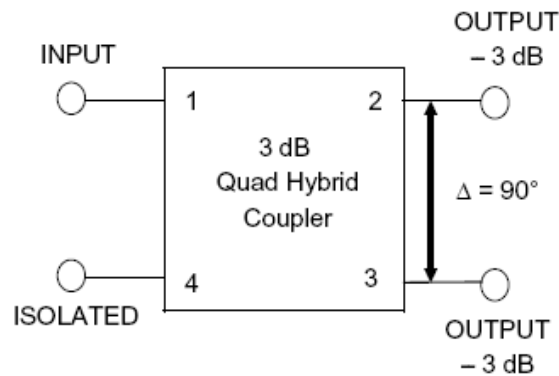
Figure 3.10: 3-dB Quadrature Hybrid Coupler

Referring to Figure 3.10, a signal applied to port 1 splits equally between ports 2 and 3 with one of the outputs exhibiting a relative 90° phase shift. If ports 2 and 3 are properly terminated into matching impedances, nearly all the signal applied to port 1 is transmitted to the loads connected to ports 2 and 3. In this circumstance, port 4 receives negligible power and is termed ''isolated''. However, if there is an impedance mismatch at port 2, for example, then signal power reflected back from port 2 will be divided proportionally between ports 1 and 4. Power is not fed to port 3. Moreover a Bi-Directional Coupler has the isolated is a four port network that has the isolated port externalized with either an RF connector or pin. One advantage of this type of coupler is that a higher power termination can be selected to suit higher input power requirements. The four port network can also act as a bi-directional coupler monitoring signals in both directions provided the coupled ports feed into a reasonably constant 50 Ohms impedance.

Implemented solution

The S-parameters Measuring System uses a Dual Directional 3-dB Quadrature Hybrid Coupler. This specific kind of coupler system is a four port network that is distinguished from the bi-directional types in that dual directional coupler is two independent four port network connected in series. It is better than the simple bi-directional coupler in that it provides higher isolation between coupled ports.

It was designed with lumped elements because our application required a size reduction and lumped or semi-lumped element devices requiring only a small area are very attractive. This proposed Dual Directional 3-dB Quadrature Hybrid Coupler is physically compact and is more convenient to circuit layout and it provides a wider bandwidth for power split in the quadrature phase, and it has a good matching and isolation (more than 50 dB) at the same time. In Figure 3.11 it is possible to see the coupler device circuit adopted for this system, after several trials, this topology reached the best performances and these values of the passive lumped elements that tuned perfectly the input frequency of 298 MHz.
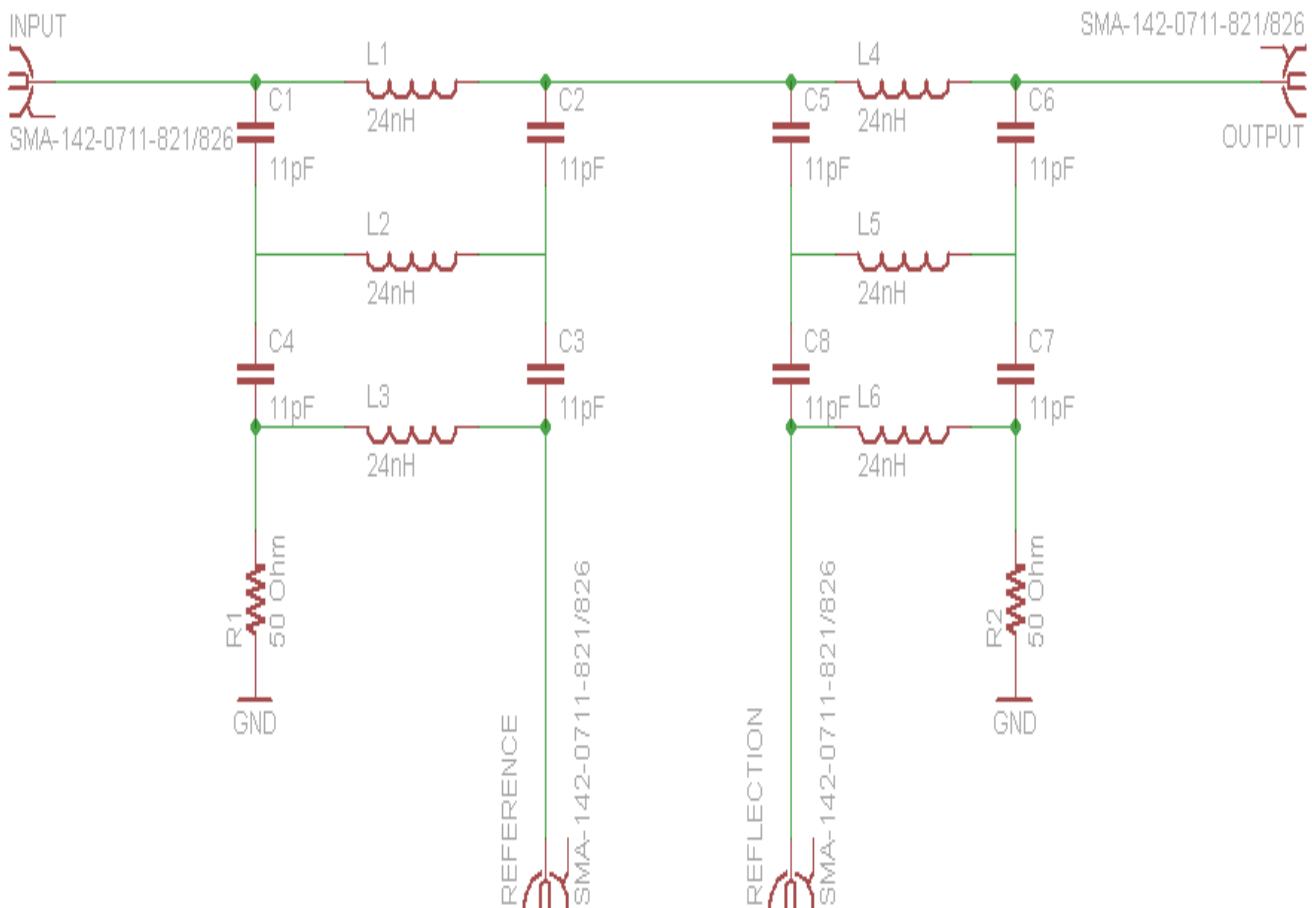
Figure 3.11: Proposed topology of a Dual Directional 3-dB Q-Hybrid Coupler with L= 24 nH and C=11 pF

The Directional Coupler is tuned for a very narrowband because in the quad hybrid coupler design there is an inevitable tradeoff between bandwidth and amplitude balance that affects overall unit complexity. For example, if satisfactory amplitude balance is to be preserved across a broader bandwidth, the immediate consequence is an increase in the required number of sections and lumped elements. With an increased number of components comes an increase in package complexity and size. This, in turn, increases insertion loss. As the package gets progressively larger, so also do the effects of stray capacitances and self-inductance. Also the coupling factor directly influences the flatness of the output power and in general, broadband couplers have high transmission losses (1dB).

3.3.3   Receiver that provides detection

General characteristics

There are two basic ways of providing signal detection in Network Analysers (Fig. 3.12):

- Diode detectors convert the RF signal level to a proportional DC level. If the signal is amplitude modulated (AC detection), the diode strips the RF carrier from the modulation. Diode detection is inherently scalar, as phase information of the RF carrier is lost.
- The tuned receiver uses a local oscillator (LO) to mix the RF down to a lower "intermediate" frequency (IF). The LO is either locked to the RF or the IF signal so that the receivers in the network analyzer are always tuned to the RF signal present at the input. The IF signal is bandpass filtered, which narrows the receiver bandwidth and greatly improves sensitivity and dynamic range.
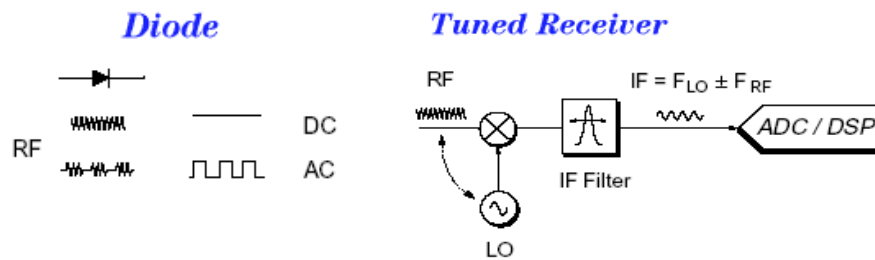
Figure 3.12: Diode VS Tuned receivers

Modern analysers use also an analog-to-digital converter (ADC) and digital-signal processing (DSP) to extract magnitude and phase information from the IF signal. The tuned-receiver approach can be used in scalar or vector Network Analysers. The main advantages of diode detectors are broadband frequency coverage (< 10 MHz on the low end to > 26.5 GHz at the high end, see Fig. 3.13) and they are inexpensive compared to a tuned receiver.


Figure 3.13: Diode detector

Diode detectors provide medium sensitivity and dynamic range: they can measure signals to - 50 dBm or so and have a dynamic range around 60 dB. Their broadband nature limits their sensitivity and makes them sensitive to source harmonics and other spurious signals. Dynamic range is improved in measurements by increasing input power. AC detection eliminates the DC drift of the diode as an error source, resulting in more accurate measurements. This scheme also reduces noise and other unwanted signals. The major benefit of DC detection is

that there is no modulation of the RF signal, which can have adverse effects on the measurement of some devices. Examples include amplifiers with large DC gain, and narrowband filters. One application where broadband diode detectors are very useful is measuring frequency-translating devices, particularly those with internal LOs. Tuned receivers provide the best sensitivity and dynamic range, and also provide harmonic and spurious-signal rejection. The narrow IF filter produces a considerably lower noise floor, resulting in a significant sensitivity improvement. For example, a microwave vector network analyzer (using a tuned receiver) might have a 3 kHz IF bandwidth, where a scalar analyzer's diode detector noise bandwidth might be 26.5 GHz (Fig. 3.14).
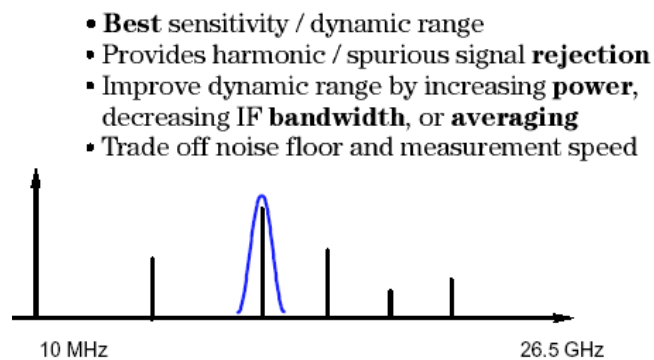
Figure 3.13: Tuned receiver

Measurement dynamic range is improved with tuned receivers by increasing input power, by decreasing IF bandwidth, or by averaging. The latter two techniques provide a tradeoff between noise floor and measurement speed. Averaging reduces the noise floor of the Network Analyser (as opposed to just reducing the noise excursions as happens when averaging spectrum analyser data) because we are averaging complex data. Without phase information, averaging does not improve analyser sensitivity. The same block diagram features that produce increased dynamic range also eliminate harmonic and spurious responses. As was mentioned earlier, the RF signal is downconverted and filtered before it is measured. The harmonics associated with the source are also downconverted, but they appear at frequencies outside the IF bandwidth and are therefore removed by filtering. Tuned

receivers can be implemented with mixer- or sampler-based front ends. It is often cheaper and easier to make wideband front ends using samplers instead of mixers, especially for microwave frequency coverage. The sampler uses diodes to sample very short time slices of the incoming RF signal. Conceptually, the sampler can be thought of as a mixer with an internal pulse generator. The pulse generator creates a broadband frequency spectrum (often referred to as a "comb") composed of harmonics of the LO. The RF signal mixes with one of the spectral lines (or "comb tooth") to produce the desired IF. Compared to a mixer-based Network Analyser, the LO in a sampler-based front end covers a much smaller frequency range, and a broadband mixer is no longer needed. The tradeoff is that the phase-lock algorithms for locking to the various comb teeth is more complex and time consuming. Sampler-based front ends also have somewhat less dynamic range than those based on mixers and fundamental LOs. This is due to the fact that additional noise is converted into the IF from all of the comb teeth. Network Analysers with narrowband detection based on samplers still have far greater dynamic range than analysers that use diode detection. Dynamic range (Fig. 3.15) is generally defined as the maximum power the receiver can accurately measure minus the receiver noise floor.

Figure 3.13: Dynamic range of Broadband detection VS Narrowband detection

There are many applications requiring large dynamic range. One of the most common are filter applications. In the case where the scalar Network Analyser was used with broadband

diode detection, a harmonic or subharmonic from the source created a "false" response. For example, at some point on a broadband sweep, the second harmonic of the source might fall within the passband of the filter. If this occurs, the detector will register a response, even though the stopband of the filter is severely attenuating the frequency of the fundamental. This response from the second harmonic would show on the display at the frequency of the fundamental. On the tuned receiver, a spurious response such as this would be filtered away and would not appear on the display.

A frequency mixer is a 3-port electronic circuit two of the ports are "input" ports and the other port is an "output" port. The ideal mixer "mixes" the two input signals such that the output signal frequency is either the sum (or difference) frequency of the inputs as shown in Fig. 3.14. In other words

$$f_{out} = f_{in1} \pm f_{in2} \tag{3.3}$$

The nomenclature the 3 mixer ports are the Local Oscillator (LO) port, the RF and the Intermediate Frequency (IF) port. The LO port is typically driven with either sinusoidal continuous wave (CW) signal or a square wave signal. The choice to apply a CW depends on the application and the mixer. Conceptually, the LO signal as the "gate" of the mixer in the sense that the mixer can be considered "ON" when the LO is a large voltage and "OFF" when the LO is a small voltage. The LO port is exclusively used as an input port.
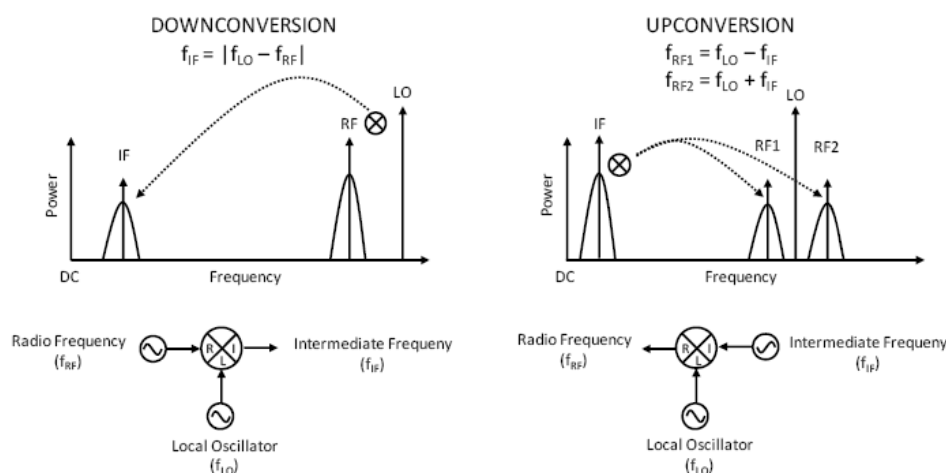
Figure 3.14: Definitions of downconversion and upconversion.

The other two ports of the mixer, the RF and IF, can be interchanged as either the second input or the output the actual configuration depends on the application. When the desired output frequency is lower than the second input frequency, then the all process is called downconversion and the RF is the input and the IF is the output. The relationship between input and output is given by:

$$f_{IF} = |f_{LO} - f_{RF}| \qquad (3.4)$$

On the other hand, when the desired output frequency is higher than the second input frequency, then the process is called upconversion and the IF is the input and the RF is output. A frequency domain representation of downconversion and upconversion is illustrated in Fig. 3.14. Take careful note of the upconversion case, the close proximity of the sum and difference frequencies (f_{RF1} and f_{RF2}) in the frequency domain implies that both a re-available at the RF output port. This type of upconversion is known as double sided upconversion.

Implemented solution

Single upconversion is also possible, in which case either the sum or the difference frequency is intentionally cancelled inside the mixer. Mixers that perform this more sophisticated functionality are called single sideband (SSB) upconverters (or single sideband modulators). As Fig. 3.14 depicts, IF/RF signals tend to be information bearing signals (as denoted by broadened spectra surrounding the RF and IF center frequencies). During frequency conversion, the information carried by the RF (IF) signal is frequency translated to the IF (RF) output. Therefore, mixers perform the critical function of translating in the frequency domain.

In this S-parameters Measuring System are used two mixers AD8343 to downconvert the RF to a lower "intermediate" frequency (IF). In particular the two RF inputs are the two output signals of the Directional Coupler, the first one is the Forward wave and the other one is the Reflected wave. both of the signals have the typical frequency used for the 7 Tesla MRI $f_{RF} = 298$ MHz. Instead the for the LO was used a frequency $f_{LO} = 298,3$ MHz . In this way we can use the

mixers to obtain as output a frequency f_{IF}=300 KHz (Fig. 3.15), that are more desirable to filter and process compare with a very high frequency of MHz.
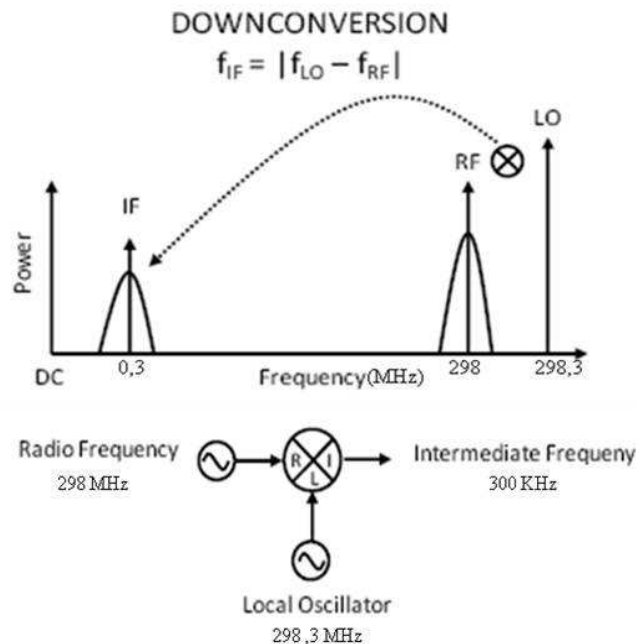
Figure 3.14: Downconversion of the S-parameters Measuring System

A serious problem that this new System had to face and solve was to make the two mixers work in a continuous magnetic field (MRI room). The first schematic used for the two mixers was designed to reach the best tradeoff between a good signal as output of the mixer and the simplicity and relatively small area occupied by the mixer itself. For this reason the schematic was designed with three baluns (each balun for every port). All of them were made with wire-wound transformers. The first two baluns were at the two input with a 1:1 impedance ratio and the third one was at the output with a 4:1 impedance ratio (see Appendix A). In the design of mixers baluns are used to link a symmetrical (balanced) circuit to a asymmetrical (unbalanced) circuit. Baluns are designed to have a precise 180-degree phase shift, with minimum loss and equal balanced impedances. In power amplifiers loss of symmetry will degrade efficiency and the symmetrical port must be well isolated from ground to eliminate parasitic oscillations. The basic design of a balun consists of two 90-degree phasing lines that provide the required

180-degree split, and this involves the use of λ/4 and λ/2. A wire-wound transformer provides an excellent balun. Miniature wire-wound transformers are commercially available covering frequencies from low kHz to beyond 2GHz. Two coils on a ferrite rod can be used as a balun by winding the individual strands of enamelled wire comprising the coil very tightly together. This winding can take one of two forms: either the two windings must be wound such that the two form a single layer where each turn is touching each of the adjacent turns of the other winding; or the two wires are twisted together before being wound into the coil. The two windings are joined to become a single coil. The end of one of the windings on one side of the coil is connected to the end of the other winding on the other side of the coil. This point then becomes the ground for the unbalanced circuit. One of the remaining ends is connected to the ungrounded side of the unbalanced circuit, and one side of the balanced circuit. Finally, the other side of the balanced circuit is connected to the remaining end. When they are realized with a centre-tapped secondary winding, if grounded this provides a short circuit to even-mode (common-mode) signals whilst having no effect on the differential (odd-mode) signal.
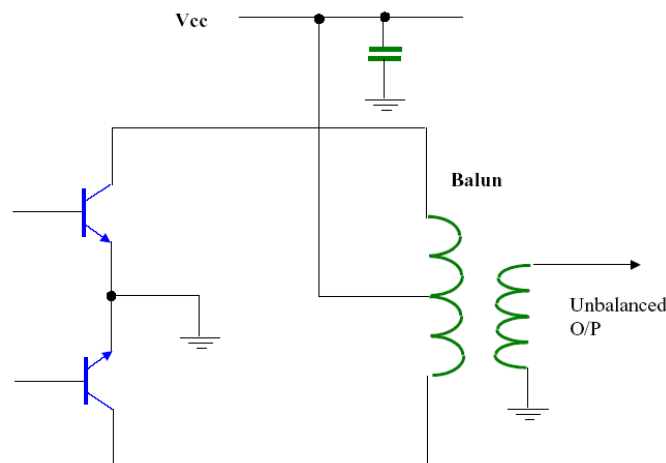
Figure 3.15: Use of a wire-wound balun on the output to provide a balanced to unbalanced conversion

Wire-wound transformers are more expensive than the printed or lumped element baluns and they are made with ferrite so they cannot be used within a magnetic field. For this reason the old baluns were substituted with lumped elements baluns, which find greater adoption in practical mixer designs. These lumped element and printed baluns do not provide the centre-tapped ground to even mode signals and this fact must be accounted for in the mixer design, but they can work in a continuous magnetic field with the same results of the previous kind of balun. The design of the balun adopted was the "L-C Balun". This design is essentially a bridge and is known as a 'lattice-type' balun. It consists of two capacitors and two inductors, which produce the ± 90 degree phase shifts. The diagram below (Figure 3.16) shows the circuit diagram of the Balun.
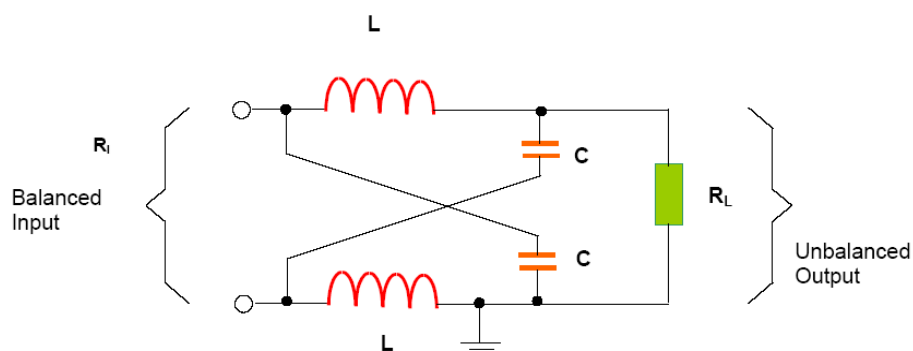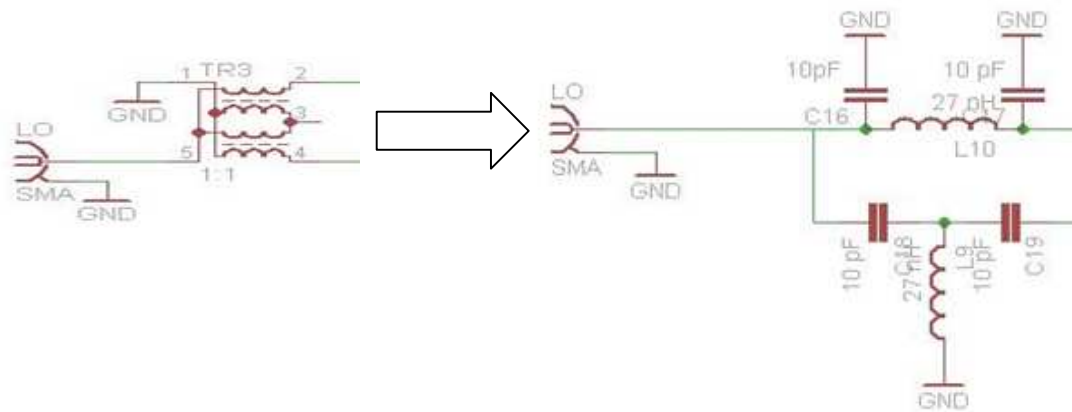

Figure 3.16: Schematic diagram of a L-C lumped balun.

When designing this circuit make sure that the operating frequency is well below the self-resonant frequencies of the components and take account of pad capacitances.

In the end the schematic of the 2 Mixers was modified and the three wire-wound baluns in the Input (Fig. 3.17), LO (Fig.3.18) and Output (Fig. 3.19), were substutited with lumped elements baluns and also it was added a differential amplifier to the Output to reach a bigger signal in magnitude (see Appendix B). The IF then signal is bandpass filtered (analogic filter), in this way was possible to narrow the receiver bandwidth and greatly improves sensitivity and dynamic range.
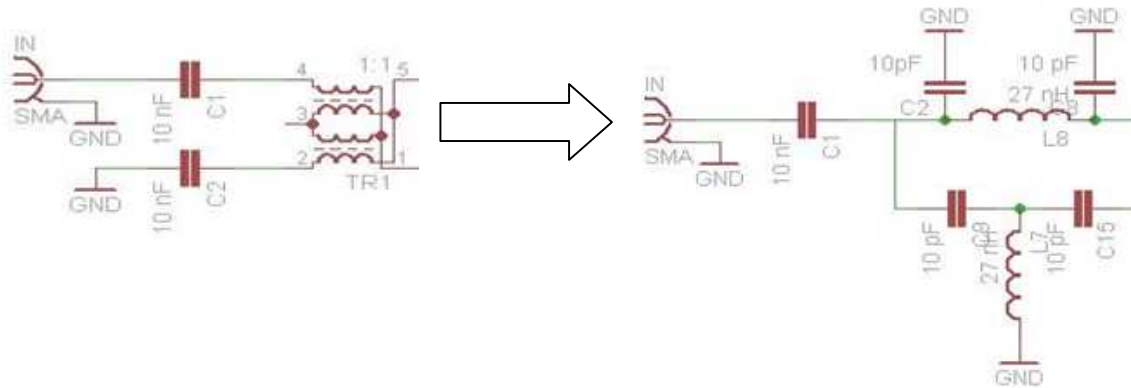
Figure 3.17: Sobstitution of the wire-wound balun with a lumped element balun

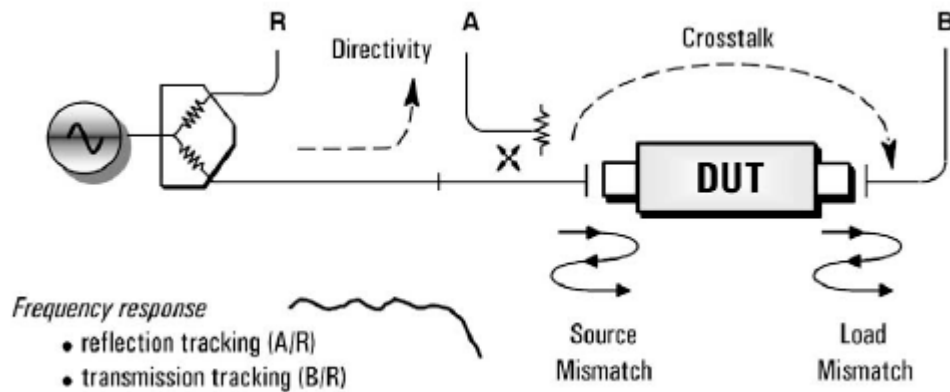**Figure 3.16**: Schematic diagram of a L-C lumped balun.

$$VO = (VIN(+) - VIN(-))(1 + RG2/RG1)$$
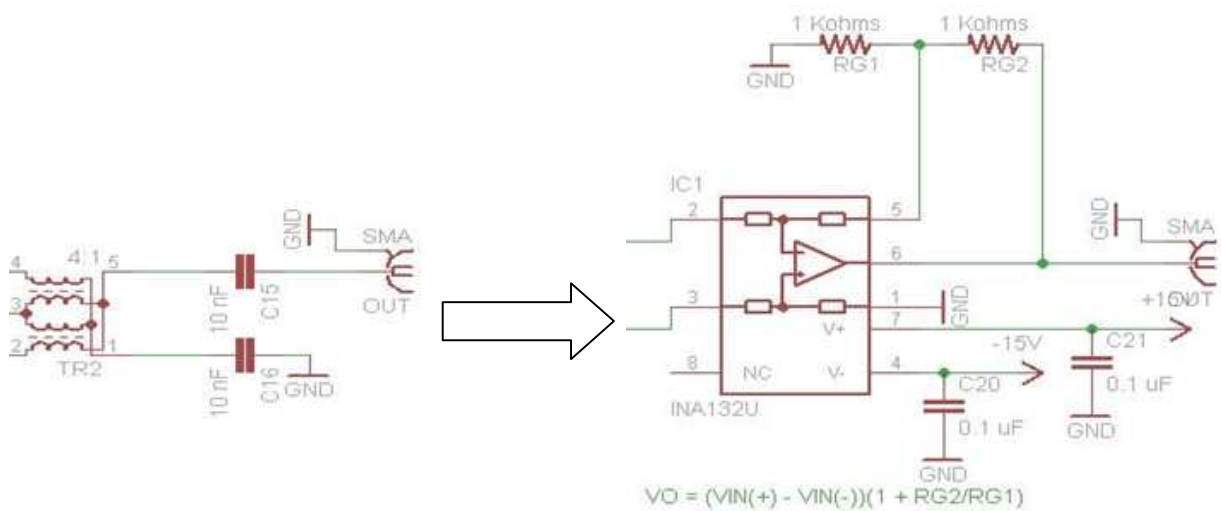
Figure 3.16: Schematic diagram of a L-C lumped balun.

3.3.4 Processor/Display for calculating and reviewing the results

General characteristics

The last major block of hardware in the Network analyser is the display/processor section. This is where the reflection and transmission data is first measured and calculated, then it is formatted in ways that make it easy to interpret the measurement results. Most Network Analysers have similar features such as linear and logarithmic sweeps, linear and log formats, polar plots, Smith charts, etc. Other common features are trace markers, limit lines, and pass/fail testing. A modern scalar Network analyser has all of the components needed for reflection and transmission measurements built-in to the instrument, such as a synthesized source, a test set, and a large display. Some scalar Network analysers even have attributes of vector analysers such as narrowband detection and vector error correction (one-port and enhanced-response calibration). These instruments exhibit very high dynamic range and good measurement accuracy and they are essential for the correction of the measurements errors. Let us look at the three basic sources of measurement error: systematic, random and drift. Systematic errors are due to imperfections in the analyser and test setup. They are repeatable (and therefore predictable), and are assumed to be time invariant. Systematic errors are characterized during the calibration process and mathematically removed during measurements. Random errors are unpredictable since they vary with time in a random fashion. Therefore, they cannot be removed by calibration. The main contributors to random error are instrument noise (source phase noise, sampler noise, IF noise). Drift errors are due to the instrument or test-system performance changing *after* a calibration has been done. Drift is primarily caused by temperature variation and it can be removed by further calibration(s). The timeframe over which a calibration remains accurate is dependent on the rate of drift that the test system undergoes in the user's test environment. Providing a stable ambient temperature usually goes a long way towards minimizing drift. Shown in Fig. 3.20 are the major systematic errors associated with network measurements. The errors relating to signal leakage are directivity and crosstalk. Errors related to signal reflections are source and load match. The final class of errors are related to frequency response of the receivers, and are called reflection and transmission tracking. The full two-port error model includes

all six of these terms for the forward direction and the same six (with different data) in the reverse direction, for a total of twelve error terms. This is why we often refer to two-port calibration as twelve-term error correction.

Figure 3.20: Schematic diagram of a L-C lumped balun.

The two main types of error correction that can be done are response (normalization) corrections and vector corrections. Response calibration is simple to perform, but only corrects for a few of the twelve possible systematic error terms (the tracking terms). Response calibration is essentially a normalized measurement where a reference trace is stored in memory, and subsequent measurement data is divided by this memory trace. A more advanced form of response calibration is open/short averaging for reflection measurements using broadband diode detectors. In this case, two traces are averaged together to derive the reference trace. Vector-error correction requires an analyser that can measure both magnitude and phase. It also requires measurements of more calibration standards. Vector-error correction can account for all the major sources of systematic error and can give very accurate measurements. Note that a response calibration can be performed on a vector Network Analyser, in which case we store a complex (vector) reference trace in memory, so that we can display normalized magnitude or phase data. This is not the same as vector-error correction however (and not as accurate), because we are not measuring and removing the individual systematic errors, all of which are complex or vector quantities.

Vector-error correction is the process of characterizing systematic error terms by measuring known calibration standards, and then removing the effects of these errors from subsequent measurements. One-port calibration is used for reflection measurements and can measure and remove three systematic error terms (directivity, source match, and reflection tracking). Full two-port calibration can be used for both reflection and transmission measurements, and all twelve systematic error terms are measured and removed. Two-port calibration usually requires twelve measurements on four known standards (short- open- load- through or SOLT). Some standards are measured multiple times (e.g., the through standard is usually measured four times). The standards themselves are defined in a cal-kit definition file, which is stored in the Network Analyser. Agilent Network analysers contain all of the cal-kit definitions for our standard calibration kits. In order to make accurate measurements, the cal-kit definition must match the actual calibration kit used! If userbuilt calibration standards are used (during fixtured measurements for example), then the user must characterize the calibration standards and enter the information into a user cal-kit file. Sources of more information about this topic can be found in the appendix.

Reflection: One-Port Model

Taking the simplest case of a one-port reflection measurement, we have three systematic errors and one equation to solve in order to calculate the actual reflection coefficient from the measured value. In order to do this, we must first calculate the individual error terms contained in this equation. We do this by creating three more equations with three unknowns each, and solving them simultaneously. The three equations come from measuring three known calibration standards, for example, a short, an open, and a Z_0 load. Solving the equations will yield the systematic error terms and allow us to derive the actual reflection S-parameter of the device from our measurements (Fig 3.21). When measuring reflection two-port devices, a one-port calibration assumes a good termination at port two of the device. If this condition is met (by connecting a load calibration standard for example), the one-port calibration is quite accurate. If port two of the device is connected to the Network Analyser and the reverse isolation of the DUT is low (for example, filter passbands or cables), the assumption of a good load termination is not valid. In these cases,

two-port error correction provides more accurate measurements. An example of a Two-Port device where load match is not important is an amplifier. The reverse isolation of the amplifier allows One-Port calibration to be used effectively.
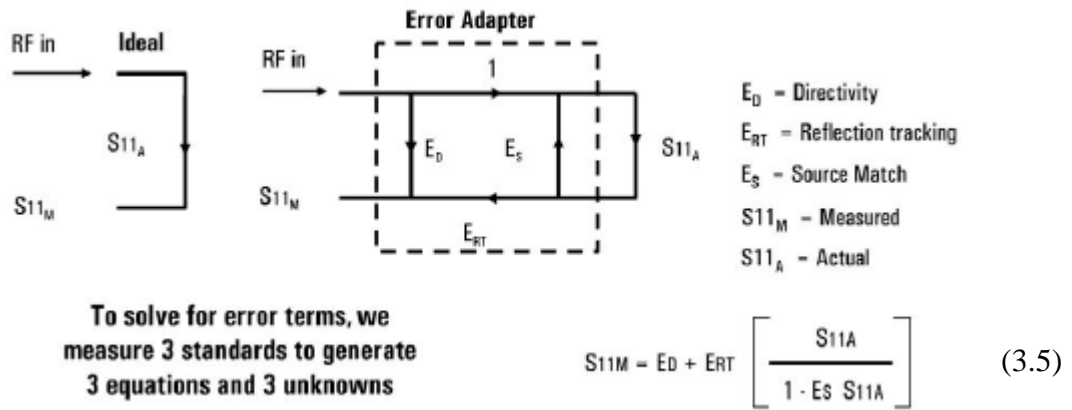

$$S_{11M} = E_D + E_{RT} \left[\frac{S_{11A}}{1 - E_S\, S_{11A}} \right] \quad (3.5)$$

Figure 3.21: One-Port Error Correction.

Two-Port Error Correction

Two-port error correction is the most accurate form of error correction since it accounts for all of the major sources of systematic error. The error model for a two-port device is shown in Fig. 3.22. Shown below are the equations to derive the actual device S-parameters from the measured S-parameters, once the systematic error terms have been characterized. Notice that each actual S-parameter is a function of all four measured S-parameters. The Network Analyser must make a forward and reverse sweep to update any one S-parameter.
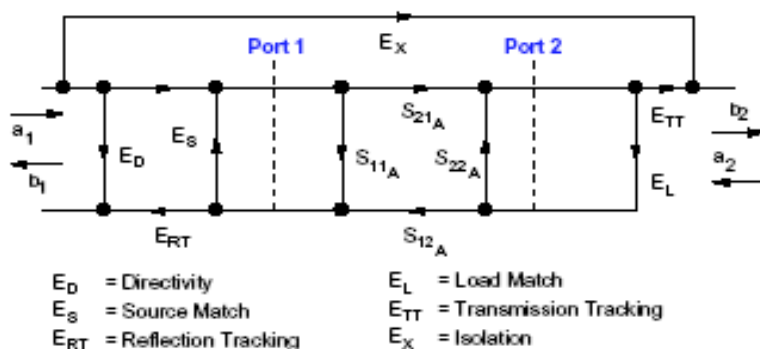
Figure 3.22: Two-Port Error Correction.

The formulas to compute each S-parameter with a Two-Port Correction are*:

$$S_{11a} = \frac{(\frac{S_{11m}-E_D}{E_{RT}})(1+\frac{S_{22m}-E_D'}{E_{RT}'}E_S')-E_L(\frac{S_{21m}-E_X}{E_{TT}})(\frac{S_{12m}-E_X'}{E_{TT}'})}{(1+\frac{S_{11m}-E_D}{E_{RT}}E_S)(1+\frac{S_{22m}-E_D'}{E_{RT}'}E_S')-E_L'E_L(\frac{S_{21m}-E_X}{E_{TT}})(\frac{S_{12m}-E_X'}{E_{TT}'})} \quad (3.6)$$

$$S_{21a} = \frac{(\frac{S_{21m}-E_X}{E_{TT}})(1+\frac{S_{22m}-E_D'}{E_{RT}'}(E_S'-E_L'))}{(1+\frac{S_{11m}-E_D}{E_{RT}}E_S)(1+\frac{S_{22m}-E_D'}{E_{RT}'}E_S')-E_L'E_L(\frac{S_{21m}-E_X}{E_{TT}})(\frac{S_{12m}-E_X'}{E_{TT}'})} \quad (3.7)$$

$$S_{12a} = \frac{(\frac{S_{12m}-E_X'}{E_{TT}'})(1+\frac{S_{11m}-E_D}{E_{RT}}(E_S-E_L'))}{(1+\frac{S_{11m}-E_D}{E_{RT}}E_S)(1+\frac{S_{22m}-E_D'}{E_{RT}'}E_S')-E_L'E_L(\frac{S_{21m}-E_X}{E_{TT}})(\frac{S_{12m}-E_X'}{E_{TT}'})} \quad (3.8)$$

$$S_{22a} = \frac{(\frac{S_{22m}-E_D'}{E_{RT}'})(1+\frac{S_{11m}-E_D}{E_{RT}}E_S)-E_L'(\frac{S_{21m}-E_X}{E_{TT}})(\frac{S_{12m}-E_X'}{E_{TT}'})}{(1+\frac{S_{11m}-E_D}{E_{RT}}E_S)(1+\frac{S_{22m}-E_D'}{E_{RT}'}E_S')-E_L'E_L(\frac{S_{21m}-E_X}{E_{TT}})(\frac{S_{12m}-E_X'}{E_{TT}'})} \quad (3.9)$$

*See article: *Applying Error Correction to Network Analyzer Measurements*, [42].

Implemented solution

The Processor used for the new System, shown in Fig. 3.23, is the **PIC32MX795F512L** with:

- MIPS32® M4K™ 32-bit core with 5-stage pipeline

- 100 Pins (soldered manually with the help of a microscope, State of Art of this lab);

- Operating voltage range of 2.3V to 3.6V;

- Internal 8 MHz and 32KHz oscillators;

- Five 16-bit Timers/Counters (two 16-bit pairs combine to create two 32-bit timers) ;

- 16channels, 10-bit Analog-to-Digital Converter (ADCs);

- 6 UART modules with: RS-232, RS-485 and LIN 1.2 support;

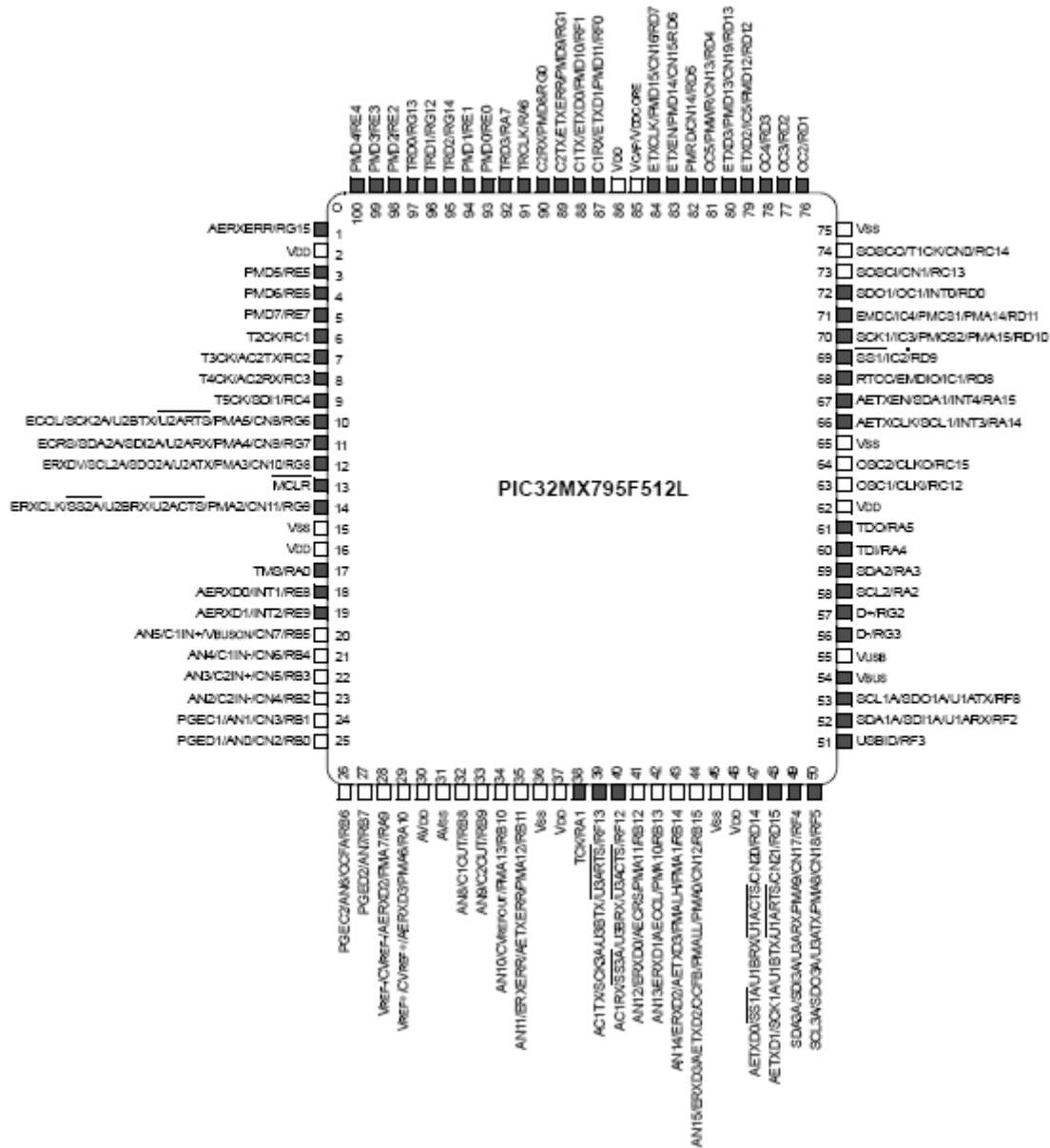- CPU with 80 MHz maximum frequency.

Figure 3.23: Pin Diagram of the PIC

 The system used for the sampling of the two signals is the Alternating Sample Mode. In this system it is used only one ADC with two input MUXs, These MUXs are used to select which analog input has to be sampled. During the Alternating Input Selections the module alternates between the MUX A inputs on one sample and the MUX B inputs on the subsequent sample. Then the pattern repeats. On this way it is possible to sample two channels at the same time and save a lot of time. The output signals of 400 KHz of frequency of the 2 Mixers are respective connected with the two input channels connected with MUX A and MUX B of the PIC and selected for the Alternating sample mode. The

Algorithm implemented in the PIC with the software MPLAB© has a maximum sampling frequency for the ADCs of the two input channels that is 30 KHz. For this reason the FORWARD and REFLECTED waves are sampled with the Undersampling technique. The Undersampling or violating the Nyquist criterion is a technique often utilized in ADC applications, RF communications and high performance test equipment. This is a 'grey' area and confusion often arises over the necessity to obey Nyquist in order to retrieve the information content of a signal. Examination of both the Nyquist and Shannon theorems will demonstrate that the choice of ADC sampling frequency has a strong correlation to the ratio of maximum input signal frequency to input signal bandwidth. Nyquist theorem states that to reconstruct an analogue signal waveform without error from sample point taken at equal time intervals, the sampling frequency must be greater than or equal to twice the highest frequency component in the analogue signal. In practice, analogue signals are not simple sine waves and usually have complex waveforms with components or harmonics at many frequencies. Therefore to reliably reproduce a square wave from time-interleaved samples, the sampling frequency according to Nyquist must be many times higher than the square wave's fundamental frequency. Sampling an analogue signal f_a, at a sampling rate f_s, actually produces two aliased components, one at $f_s + f_a$ and the other at $f_s - f_a$. The frequency domain representation of this is shown in Figure 3.24.
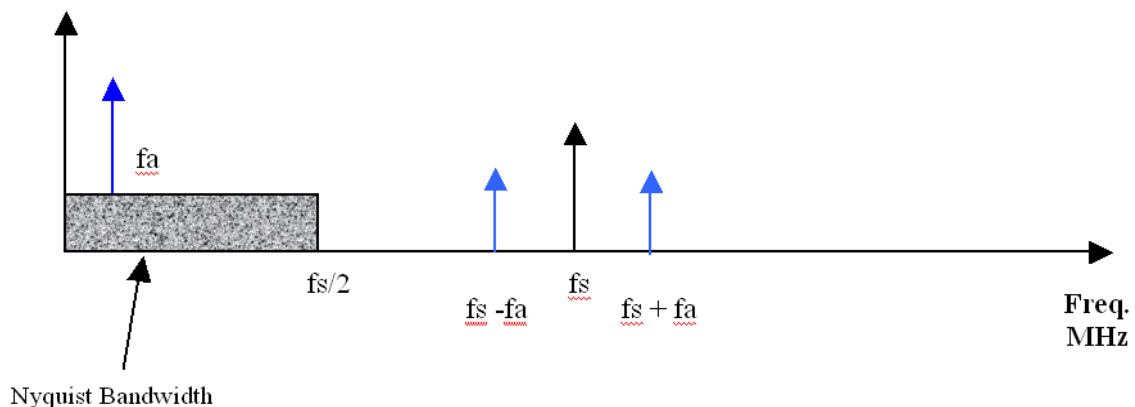
Figure 3.24: Signal Sampling Produces Aliased Components

Generally, it is only the lower alias component which may cause problems because it can fall within the Nyquist bandwidth and corrupt wanted signals. Based on the aliasing phenomenon of sampling systems the Nyquist criteria requires sampling at a rate of $f_s > f_a$

in order to avoid overlapping aliased components into the first Nyquist zone. To prevent unwanted interference, any signals which fall outside the bandwidth of interest should be filtered before sampling. This explains the necessity for anti-alias filters in many sampling systems. However, methods exist which use aliasing to one's advantage in signal processing applications. One can quickly see the limitations implied by the Nyquist theorem. Nyquist assumes that the desired information bandwidth is equal to the Nyquist bandwidth or half the sampling frequency. It should be observed that the required minimum sampling frequency is actually a function of the input signal bandwidth. Shannon's theorem examines this further. An analogue signal with a bandwidth f_b, must be sampled at a rate of $f_s > 2f_b$ in order to avoid the loss of information. The signal bandwidth may extend from DC to f_b (baseband sampling) or from f_1 to f_2 where $f_b = f_2 - f_1$ (undersampling). So Shannon's theorem states that the actual minimum required sampling frequency is a function of the signal bandwidth and not only its maximum frequency component. In general the sampling rate must be at least twice the signal bandwidth and the sampled signal must not cross an integer multiple of $f_s/2$ to prevent overlapping of the aliased components. Note that for large ratios of f_{MAX} (maximum frequency component of the analog signal) to signal bandwidth B, the minimum sampling frequency approaches 2B. In many applications this greatly reduces the demand placed on the ADC required. Sampling a signal with a maximum signal frequency of 150MHz but with a bandwidth of 10MHz would require perhaps a 22 *msps* ADC instead of a bigger than 300 *msps* ADC as stipulated by Nyquist. Otherwise stated, due to harmonic folding or undersampling, every ADC input frequency component outside the Nyquist bandwidth is always folded back into the first Nyquist zone. Sub-sampling has many uses in practical electronic systems. One such popular application of undersampling is in digital receivers. Lets first explain in a little more detail the process of sub-sampling. The process of sub-sampling or folding can be thought of as mixing the ADC input signal with the sampling frequency and its harmonics. This means that many frequencies can be mixed down to DC and their original frequency can no longer be determined (Fig. 3.25). Sub-sampling cannot be used if the original input frequency must be determined at the ADC output. This is because the Nyquist criteria is violated. Sub-sampling still proves useful if there is no need to determine the carrier frequency at the ADC output.
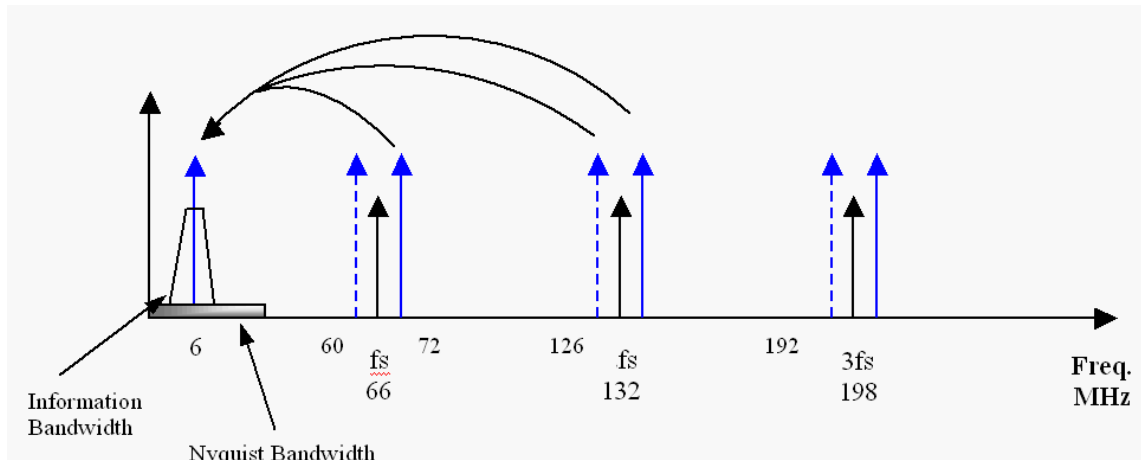
Figure 3.25: Many Frequencies are mixed down towards DC when Sub-Sampling

The process of sampling a signal outside the first Nyquist zone is often referred to as *Undersampling*, or *harmonic sampling*. Note that the first Nyquist zone image contains all the information in the original signal, with the exception of its original location. Notice also that there is no mention in the Shannon's theorem of the absolute *location* of the band of sampled signals within the frequency spectrum relative to the sampling frequency. The only constraint is that the band of sampled signals be restricted to a *single* Nyquist zone, i.e., the signals must not overlap any multiple of $f_s/2$. For example supposed that the signal frequency of the input is $f_{in} = 36$ MHz and the sampling frequency is $f_s = 20$ MHz. This is the case shown in Fig 3.26 where $f_{in} > f_s$, for this reason the best choice is to use the Undersampling technique and it is easy to note that the harmonic $2f_s - f_{in} = 4$MHz is inside the first Nyquist zone and contain all the information of the original signal. So it is clear that choosing the correct sampling rate ADC for an application requires more than just knowledge of the highest analogue frequency for conversion. Shannon's theorem demonstrates that signal bandwidth is of equal importance. We have also discovered that sampling at greater than the Shannon rate brings other benefits such as vast improvements in dynamic range brought about by processing gain. Armed with this knowledge, a system designer can make the right choice for ADC sampling frequency and resolution based upon readily available and affordable standard ADCs.
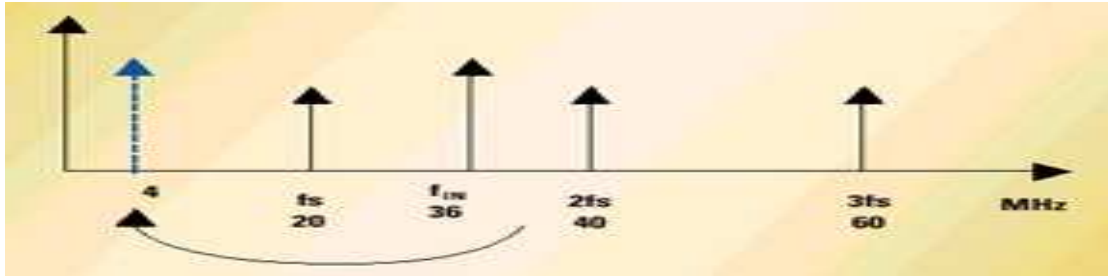
Figure 3.26: Undersampling technique

Then all the harmonics associated with the two signals are also removed by digital filtering. Then, after the conversion and filtration of the signals of the two channels, the Algorithm finds the max and the min values of the two sinusoids and it computes the mean value of the reflected signal with:

$$(\text{max} + \text{min}) / 2 \qquad (3.10)$$

This value is called "offset" and it is used as a reference to compute the Phase of the S-parameter as the phase shift for both signals. The phase shift is computed as the difference between two values. These values represent the two times when the sinusoid goes through the offset and it is increasing (from a value smaller than the offset to a value bigger than the offset). So it is possible to see the phase shift as:

$$\text{phase shift} = t_2 - t_1 \qquad (3.11)$$

with t_2 as the time when the FORWARD wave is passing through the offset and t_1 as the time when the REFLECTED wave is passing to the offset. Then it is compute the Modulus of the S-parameter such as the amplitude of the REFLECTED wave divided by the amplitude of the FORWARD wave:

$$\text{modulus} = (\text{max1-min1})/(\text{max2-min2}) \qquad (3.12)$$

with max1 and min1 as respectively the maximum and the minimum values of the REFLECTED wave and max2 and min2 as respectively the maximum and the minimum values of the FORWARD wave. The Algorithm uses this process iteratively to compute the four Phases and the four Modulus of the four S-parameters needed for the One Port calibration. Every time that the process is repeated what changes is the impedance acquired by the system. First is acquired the Phase and Modulus values of the S-parameter without the calibration and then the three Phases and Modulus values of the S-parameters with an impedance respectively equal to a Short, Open and Z_0 (characteristic impedance). Last but not the least there is an external PC connected with the Processor through an optic fiber. Thanks to this connection the System can send for the One Port Error Correction all four S-parameters measurements to the PC. Then all these values are collected and used for the computation of the S-parameter after the calibration and the impedance measurement. The software used to analyze and process the measurements was MATLAB©. The different measurements, done by the system during the calibration, were first saved in the PIC in a buffer and then sent all together through the optic fiber to the PC. Then thanks to MATLAB was possible to compute the three error terms E_D, E_{RT} and E_S and then the S-parameter calibrated after solving a system with 3 equations and three unknowns:

$$E_D = S_{load} \tag{3.13}$$

$$E_S = \frac{(2 \times S_{load}) - (S_{short} - S_{open})}{(S_{short} - S_{open})} \tag{3.14}$$

$$E_t = \frac{2 \times (S_{open} + S_{load}) \times (S_{short} + S_{load})}{(S_{short} - S_{open})} \tag{3.15}$$

with S_{load} as the S-parameter measured with an impedance equal to Z_0, S_{open} as the S-parameter measured with an open and S_{short} as the S-parameter measure with a short. Then the calibrated S-parameter is computed with the equation (3.5). Finally with the calibrated S-parameter it is easy to achieve the impedance value that is the result the system was designed for. Because the S-parameter computed belongs to an unique

Directional Coupler so it refers only to one impedance measurement of only one channel of the DUT and therefore it is called for example S_{11}. It is known with the relationship (2.21) that the S_{11} is equal to the reflection coefficient and from equation (2.23) it is trivial to obtain:

$$Z_l = \frac{Z_0\,(\Gamma_0 + 1)}{1 - \Gamma_0} \qquad (3.16)$$

with Γ_0 as the reflection coefficient and Z_l as the impedance at the load level, that it is the scope of the system. In Fig.3.27 it is shown the general schematic for this system
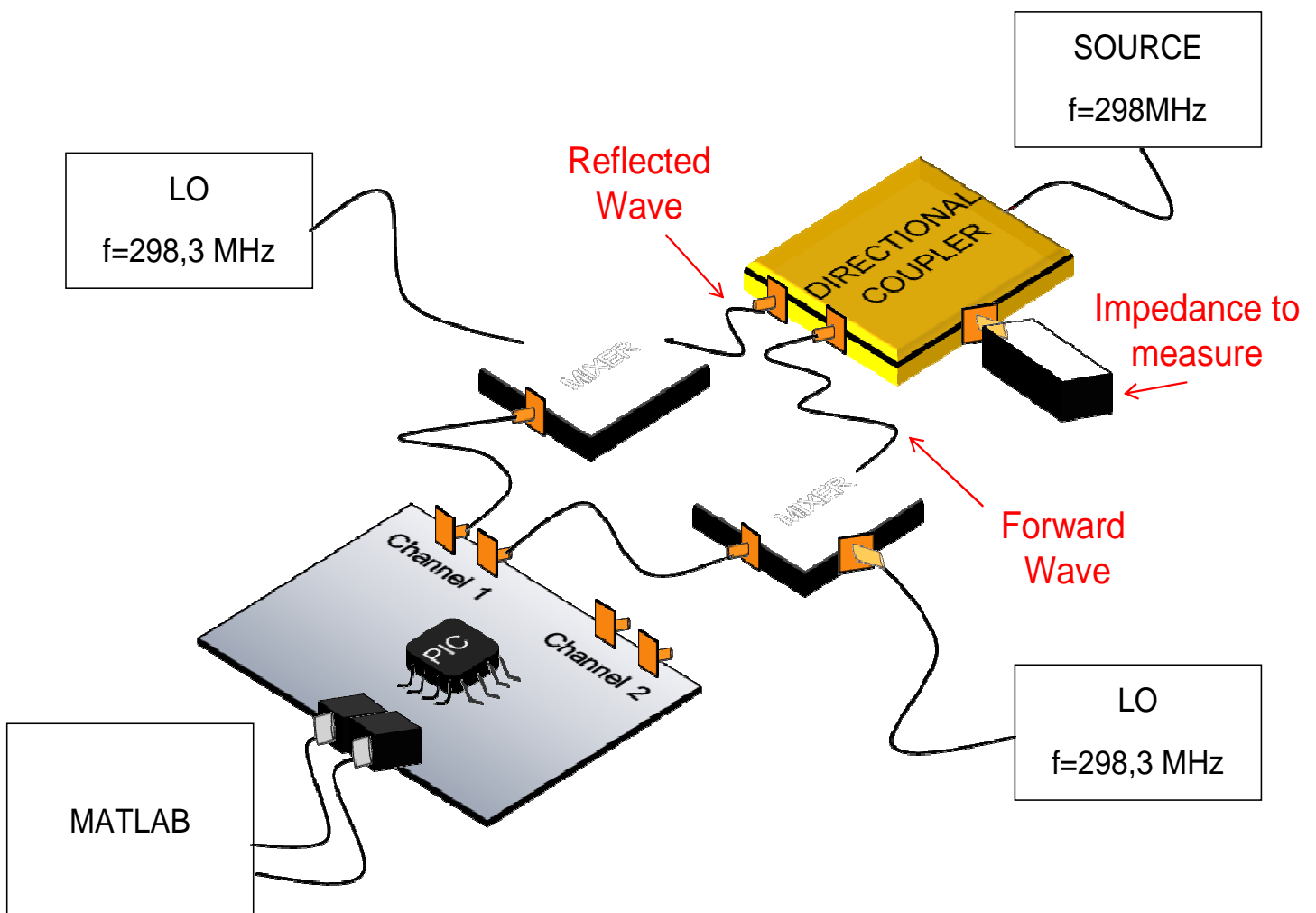
Figure 3.27: General view of the system implemented with all the most important parts: Sources (2 Local Oscillators and the source for the stimulus); Directional Coupler (hat splits the source signal in FORWARD and REFLECTED waves); Mixers (that downconvert both waves to an intermediate frequency); Processor (with the PIC inside); Display (with Matlab); Impedance to measure.
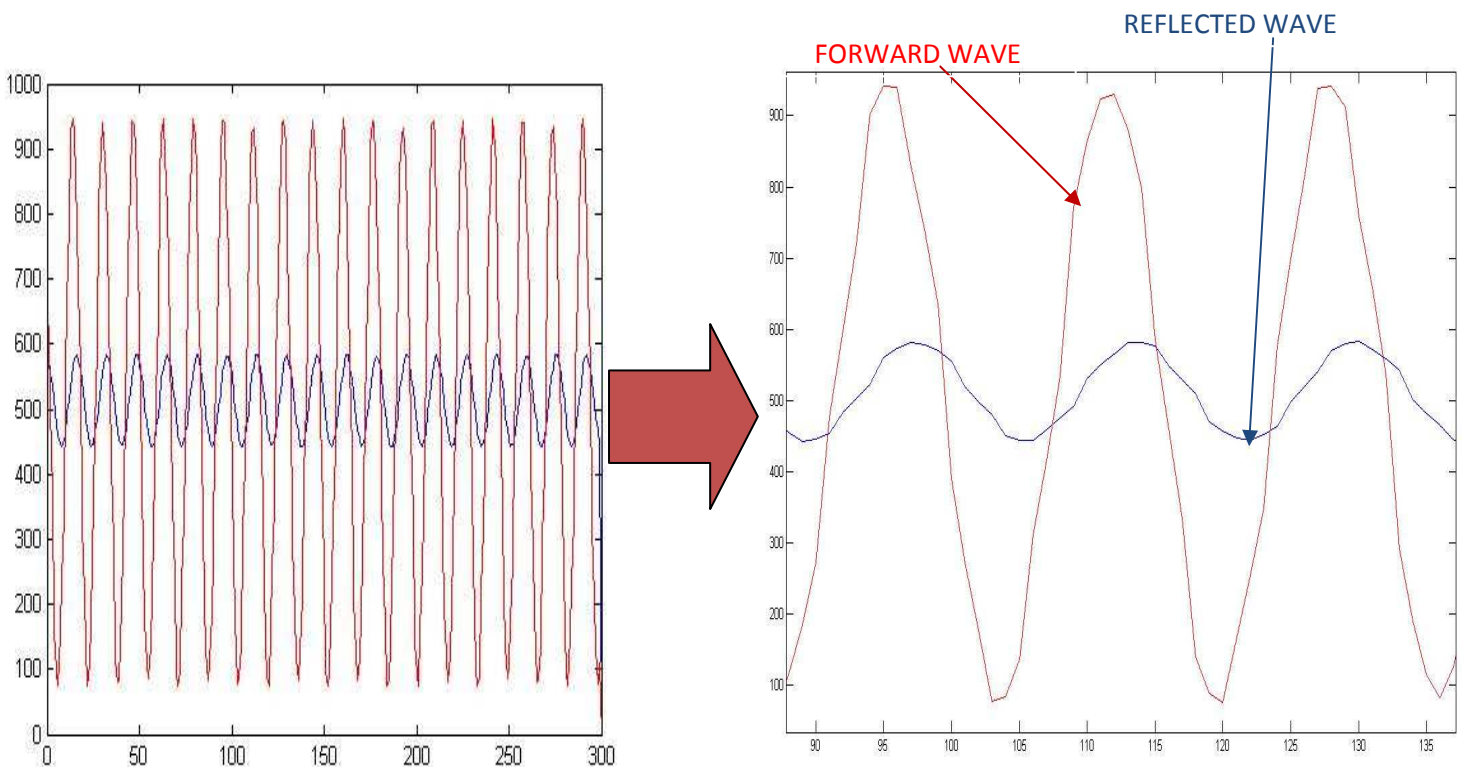
Chapter 4

Results and Conclusions

This Chapter shows and explains the different results obtained by a qualitative analysis, showing graphs and images of the signals, and a quantitative analysis of the probability, computing some important values to quantify the quality of the Scattering-Parameters measurement system for automatic matching network setup for MRI. First, it provides the filtering analysis of the FORWARD and REFLECTED waves from the mixers and connected with the processor part and the correspondent results after the digital filtration. Second, it describes how to apply One Port calibration and the error correction process to the impedance measurement to this system. Every time providing the output waves correspondent to every case of the calibration Short-Open-Load and it compares the values of the impedance measured before and after the calibration. In the third part, it compares the comparison of the measurements of 125 different impedances between the Network Analyser (considered the Gold Standard) and the new system implemented at the end of this part are also computed some basic probabilistic values to quantify how much the two setup differ from each other:

- Mean Value;

- Error Correction;

- Standard deviation.

Furthermore, there is a brief discussion about the results recorded by the compared measurements, in the MRI lab with the simulated changes of the impedance, of the S-Parameters Measurement System and the Network Analyser. The chapter concludes with the pros and cons of the system implemented in this thesis, the possible improvements and the future application of the system in a 7 Tesla MRI.

4.1 Digital Filtering

When arriving at the processor from the mixers, the two signals, FORWARD and REFLECTED, still contain a wide range of frequencies, not just one. The presence of these multiple frequencies with also harmonics can cause the instability of the two waves. Therefore, first, the two signals have been processed by the 10-bits ADCs and the analog signals became discrete numbers. Then, they are digitally filtered by a digital filter in the algorithm of the PIC. The 50th order filter, applied to both waves, permits, with only few lines of code, to have output signals without harmonics and increased stability. Depicted in Figures 4.1 and 4.2 are the two signals respective before and after filtering. As it is possible to see from these two images the filtered signals are much more stable and their bandwidths are narrower and without harmonics less noise, caused by the presence of several harmonics, that can affect the quality of the measurement procedure.

**Figure 4.3**: Original signals before digital filtering with several harmonica and not very stable;
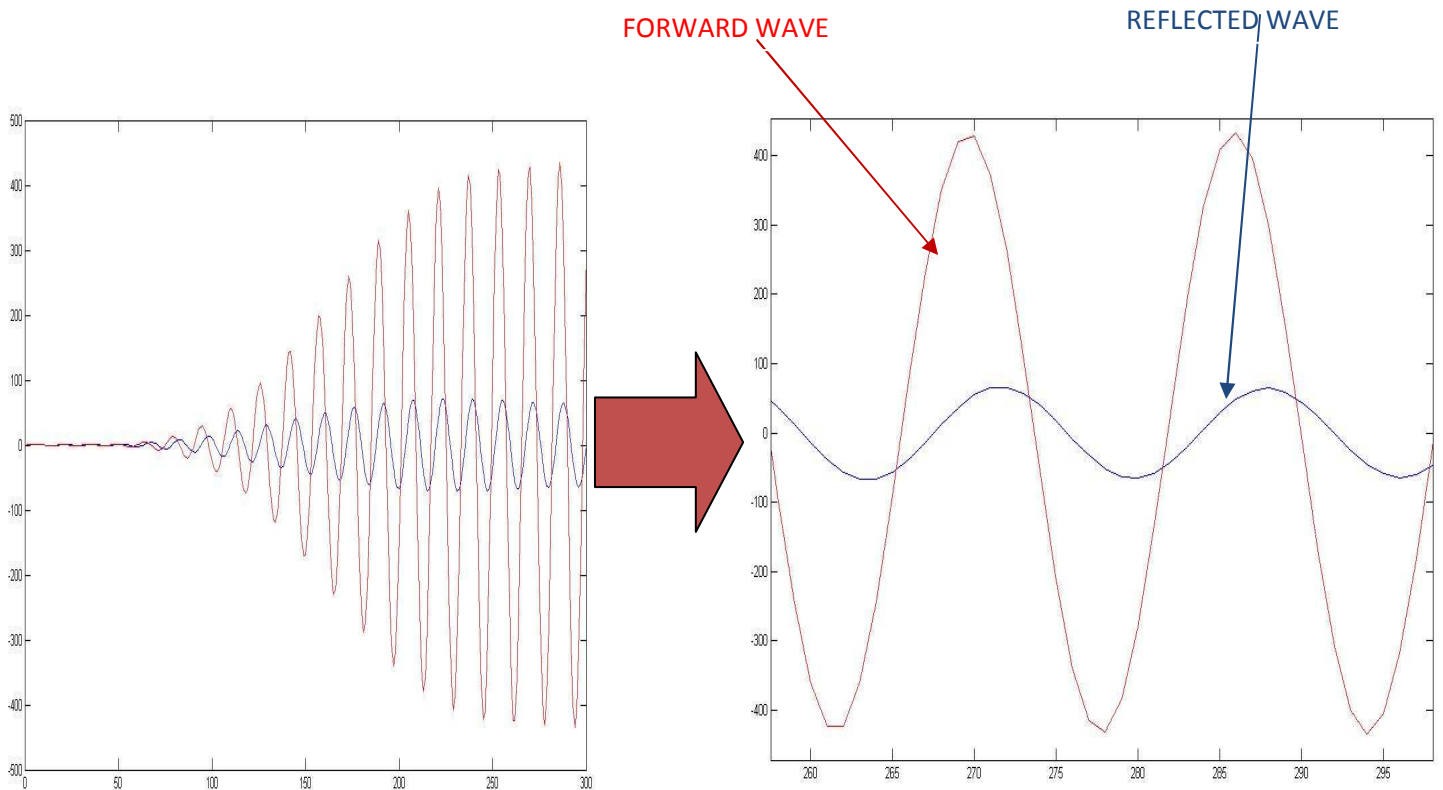
Figure 4.2: Filtered signals much more stable and without harmonics

4.2 System Calibration

As already described in Paragraph 3.4 of Chapter 3: The Algorithm used by the PIC iteratively computes the four Phases and the four Modulus of the four S-parameters needed for the One Port calibration. Every time the process is repeated what changes is the impedance acquired by the system in one of the input of the double hybrid. Following the Algorithm; it acquires the Phase and Modulus values of the S-parameter of the impedance to measure without the calibration, then the Algorithm acquires the two waves and computes the three Phases and Modulus values of the S-parameters with an impedance respectively equal to a Short, Open and Z_0 (characteristic impedance). To do the calibration, a specific standard calibration kit Short-Open-Load ha been used. In Figure 4.3, represents the three basic reference points needed for a One Port calibration. All these values, computed and saved in the PIC, are sent to the PC through optic fiber with UART modules RS-232.
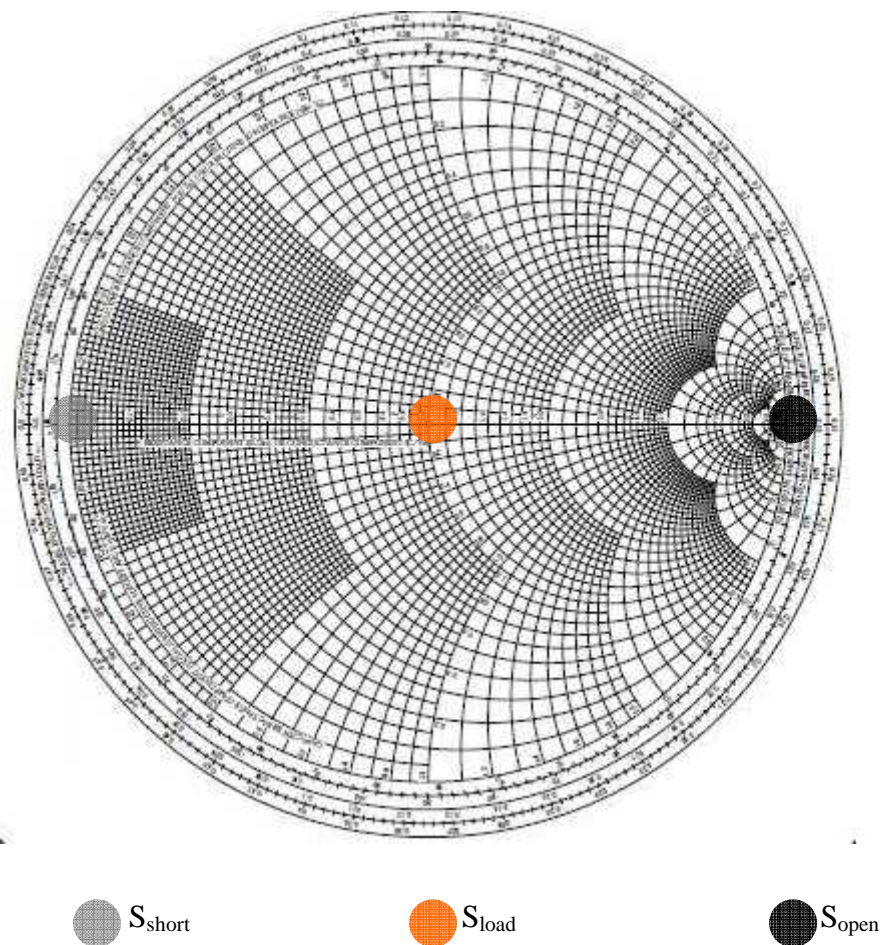
**Figure 4.3**:Basic reference points for One Port calibration

During the calibration the FORWARD and REFLECTED signals change the phases or the modulus according to the changes of the impedance at the input of the transmission line of the Directional Coupler. Below is described the three different behaviours of the two signals of the S-Parameters Measurement System when:

1) The transmission Line is terminated with Open reflects all the power back. In this case the reflection coefficient is equal to $\Gamma = 1$ (full reflection) and the impedance should be equal to $Z = 0$. The result signals have the modulus that doesn't change and they are in phase (Figure 4.4).
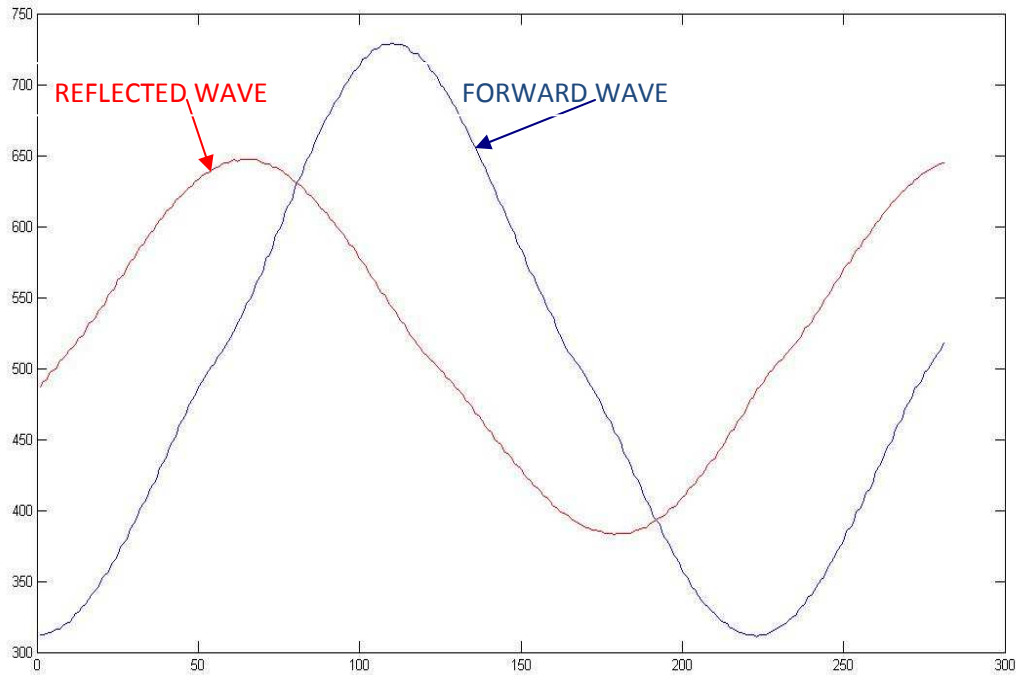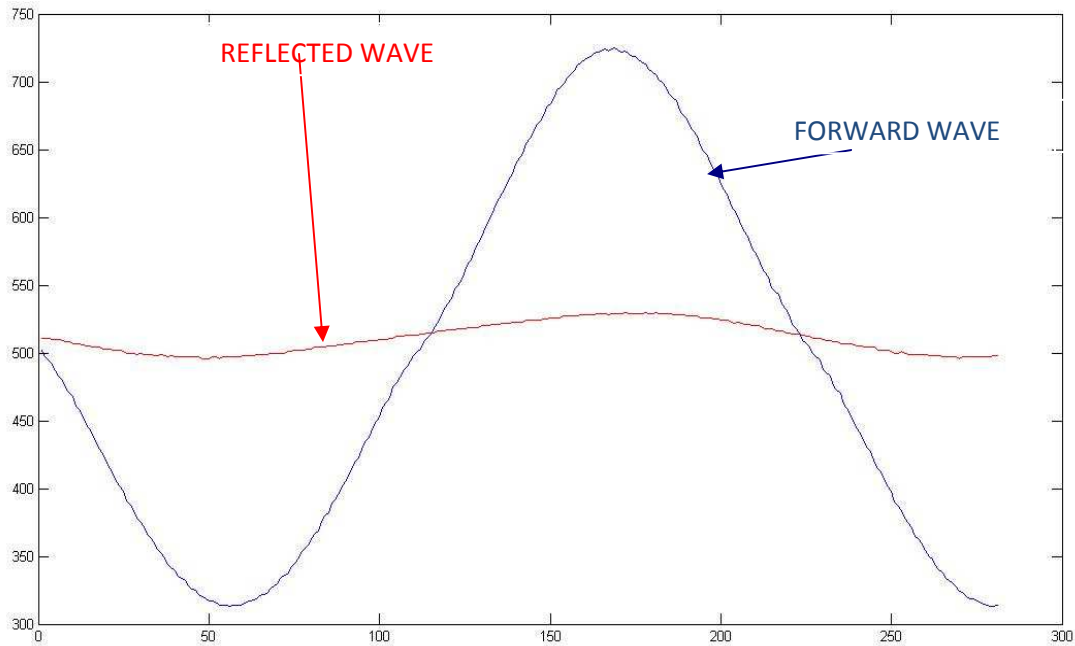
Figure 4.4: FORWARD (blue) and REFLECTED (red) waves when the transmission line is terminated with an Open

2) The transmission line is Short circuited and it reflects all the power back. In this case the reflection coefficient is equal to $\Gamma = 1$ and the impedance is equal to $Z = 0$. The resulted signals have the Modulus that do not change but they are out of phase by $180°$ (Figure 4.5).
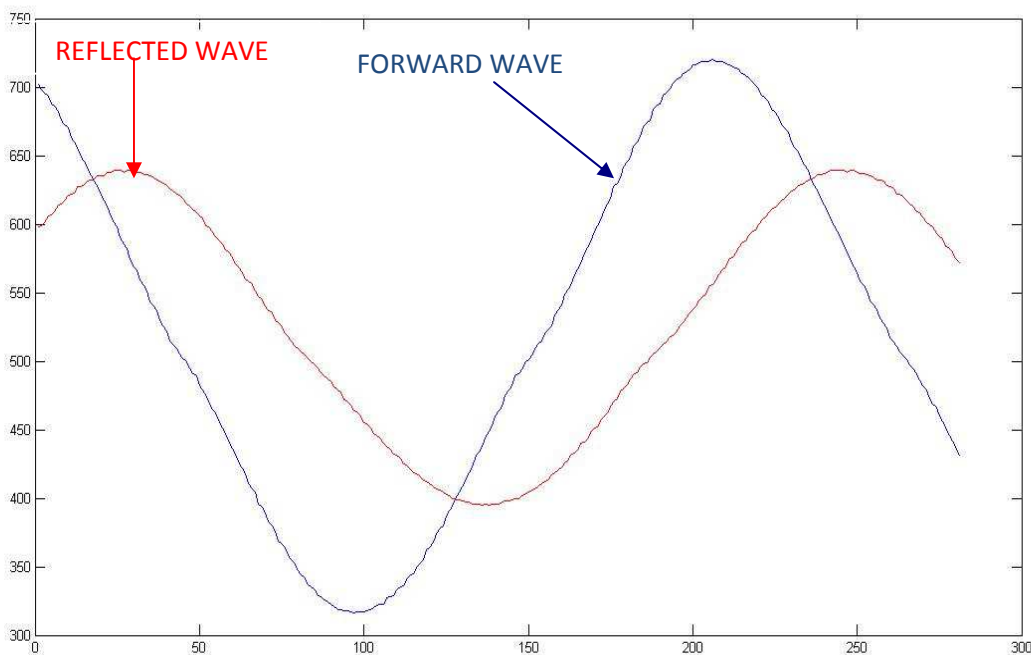

Figure 4.5: FORWARD (blue) and REFLECTED (red) waves when the transmission line is terminated Shorted

3) The transmission line is terminated with Z_0 and, in perfect conditions, all the incident power is absorbed in the load (Vrefl = 0). Experimentally, not all but almost all the power is reflected in the load. In this case the reflection coefficient is almost equal to $\Gamma = 0$ and the impedance is equal to $Z = Z_0$. The resulted signals have the Modulus of the FORWARD wave that doesn't change but the Modulus of the REFLECTED wave is almost equal to zero (Figure 4.6).


Figure 4.4: FORWARD (blue) and REFLECTED (red) waves when the transmission line is terminated with an Open

Then, thanks to the connection of the system between the processor part and the display, it is possible to send, for the One Port Error Correction, all four S-parameters measurements to the Computer. The different values of the S-parameters, done by the system during the calibration, have been used, with the software MATLAB, to compute the three error terms (E_D, E_{RT} and E_S) and then the S-parameter calibrated after solving a system with the 3 equations and three unknowns (3.13), (3.14), (3.15). Once these three terms are known, the calibrated S-parameter is computed with the equation (3.5). Here below there are three examples of comparisons between the S-parameter measurements done with and without calibration. Where: S_{load} is the S-parameter measured with an impedance equal to Z_0; S_{open} is the S-parameter measured with an open; S_{short} is the S-parameter measure shorted.
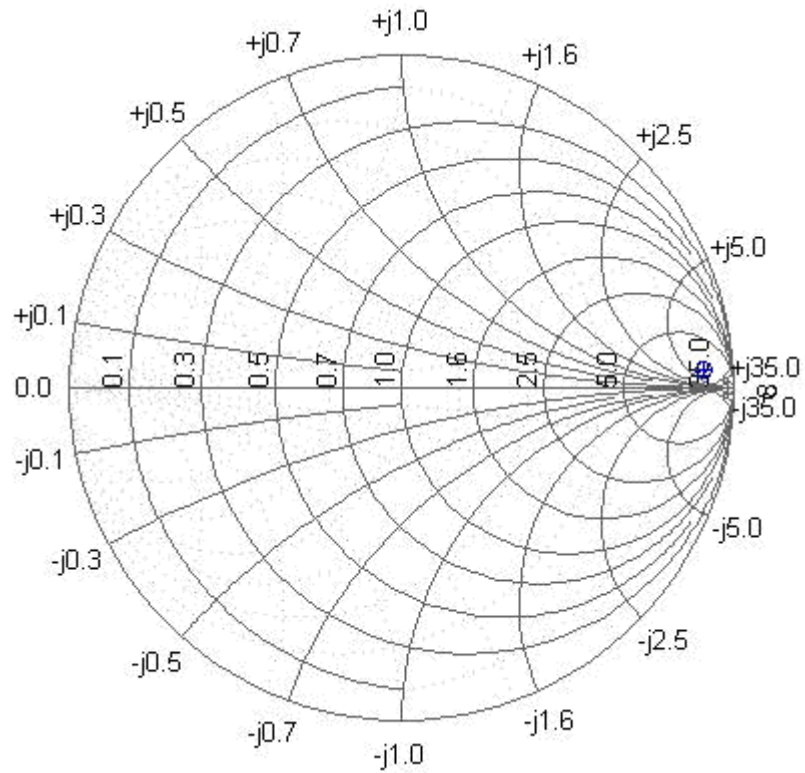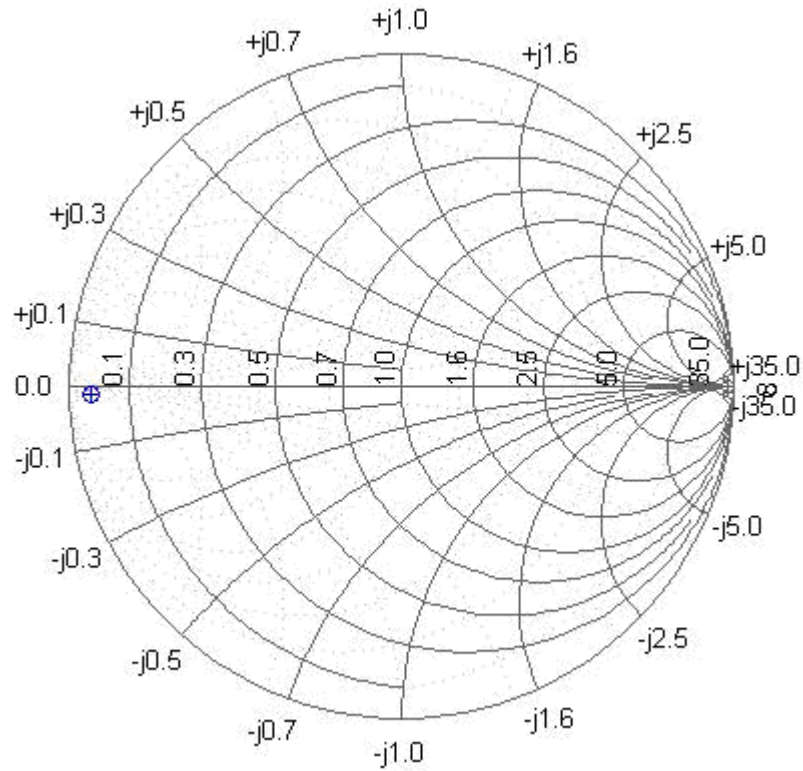
Figure 4.5: S-parameter of a open circuit measured WITHOUT calibration
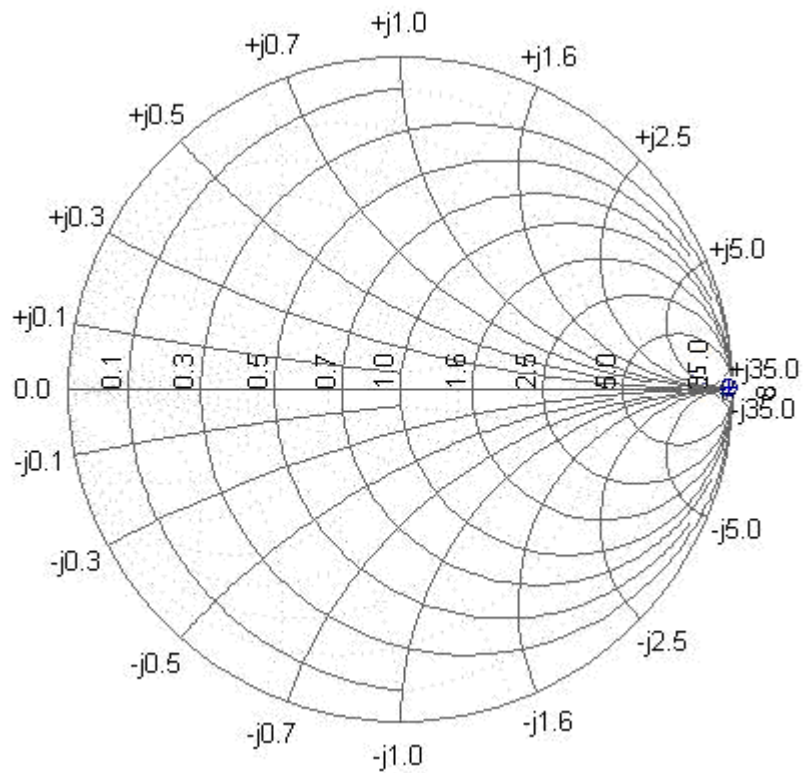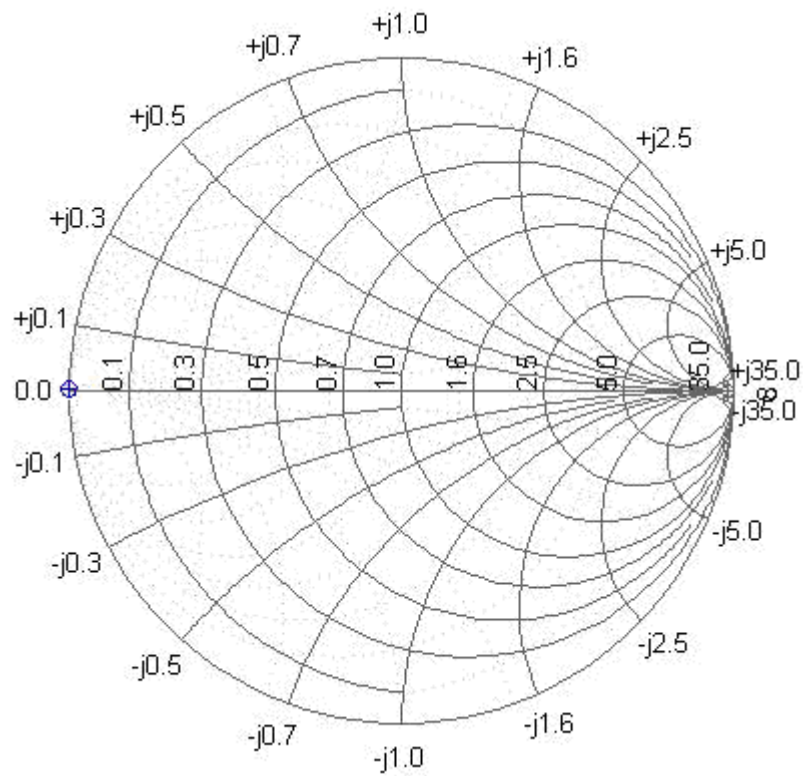
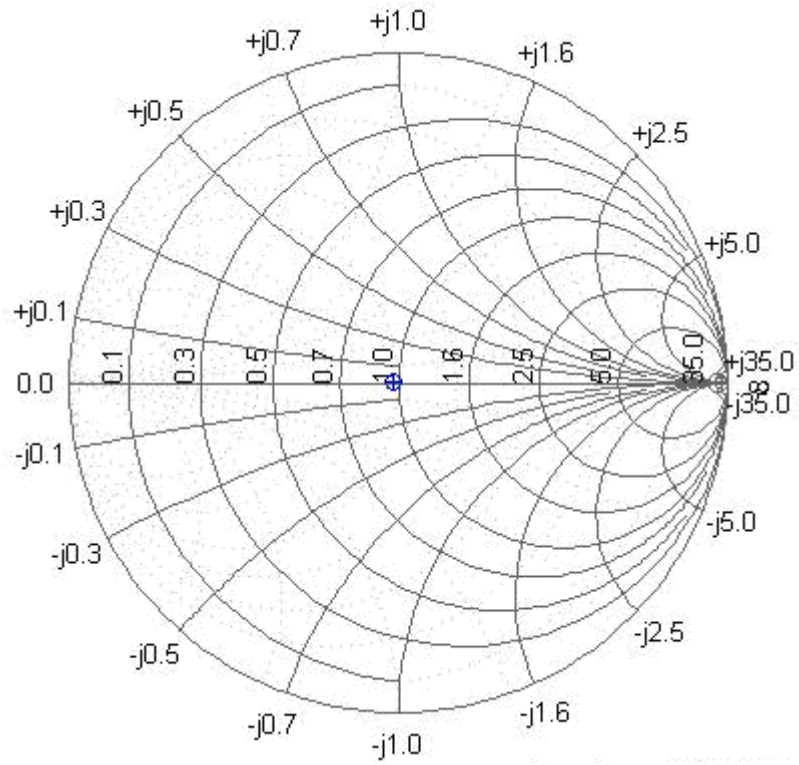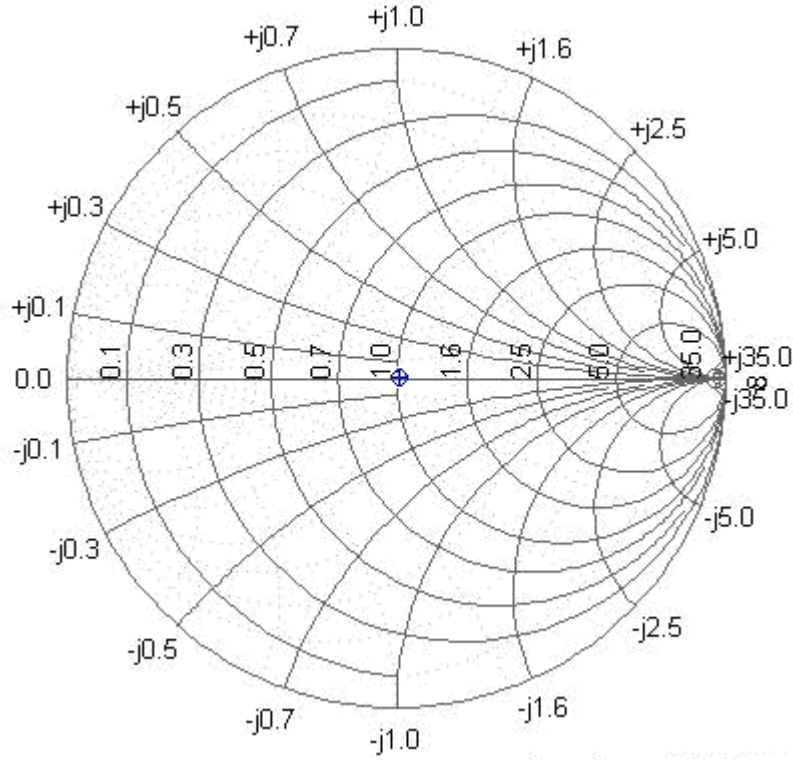**Figure 4.6**: S-parameter of a open circuit measured WITH calibration

Figure 4.7: S-parameter of a short circuit measured WITHOUT calibration

Figure 4.8: S-parameter of a short circuit measured WITH calibration

**Figure 4.9**: S-parameter of a load equal to 50 Ohms measured WITHOUT calibration

Figure 4.10: S-parameter of a load equal to 50 Ohms measured WITH calibration

4.3 Network Analyser vs S-Parameters Measurement System

Once all the reference S-parameters have been measured and computed and the system has been calibrated, it is possible to proceed with the computation of the real impedance at the input of the system. To understand the quality of the results given by this new system, an algorithm has been written to measure 125 different impedances and to compare the value of the respective impedance measured by the Network Analyser and the implemented system. The setup for this test has been developed and completed in the MRI lab of the Biomedical Department. The Network Analyser has been connected with a switch to the processor part of the System concerning the thesis. The processor, also has been connected to the computer through fiber optics. An algorithm has been implemented in the computer that starts from the characteristic impedance and then it changes the value of the impedance for 125 times all around the Smith Chart with a spiral trajectory. Every time the algorithm changes the impedance, the computer first acquires the value measured by the Network Analyser, then, the same value of impedance is also measured and saved in the PIC of the new system and sent in the same array. Next the process is repeated iteratively for 125 times and in the end the array on the computer has 125 values acquired by the Network Analyser and 125 values by the new system. So, finally, it is possible to compare the results recorded by this test and better understand how much the values of the impedance measured by this system are different from the Network Analyser (considered as "Gold Standard"). To quantify the difference in percentage between the two techniques some basic probabilistic values such as: Mean Value; Error Correction; Standard deviation have also been computed. Figure 4.11 shows the results of the experimental test. It can be seen that the measured and computed values of the impedance form the two different systems are equal, close to the reference points (Short-Open-Load). However when the values of the impedance are far away form these reference points, the two techniques show the same value of modulus, but different values of phase. In contrast, it is almost clear that the difference of phase between the two different technologies of the values related with the measured impedance is always constant. So, probably, with some further computation it will be possible to delete this difference of phase and to have a S-parameter measuring system that provides results very close to or even the same as that of the Network Analyser.
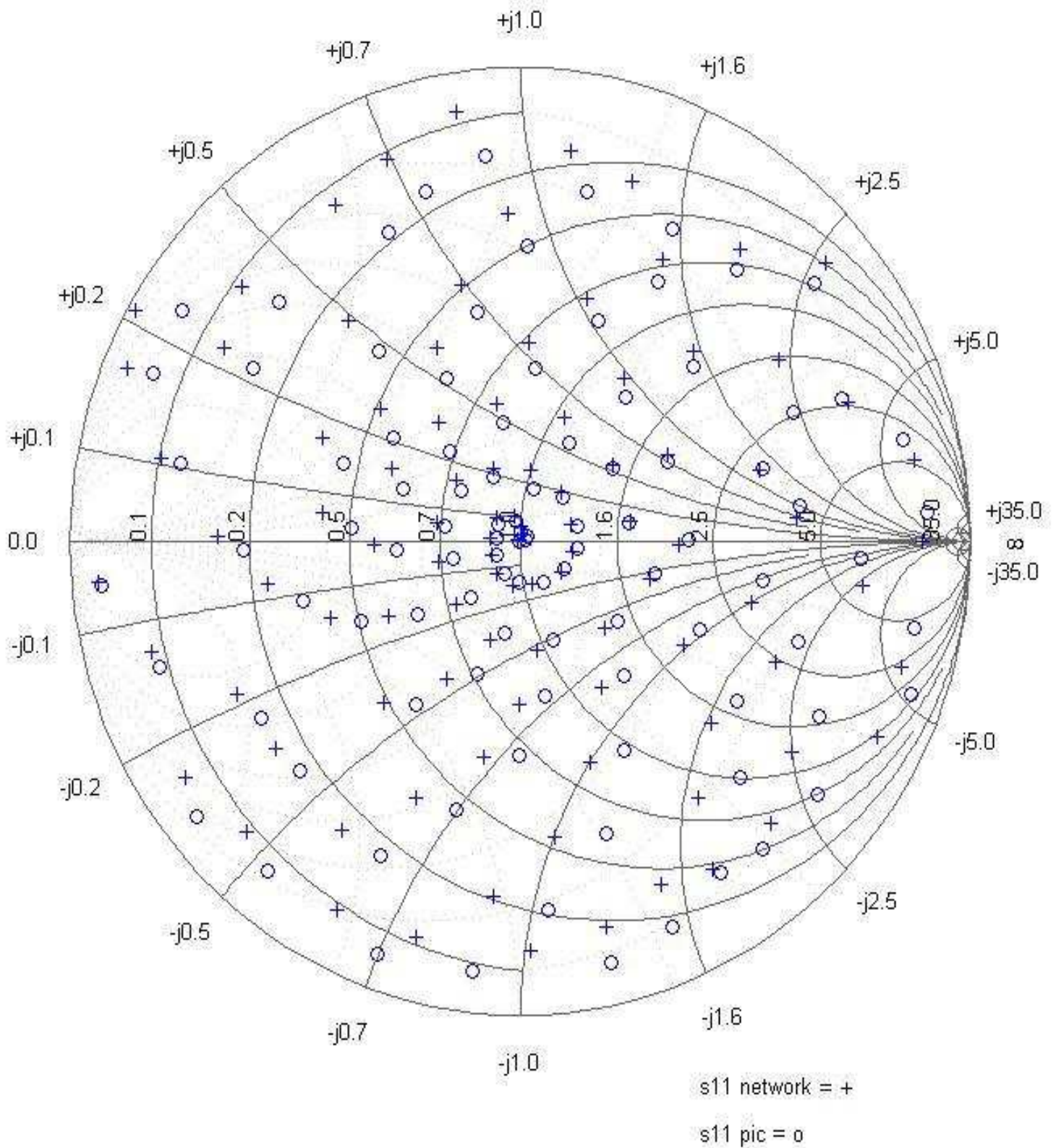
Figure 4.11: Comparison between the Network Analyzer (+) and the new System (o)

Moreover it is possible to make a further comparison of the same probabilistic values between the two different impedance measuring system setup. The first setup has been obtained by the RF gain and phase detector chip of the Modular Automatic Matching Network (AMMN) implemented by Pavan. The second is the S-Parameters Measurements System implemented in this thesis and goes to substitute the part related with the impedance measurement and absolutely compatible with the rest of the AMMN.

The probabilistic values computed with the results of the RF gain and phase detector chip are:

- mean_error =   0.0506

- standard_deviation =   0.0302

- error_in_percent = 2.0306 %

The probabilistic values computed directly form the results obtained by this experimental setup are:

- mean_error =   0.0606

- standard_deviation =   0.0402

- error_in_percent = 3.0306 %

On one hand, these values say that the mean error and the standard deviation are very good in both setups, but still in Pavan's system they are a bit better. For this reason the error in percent, concerning this work, is just 1% more than the previous one- In contrast, the system implemented in this work has the big advantage to reach an excellent linearity in the computation of the phase shift for the impedance measurement. Figure 4.12 shows the two different behaviour of the two system concerning the computation of the phase shift.
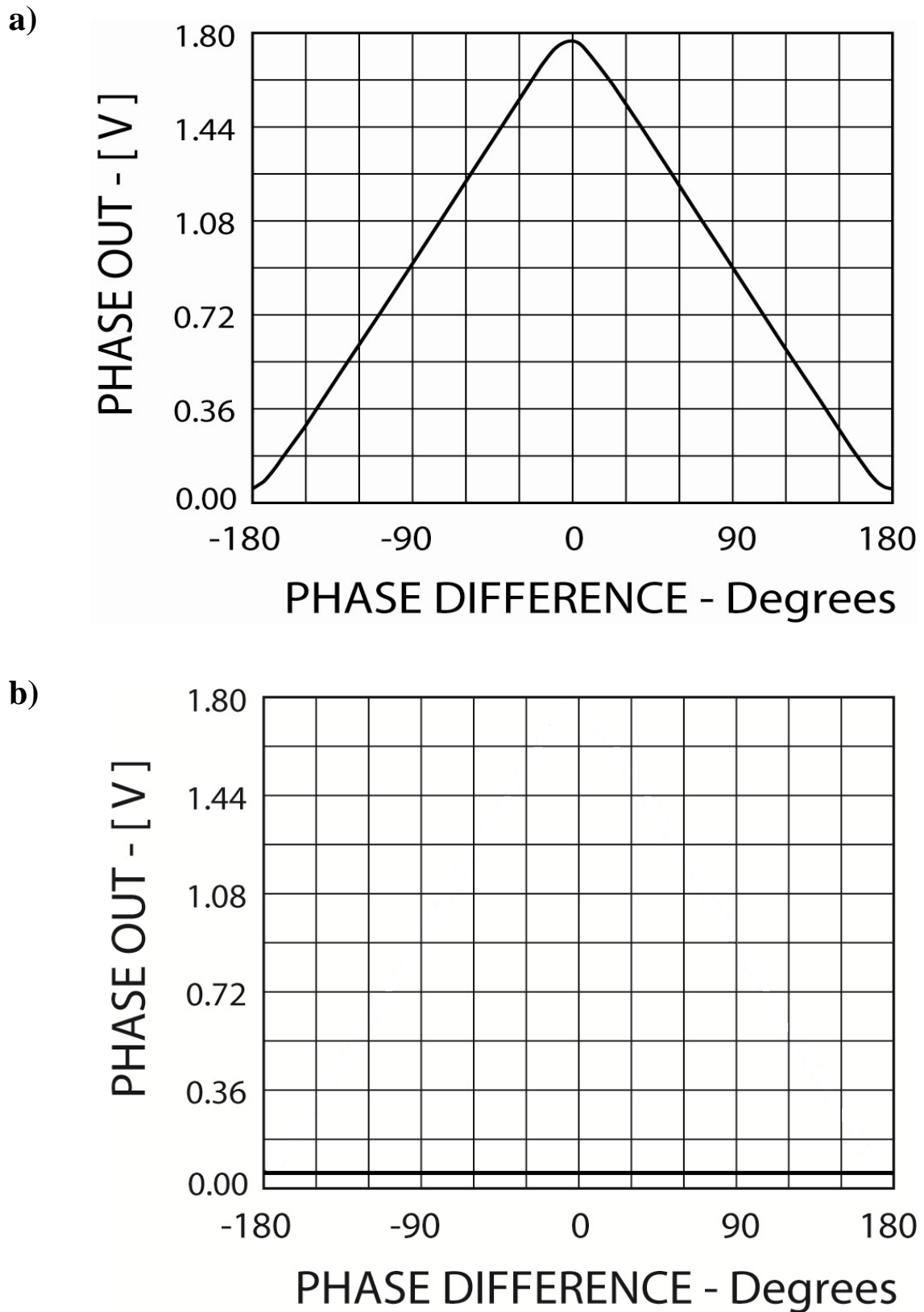
Figure 4.12: a) Non linear behavior of the RF gain and phase chip detector; b) Perfect linear behavior of the algorithm in the PIC of the S-Parameters Measuring System .

4.4   Conclusions

This thesis has been developed entirely at the MRI Lab of the Biomedical Department of the ETH University of Zürich, under the careful supervision of the PhD Matteo Pavan and the expert coordination of Prof. Klaas Prüssmann in ETH and of Prof. Andrea Aliverti in Politecnico. The scope of the thesis was to improve the previous system used by *Pavan* through the creation and application of an innovative way to measure the respective impedance for the automatic matching network setup. This network is used to keep the coil matched to the impedance that gives the best noise figure of the preamplifier, especially when coil loading conditions are changing. When coils can be stretched to adapt to the anatomic region to be pictured, obtaining an optimum SNR with an extraordinary high resolution of the images. The work can be divided in three main parts.

The first part was spent on studying all the past literature about this topic: After a general overview about the basic processes of a 7 Tesla MRI, the period of study was focused on understanding specifically: What a matching network is; Where possible it is to use it, and; Which kind of matching network had been created in the past through til Pavan's Automatic Modular Matching Network (AMMN).

The second part was based on the design and manufacture of the hardware part of the system. The design process started with the creation of a double hybrid Directional Coupler to reach the best performances for this kind of system. Then it has been designed and manufactured two mixers that were able to receive an RF sinusoidal signal as input and mix down to an Intermediate Frequency (IF) the output in a range of KHz and with only components used inside the MRI room (only lumped elements). The hardware finishes with the realization of the processor part with the PIC32MX795F512L and the connection between the processor with computer through optic fiber.

The final part refers to the creation of the algorithm used to compute the impedance. The algorithm implemented receives the two analogic signals from the two mixers, the FORWARD and the REFLECTED waves, and it processes both of them with the ADCs with the sample frequency of 300 KHz, using the oversampling technique. Then there is a digital filter to remove all the harmonics associated with the two signals and obtain more stable signals, very useful for the next steps. Once the signals are filtered, the algorithm memorizes the max and min values of both signals and then computes the modulus, with

the formula (3.10) and then the phase shift, using the relationship (3.11) of the two waves. Afterwards it iteratively computes the the modulus and phase shift of the S-parameter of the impedance to measure and then makes the calibration computing the same values for the S-parameters of Short-Open-Load. In the end the algorithm computes the three error terms to compute S-parameter calibrated and send all these values to MATLAB that computes, first the S-parameter calibrated, and then the respective value of the impedance, through the relationship (3.16).

To sum up, a New System has been developed very easy to use This system includes the Directional Coupler connected with two mixers and every mixer receives one of the two waves (forward or reflected). Two external mixer frequency generators provide the input signal, one for the Double Hybrid and the other one as the Local Oscillator (LO) for both mixers. The two outputs of the mixers are bandpass filtered and then sampled and analysed through the PIC microcontroller to obtain the impedance values for the computer. This System was designed for a 7 Tesla MRI and it can compute every impedance in less then 100 ms and the setup is implemented and positioned totally inside the MRI room. This work goes to substitute the Gain and Phase detector chip, including the Hybrid and the VCO, of Pavan´s System (showed in Figure 1.14). It replaces this part with a new S-parameter Measuring System. Entirely compatible with the rest of AMMN implemented from Pavan with several advantages and improvements and also some limits.

Through, this system has some limits, these restrictions concern the results found by comparing the probabilistic values computed during the comparison between the Network Analyser (NA) and the System implemented in this thesis and the comparison between the same NA and Pavan´s System. These results say that the mean value and the standard deviation of the first comparison (NA and new system) not as accurate as than the ones of the second comparison (NA and previous system). The Impedance Error value in both systems are good but the new system is still marginally poorer than the previous one. This means that the System implemented, is less precise and the measurements are less equal to the ones done by Pavan´s System.

On the other hand, this system has several advantages and improvements compared with the old system; one of the advantages of the system is the fact that it is the linearity of the system, t this system has a perfect linear behaviour when it measures the S-parameters, instead Pavan´s system is characterized by a big non-linearity, caused by the detector chip,

and it needs a Lookup Table. For this reason it computes all the possible values in the Smith Charts without a problem, compared with the other system where it was impossible to distinguish the impedance of 180° difference. Another advantage is the capability that the new system permits to measure the forward wave and the reflected wave in separate ways, instead the chip used by the older system has to measure both waves at the same time as input and it gives two voltages. Thanks to this the new system is able to compute, S_{11} and S_{22}, but also the S_{21} Parameter (and S_{12}) without any addition or change in the hardware, instead of only the S_{11} and S_{22} computed by the previous system.

The Possible improvements that can be adopted without increasing the time to measure an impedance could be:

1) Optimization of the undersampling with a better digital filter that can decrease the Impedance Error of the System and in this way, reach measurements more close to the Network Analyser.

2) Improvement of the quality of the signal from the mixers in such a way to have bigger difference between the two signals and compute more precisly the phase shift between the FORWARD and the REFLECTED waves.

3) Implementation of the algorithm totally inside the PIC. This way it is possible to speed up the process of measuring the impedance, since the PIC is much more faster than the normal communication between the PIC and computer through fiber optics.

4) Increasing the number of channels from two (already implemented and tested) to a max of 16 channels, to have the possibility to measure a lot of different channels at the same time.

In the end it is possible to conclude that the thesis offers the opportunity to study what happens when the MRI receives coils are coupled in different ways thanks to the computation not only of the reflection S-parameters (S_{11} and S_{22}) but also of the transmission S-parameters (S_{12} and S_{21}). This is a critical topic in Magnetic Resonance

such that still nobody has been able to study and analyse in a constant way. General hypotheses must be verified since a written theory is not yet in existence. This wok provides a lot of help and insight to this topic which should be developed in year to come.

Bibliography

1. C. P. Slichter. Principles of Magnetic Resonance. *Harper & Row, New York, 1963.*

2. E. Fukushima and S. B. W. Roeder. Experimental Pulse NMR: A Nuts and Bolts Approach. *Addison-Wesley, Redwood City, 1981.*

3. Thomas C. Farrar. Pulse Nuclear Magnetic Resonance Spectroscopy. *Farragut Press, Chicago, 1989.*

4. D. C. Ailion, Methods of Experimental Physics. *Academic Press, New York, Vol. 21, 1983 pp. 439-482.*

5. R. J. Abraham, J. Fisher, and P. Loftus. Introduction to NMR Spectroscopy. *John Wiley & Sons, New York, 1988.*

6. Wendell A. and Gibby MD. Basic principles of magnetic resonance imaging. *Neurosurgery Clinics of North America*, 2005.

7. Mark A. Brown and Richard C. Semelka. *MRI, Basic principles and applications*. John Wiley and Sons, 2003.

8. Pottumarthi V. Prasad. *Magnetic resonance imaging*. Humana Press, 2006.

9. Matteo Pavan. *Hardware advance in Magnetic Resonance Imaging*. 2008

10. Chris Bowick. *RF Circuit Design*. Newnes, 1982.

11. Reinhold Ludwig and Pavel Bretchko. *RF circuit design, theory and applications*. Prentice Hall, 2000.

12. Reinaldo Perez. *Design of medical electronic devices*. Academin press, 2002.

13. David M. Pozar. *Microwave Engineering*. John Wiley and Sons, 1998.

14. Patrick L. Jaskolski, Wauwatosa. Mutual Inductance NMR RF coil Matching Device. *U.S. Patent Documents,* 1987

15. William H. Harrison. Remotely Adjustable MRI RF coil impedance Matching Circuit with Mutually Coupled Resonators. *U.S. Patent Documents*, 1989Jerzy.

16. F. Hwang, D. I. Hoult. Automatic Probe Tuning and Matching. *MRM 39214-222 (1998)*

17. Bodurka, Patrick J. Ledden, Peter van Gelderen, Renxin Chu, Jacco A. de Zwart, Doug Morris, and Jeff H. Duyn. Scalable multichannel mri data acquisition system. *Magnetic Resonance in Medicine*, 2004

18. Pekka Sipila , Rolf F. Schulte, Gerhard Wachtuka, Florian Wiesinger. Digital Multiband Receiver for Magnetic Resonance. *Concepts in Magnetic Resonance Part B (Magnetic Resonance Engineering), Vol. 35B(4) 210–220 (2009*

19. J.A. Nordmeyer-Massner, N. De Zanche, and K.P. Pruessmann. Mechanically Adjustable Coil Array for Wrist MRI. *Magnetic Resonance in Medicine 61:429–438 (2009)*

20. Nicola De Zanche, Jurek A. Massner, Christoph Leussler, and Klaas P. Pruessmann. Modular design of receiver coil arrays. *Magnetic Resonance in Medicine*, 2008.

21. M. Pavan, K. P. Pruessmann. A Modular Matching Metwork System. 2010

22. R. Sarpeshkar, T. Delbruck, and C. A. Mead. White noise in mos-transistors and resistors. *IEEE Circuits Devices Mag.*, 1993.

23. J. J. van der Klinkd. The nmr reciprocity theorem for arbitrary probe geometry. *Journal of Magnetic Resonance*, 2001.

24. *Applying Error Correction to Network Analyzer Measurements*, Hewlett-Packard Application Note 1287-3.

25. *Understanding the Fundamental Principles of Vector Network Analysis,* Agilent application note 1287-1.

26. *Exploring the Architectures of Network Analyzers,* Agilent application note 1287-2.

27. *Network Analyzer Measurements: Filter and Amplifier Examples,* Agilent application note 1287-4.

28. *Specifying Calibration Standards for the Agilent 8510 Network Analyzer,* Agilent product note 8510-5A.

29. *Applying the Agilent 8510 TRL Calibration for Non-Coaxial Measurements,* Agilent product note 8510-8A.

30. Jian-An Hou, Yeong-Her Wang. A Compact Quadrature Hybrid Based on High-Pass and Low-Pass Lumped Elemets. *Member IEEE 1531-1309,* 2007

31. *Quadrature Hybrids 90° power/combiners 10 KHz to 40 GHz General Information*,

32. *Directional Couplers Lumped Element & Stripline 100 KHz to 65 GHz General Information*

33. Mixer Evolution, The Balanced Mixer Family Circle." Application Note. http://ww w.markimicrowave.com/menus/appnotes/balanced.pdf.

34. Henderson, B. C., "Predicting Intermodulation Suppression in Double-Balanced Mixers," WatkinsJohnson Company Technical Notes. Vol. 10, No. 4, July/August 1983.

35. Pablo Pèrez, Andrès Santos, and Juan Josè Vaquero. Potential use of the undersarnpling technique in the acquisition of nuclear magnetic resonance signals. *Magnetic Resonance Materials in Physics, Biology and Medicine*, 2001.

36. J. Yuan, P. Qu, J. Wei, and G. X. Shen. Noise figure and dynamic range optimization in optical links for mri applications. *Proc. Intl. Soc. Mag. Reson. Med. 14*, 2006.

37. R. Hernandez, A. Rodriguez, P. Salgado, F.A. Barrios. Concentric dual-loop RF coil for Magnetic Resonance Imaging. *Revista Mexicana de Fisica 49 (2) 107-114*. April 2003

38. S.P. Appelbaum, *IEEE AP 24, pp. 585-598, 1976*

39. K.P. Prüssmann et. al: *MRM 42, pp. 952-962, 1999*

40. J. Engberg et. al: *ISBN 0-471-94825-X, 1995*

41. A. Reykowski et. al: *ISMRM 2000, p. 1402*

42. C. Findeklee1. Improving SNR by Generalizing Noise Matching for Array Coils. *Proc. Intl. Soc. Mag. Reson. Med. 17 (2009)*

43. P.J. Cassidy, K. Clarke, D.J. Edwards. Determining the Tuning and Matching Requirements of RF Coils Using Electromagnetic Simulation and Electric Circuit Analysis. *Concepts in Magnetic Resonance Part B (Magnetic Resonance Engineering), Vol. 25B(1) 27–41 (2005)*

44. Ross D. Venook, Brian A. Hargreaves, Garry E. Gold, Steven M. Conolly, and Greig C. Scott. Automatic Tuning of Flexible Interventional RF Receiver Coils. *Magnetic Resonance in Medicine 54:983–993 (2005)*

45. Gonzalez, Guillermo; Microwave Transistor Amplifiers, Analysis & Design; Second Edition, Prentice Hall, Upper Saddle River, New Jersey 07458.

46. Bowick, Chris; RF Circuit Designs; Howard W. Sams & Co. Inc., a publishing subsidiary of ITT.

47. M. Pavan. Hardware Advanced in Magnetic Resonance Imaging. *Magnetic Resonance Imaging RF laboratory Institute for Biomedical Engineering University and ETH Zuerich*. 2008

48. Ferenc Marki ,Christopher Marki, Ph.D. Mixer Basics Primer A Tutorial for RF & Microwave Mixers. http://www.markimicrowave.com/menus/appnotes/mixer_basic s_primer.pdf.

49. Marki, F.A., "Miniature Image Reject Mixers And Their Use In Low-noise Front-ends In Conjunction With Gaas Fet Amplifiers," *Circuits, Systems and Computers, 1977. Conference Record. 1977 11th Asilomar Conference on* , vol., no., pp. 159-1 6 7-9 Nov 1977. http://www.markimicrowave.com/menus/appnotes/noise.pdf.

Appendix A

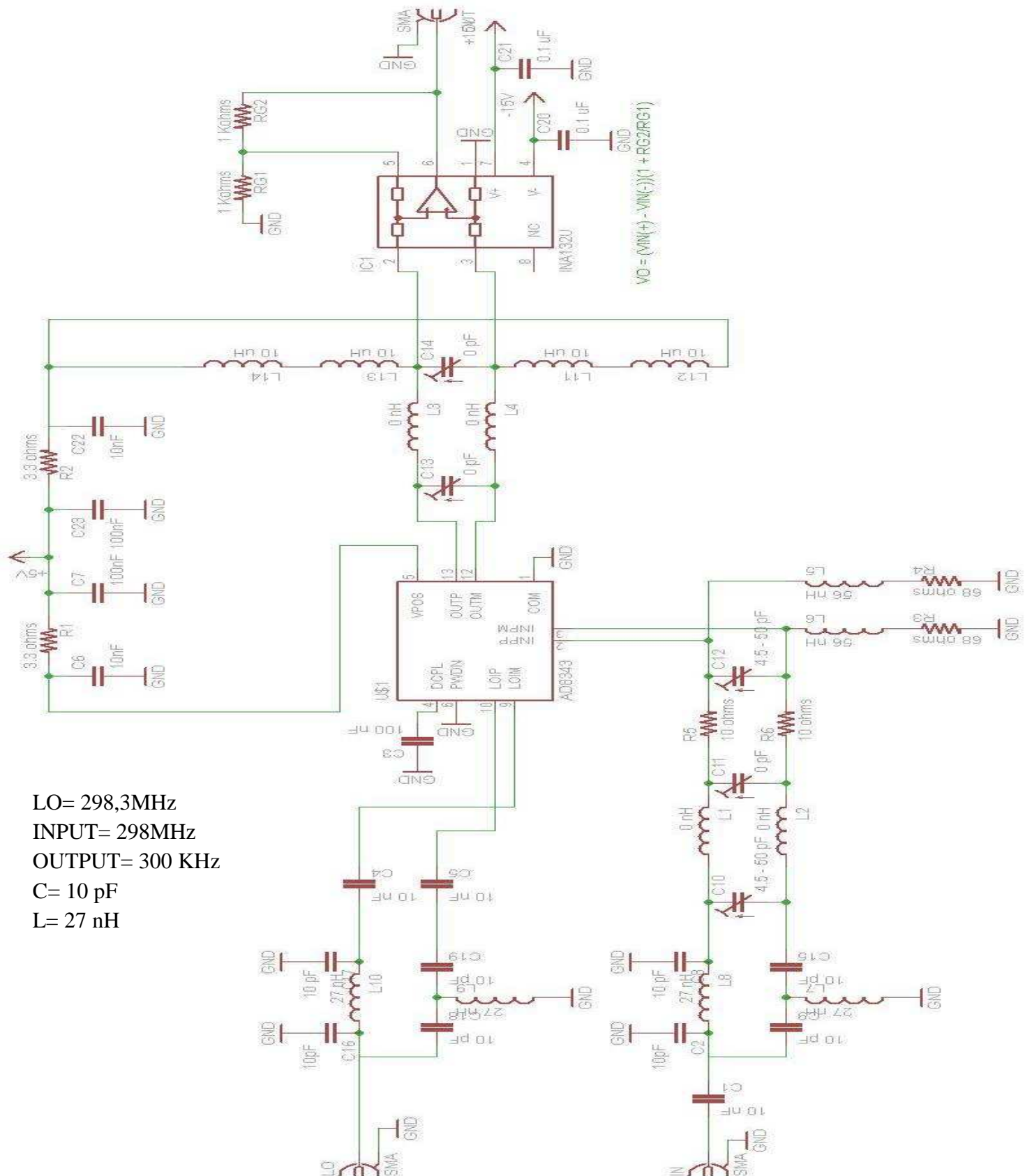It is shown the schematic of the mixer with normal baluns :
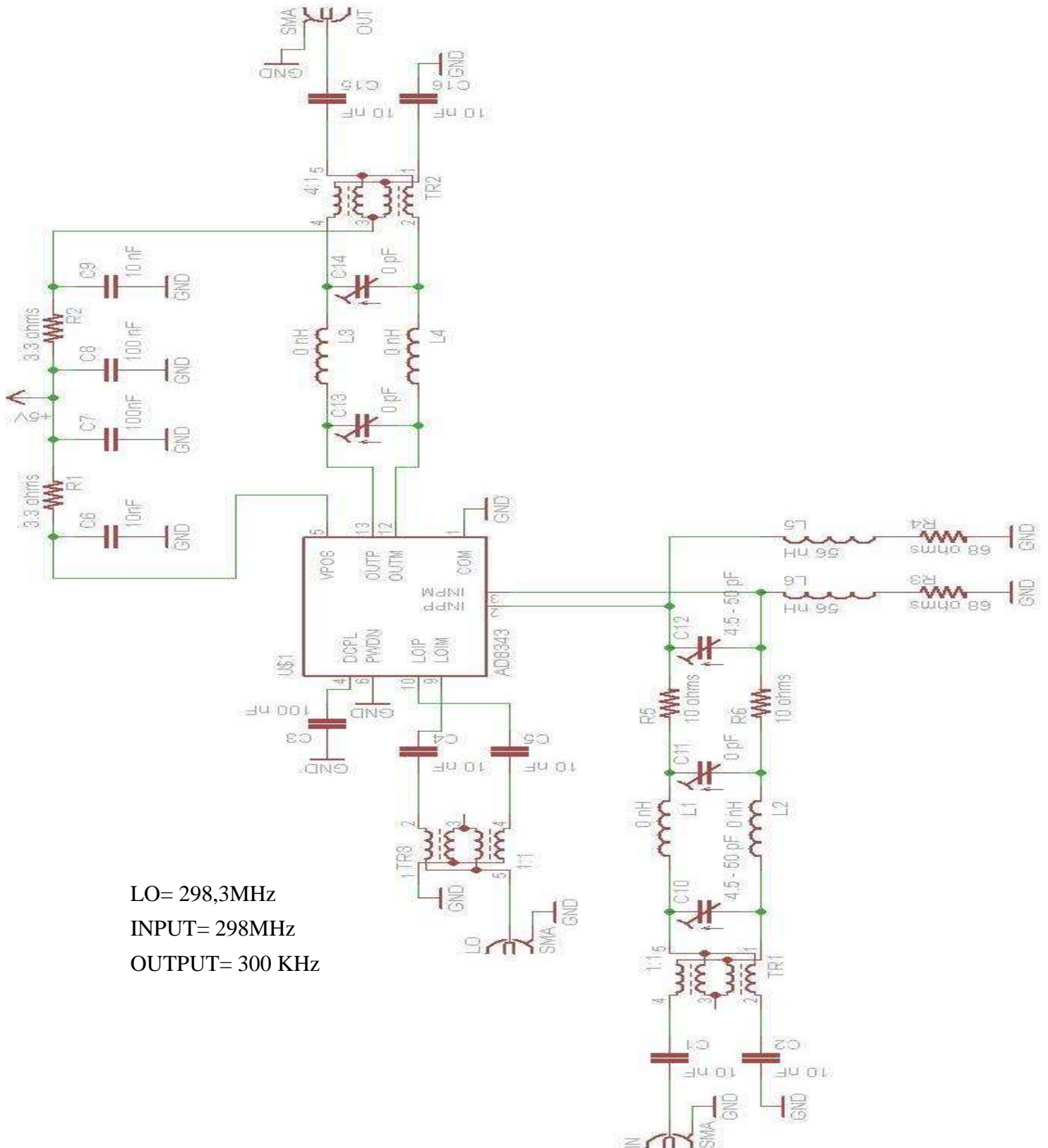
LO= 298,3MHz
INPUT= 298MHz
OUTPUT= 300 KHz

Appendix B

It is shown the schematic of the mixer with lumped elements baluns :

LO= 298,3MHz
INPUT= 298MHz
OUTPUT= 300 KHz
C= 10 pF
L= 27 nH